Can Geopolymer Concrete Become A Key Material To Utilize Basic Oxygen Furnace Slag (BOFS) As Construction Material?

Gulfairuz Kareken, Bachelor of Engineering

Submitted in fulfilment of the requirements

for the degree of Master of Science

in Civil & Environmental Engineering

NAZARBAYEV UNIVERSITY

School of Engineering and Digital Sciences

Department of Civil & Environmental Engineering

Nazarbayev University

53 Kabanbay Batyr Avenue,

Nur-Sultan, Kazakhstan, 010000

Supervisors: Chang-Seon Shon

Co-Supervisors: Dichuan Zhang

March 2023

Declaration

I hereby, declare that this manuscript, entitled “Can Geopolymer concrete become a key material to utilize Basic oxygen furnace slag (BOFS) as construction material?” is the result of my own work except for quotations and citations which have been duly acknowledged.

I also declare that, to the best of my knowledge and belief, it has not been previously or concurrently submitted, in whole or in part, for any other degree or diploma at Nazarbayev University or any other national or international institution.

Gulfairuz Kareken

April 2023

Shon Chang Seon

Abstract

Basic oxygen furnace slag (BOFS) is the hard waste created when molten iron is treated in a basic oxygen furnace during the steelmaking process. Despite its good hardness and strength properties, the free lime (f-CaO) and free magnesia (f-MgO) in BOFS limit the utilization of BOFS as an aggregate used in construction applications due to the expansion characteristics of their hydration products. However, the interaction between f-CaO and f-MgO and free silicon (f-Si) that come from sodium silicate (Na_2SiO_3) in geopolymer concrete/mortar mixture can create stable substances like wollastonite ($CaSiO_3$) and enstatite ($MgSiO_3$), and the expansion issue in BOFS may be reduced. In this research, therefore, a total of 15 geopolymer mortar mixtures were designed: 4 geopolymer mortar mixtures that comprise a partial substitution of river sand (RS) with BOFS aggregate (25%, 50%, 75%, and 100%) and one control mixture (100% RS) with fixed parameters, which contain Na2SiO3 ratio of 1, 1.5 and 2 with 10 Molarities of NaOH and the combined binder contents with 40% ground granulated blast furnace slag (GGBFS) and 60% ASTM Class F fly ash (FA). Then, the fresh and hardened properties of geopolymer mortar (GPM) mixtures were evaluated. Test results presented that increasing BOFS aggregate content up to 75% substitution of RS increases the GPM mixture's relative flowability. However, the air content and setting time of the GPM mixture decreased with increasing BOFS aggregate content. For compressive and flexural strengths, the GPM mixtures containing BOFS aggregate had comparative strength or higher strength than that containing 100% RS. The GPM mixture with higher compressive strength showed higher shrinkage than other mixtures. Finally, regardless of water and 1 M NaOH solution submersions, all GPM mixtures have less than 0.1% expansion value except for the mixture [25%RS+75%BOFS and 25%RS+100%BOFS] submersed in NaOH solution.

Acknowledgments

First and foremost, I would like to thank my supervisor, Dr. Chang-Seon Shon, of the Civil Engineering Department at Nazarbayev University. Throughout my study, Professor Shon provided supervision and instruction whenever he believed I needed it. Furthermore, he gave substantial financial assistance in purchasing the necessary lab equipment and materials. I am quite appreciative for the hours of conversation, as well as the helpful remarks and criticism that enabled me to successfully complete this Master's program.

I would also want to thank Nurtay Kozhageldi, Madiyar Mardenov, and Aizhan Tukaziban for their invaluable assistance in completing this research work.

In the end, I would like to thank my family and friends. This journey would not have been possible without your support. To my family, thank you for encouraging me in all of my pursuits and inspiring me to follow my dreams. I am especially grateful to my parents, who supported me emotionally and financially. I always knew that you believed in me and wanted the best for me. Thank you for teaching me that my job in life was to learn, to be happy, and to know and understand myself. Your love and support mean the world to me.

Table of contents

List of Abbreviations

ASR	Alkali-silica reaction
ASTM	American society of testing and materials
BOFS	Basic oxygen furnace slag
GGBFS	Ground granulated blast furnace slag
F-FA	F class Fly Ash
NaOH	Sodium Hydroxide
Na_2SiO_3	Sodium Silicate
GPM	Geopolymer Mortar
AAS	Alkali Activated Solution
OPC	Ordinary Portland cement
PSD	Particle size distribution
SEM	Scanning electron microscope
SG	Specific gravity
XRD	X-ray diffraction
XRF	X-ray fluorescence
ITZ	Interfacial Transition Zone
ASR	Alkali silica reaction
RS	River sand
RSM	Response surface methodology
GPC	Geopolymer concrete
NS	Sodium silicate

List of tables

List of Figures

Chapter 1 . Introduction

1.1. Background

The leading cause of modern climate change has been recognized as carbon dioxide (CO_2) emissions from fossil sources and human activities such as the disposal of municipal wastes through burning and resource consumption to produce industrial products. Cement manufacture is a major source of industrial and energy-related CO_2 emissions across the world. 5-8% of the world's carbon dioxide emissions come from cement production. Cement production accounts for 5-8% of global CO_2 emissions.

Using an alternate binder material in the concrete manufacturing process may be a workable substitute for cement to reduce this gas emission [Rao et al., (2020)].

Geopolymer concrete (GPC), known as alkali-activated concrete (Fig.1), can be a solid potential to replace cement because it can reduce CO_2 emissions and improve mechanical and durability compared to Ordinary Portland Cement (OPC) concrete. The main components of GPC are aluminosilicate minerals, alkali activators such as sodium hydroxide (NaOH) and sodium silicate (Na2SiO3), and fine and coarse aggregates [Azarsa et al. (2020)]. Mainly, aluminosilicate minerals include a variety of by-products, including fly ash (a derivative of coal combustion power station), ground granulated blast furnace slag (a product of steelmaking), silica fume (a by-product of ferrosilicon alloys or silicon metal), or rice husk ash (agricultural by-product). Aluminosilicate minerals are mixed with fine and coarse particles in GPC after being activated with an alkali activator during manufacturing. In comparison to OPC concrete, the GPC may be utilized in construction due to its adequate or similar mechanical properties (compressive and flexural strengths) and excellent durability [Ma et al., (2021)]. As a result of its potential to preserve natural resources and minimize CO_2 emissions, GPC can become an ecologically friendly competitive alternative to OPC concrete. [Ding et al., (2017)].

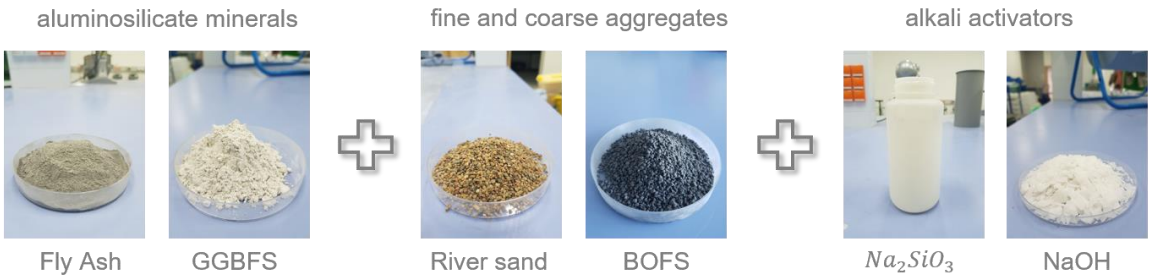

Figure 1.1. Content of geopolymer concrete

1.2. Problem statement

Meanwhile, basic oxygen furnace slag (BOFS), a by-product of the steelmaking process, is the hard waste created when iron ore is treated in a basic oxygen furnace, as shown in Fig.2. This material has good mechanical and physical qualities, such as a reduced abrasion ratio, greater compressive strength, and solid hardness [Lee et al., (2020)]. BOFS can create structural materials, road pavements, and other things instead of using natural aggregates.

Due to the concentration of free lime (f-CaO) and free magnesium oxide (f-MgO) found in the BOFS, one of the significant downsides of BOFS is its propensity to expand, which limits recycling, and reuse or utilization of BOFS as alternative aggregates used in the construction application [Yunxia et al., (2008)]. The hydration process in f-CaO or f-MgO occurs when the BOFS comes into contact with water, resulting in volume expansion. In other words, when the BOFS absorbs moisture, as shown in Eq. (1) and (2), f-CaO and f-MgO transform into calcium hydroxide ($Ca(OH)_2$) and magnesium hydroxide ($Mg(OH)_2$), respectively. The bonding structure disintegrates due to this reaction, resulting in a significant volume expansion (Fig.3) and loss of strength. The scope of using BOFS as aggregates, thus, is restricted to building materials to make OPC concrete [Kabay et al., (2021)]. As a result, BOFS is typically landfilled and considered waste materials.

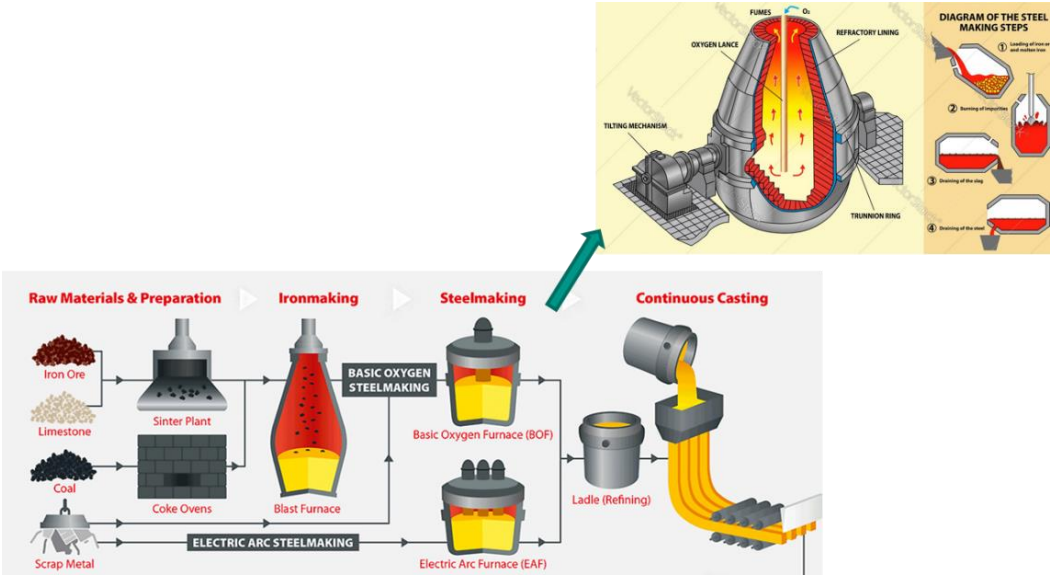

Figure 1.2. Steel making process

$$f\text{-}CaO + H_2O \rightarrow Ca(OH)_2 \quad (1)$$

$$f\text{-}MgO + H_2O \rightarrow Mg(OH)_2 \quad (2)$$

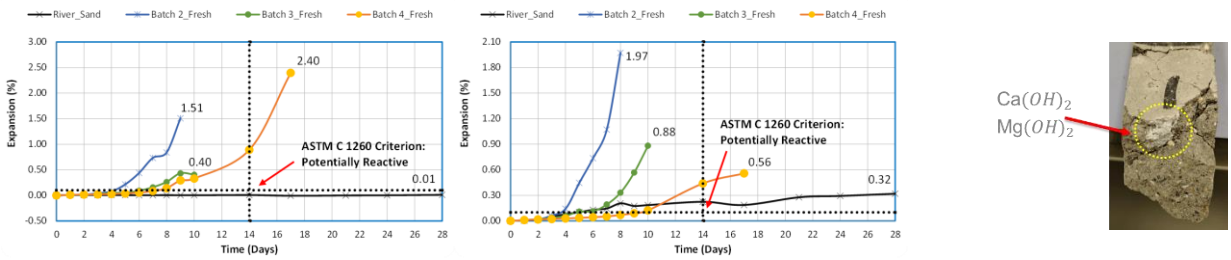

(a) (b) (c)

Figure 1.3.. (a) Expansion characteristic at the water (a) and at 1 M NaOH solution (b); (c) appearance of hydroxide in BOFS-based concrete

1.3. Possible solution

However, GPC can be a game changer for utilizing BOFS aggregate. In the GPC, the aluminosilicate (Si-O-Al) framework constitute on the solid particle surface during the polymerization process, together by Si-gel, and Al-gel are created, shown in Eq. (3). All of the O_2 atoms in the tetrahedra of silicate (SiO_4) and aluminate (AlO_4) are shared by this linked atoms. These complicated geopolymer reactions are exothermic and include a lot of free silicon (f-Si). This f-Si could react with f-CaO and f-MgO in the BOFS aggregate, which resulting in the formation of stable substances such as wollastonite ($CaSiO_3$) and enstatite ($MgSiO_3$), which restricts volumetric growth of BOFS aggregates, as shown in Eq. (4) and (5).

$$SiO_2 + Al_2O_3 \rightarrow Al_2SiO_5 \quad (3)$$

$$f\text{-}CaO + SiO_2 \rightarrow CaSiO_3 \quad (4)$$

$$f\text{-}MgO + SiO_2 \rightarrow MgSiO_3 \quad (5)$$

Mineral sequestration or carbonation process, have shown in Eq. (6) and (7). Ca and Mg are alkaline earth elements that can create carbonate minerals when they react with water and CO_2 gas. These weathering or carbonation processes could be improved and then employed industrially to bond gaseous carbon dioxide into a solid carbonate, preventing the emission of CO_2 into the environment (Huijgen, 2007).

Following the geopolymer reaction is finished, and if additional conditions cause the geopolymer matrix and/or BA and BOFS aggregates to break over time, the geopolymer composite

can be subjected to the mineral carbonation process. Eq. (8) and (9) show their overall reaction conversions to stable calcites (Lee et al., 2020). Therefore, geopolymer technology and CO_2 treatment can play a key in forming a stable calcium silicate/magnesium silicate to prevent expansion (Lee et al., 2020). These two concepts can manufacture new green, durable, and geopolymer-based construction materials.

$$CaO\ (s) + CO_2\ (g) \rightarrow CaCO_3\ (s) \quad (6)$$

$$MgO\ (s) + CO_2\ (g) \rightarrow MgCO_3\ (s) \quad (7)$$

$$CaSiO_3(s) + CO_2(g) + 2H_2O(l) \rightarrow CaCO_3(s) + H_4SiO_4(aq) \quad (8)$$

$$MgSiO_3(s) + CO_2(g) + 2H_2O(l) \rightarrow MgCO_3(s) + H_4SiO_4(aq) \quad (9)$$

Currently, Kazakhstan faces considerable difficulties in properly disposing of its industrial waste, just like any other nation. Moreover, environmental issues, including CO_2 emission, land scarcity, and the high costs of management and treatment connected to the disposal of industrial/municipal waste products, are currently gaining attention on a global scale. Therefore, Kazakhstan investigates the possibility of building a capability for industrial by-product management that goes beyond national demands and pollution prevention and cleaning. It is worthwhile to think about creating a project to look into the possible use of BOFS produced in Kazakhstan as construction materials and their application, starting with sustainable development and the reuse of waste resources.

1.4. Objective of study

The primary purpose of this study is to solve environmental problems such as gas emissions, the scarcity of land, and the high costs of management and treatment of industrial waste materials. Therefore, this study aims to utilize BOFS in geopolymer mortar (GPM) as an aggregate source and develop an optimum user-friendly mix design of GPM mixture without expansion problems. BOFS, GGBFS, FA, and two different alkali activators (NaOH and Na_2SiO_3 solutions) were used as the main components to make BOFS aggregate-based GPM mixture in this study. Five different combinations of natural river sand (RS) and BOFS aggregate were variables to determine an optimum BOFS aggregate-based GPM mix design under fixed other parameters of 10 Molarities of NaOH and 1, 1.5, and 2 ratios of Na_2SiO_3 to NaOH and the combined binder contents with 40% ground granulated blast furnace slag (GGBFS) and 60% ASTM Class F fly ash (F-FA). Moreover,

the carbonation curing technique will be used to characterize the expansion behavior of BOFS-based GPM.

1.5. Structure of thesis

There are five chapters in this thesis. The first chapter focuses on the study's introduction, where the issue statement is stated and the solution, together with the expected findings, is provided. Next, the second chapter is a literature review, where the background and properties, such as hardened strength and durability of binders such as Fly ash and GGBFS, and BOFS aggregate and Geopolymer, were explained regarding the current study. This chapter also discusses the material's characteristics.

The third chapter is the applications section. This chapter includes material characterization tests, mix design, fresh property tests, and hardened and durability properties of the mixtures. Additionally, mixing proportions and experimental design were incorporated. The casting and curing techniques for the mortar sample were also demonstrated. Chapter four included discussions of the test results and their analysis results. The final chapter finished with the research's key conclusions, as well as its limits and suggested next steps.

Chapter 2 . Literature review

2.1. Geopolymer concrete

2.1.1. Background

The cement - used in construction fields, satisfies only some of the requirements for green infrastructure development. The world needs to decrease Carbon dioxide emissions or limitation of it. While making cement, coal burning produces a tremendous amount of carbon dioxide, contaminating the air and other pollution like acidification and eutrophication [Pradhan et al., 2022]. Several methods can be provided to reduce this outgassing. One of them is using alternative cementitious material, using other fuel options in clinker cement manufacture, replacing the binder type during cement production, or changing/improving the cement manufacturing process [Farooq et al., 2021]. Researchers have been working on developing new materials to replace ordinary Portland cement for several decades [Ahmed et al., 2022]. Geopolymer concrete is one of the best sustainable options for replacing OPC concrete. Using Geopolymer concrete in the construction industry can reduce gas emissions and energy utilization [Farooq et al., 2021]. According to Hamdane et al., 2021, geopolymer properly regard as a cementitious material in the construction area, which is green and eco-friendly.

Industrial waste is expanding year after year across the world, and it has become the primary cause of pollution of the environment, air, water, and land. Studies investigated that the recycling of waste could save our environment. One of the best options for converting industrial materials is using them as a binder or cementitious material in the making process of geopolymer [Farooq et al., 2021].

Geopolymer concrete includes an abundant amount of aluminosilicates, which has a similar characterization to cementitious materials. Geopolymer concrete is often created by combining aluminosilicate and alkali activator reagent solutions such as sodium hydroxide (NaOH) or potassium hydroxide (KOH) with dissoluble silicates such as gelatine silicate [Farooq et al., 2021]. As aluminosilicate materials, natural minerals or industrial by-products can be used. For example, fly ash, slag, rice husk (amorphous silica) or kaolin, and bentonites (aluminum) [Shehata et al. 2022]. Figure 1 shows the primary materials for obtaining Geopolymer concrete.

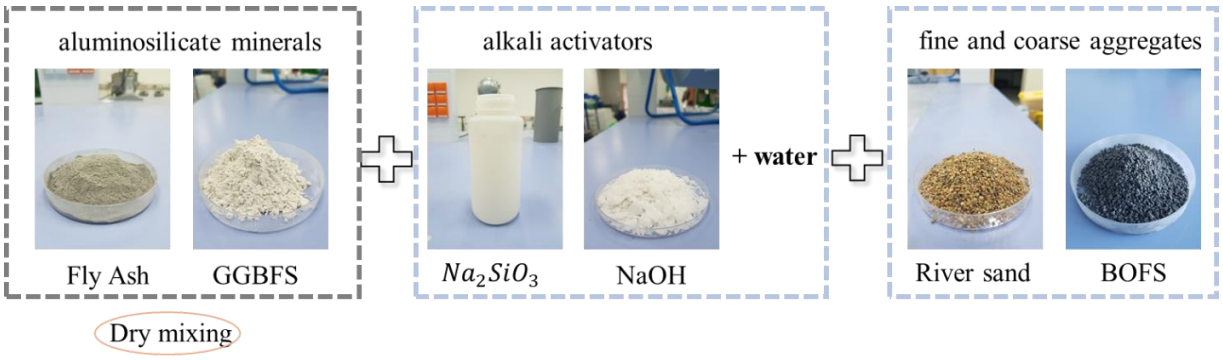

Figure 2.1.. Content of Geopolymer concrete/mortar

The conceptual process of geopolymerization includes the dissolution of blended aluminosilicate materials with an alkali solution, then oligomerization of tetrahedral frameworks, and after oligomerization of Si and Al by bonding electron framework (Fig.2).

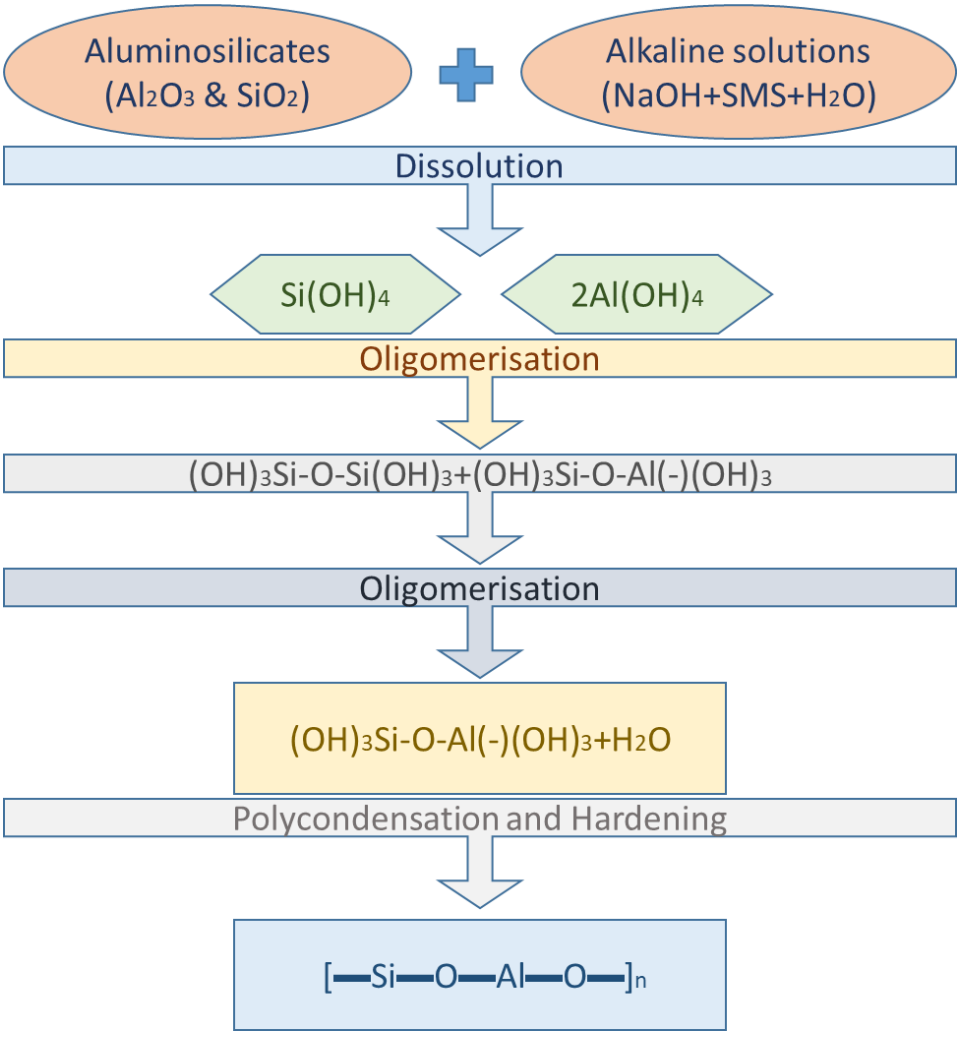

Figure 2.2. Process of geopolymerization

The first step of the geopolymerization process is association. The aluminosilicates in raw material bond with water through siloxane (—Si—O—Si—). This bond head of formation of highly reactive subsidiary silicon elements. Due to its extremely reactive nature, the intermediate pentavalent silicon undergoes fast dissociation from silanols and has a deformed trigonal bipyramid structure.

The second step is dissociation. The mechanism of the bimolecular nucleophilic substitution (SN_2) dissociates with subsidiary silicon and makes silanol (>Si—OH) and aluminol (>Al—OH).

In the third step, the result from 2nd step, silanols, react further and forms silanediol $SiO(OH)_2$, silanetriol $SiO(OH)_3$, and silanetetraol $Si(OH)_4$. The silica elements, which are hydrated, become more like an acidic oxide, with a propensity to dissolve in solution and the presence of an alkaline solution. Additionally, siloxane bridges are destroyed by OH ions, which leads to the development of alkaline silicates.

The fourth step is similar to the previous step, but aluminosilicate reacts with others instead of silicates. The aluminol, because Al^{3+} supplied only three electrons to the bonding framework in place of four silicon atoms, which would have resulted in a fourfold coordination structure, carries one negative charge.

2.1.2. Properties of geopolymer concrete

Fresh properties of geopolymer concrete

Ghafoor et al. (2021) show that FA and GGBFS-based GPC have good workability. The Molarity of NaOH was 8, 10, 12, 14, and 16, while the Na_2SiO_3 ratio was 1.5, 2.0, and 2.5. With the increasing of Molarity of sodium hydroxide, the fresh properties of samples were improved. Handling fresh concrete was easy, and the compacting and finishing showed no problems. Furthermore, increasing the AAS/binder ratio improved the workability of fresh GPC, where the alkaline activator to FA ratio was 0.4, 0.5, and 0.6. The increase in the AA/FA ratio from 0.4 to 0.6 boosted the workability of GPC by approximately 333%. The reason for good fresh performance because of high concentration of sodium hydroxide, which react with aluminosilicate minerals and gives great slump test results.

Hardened properties of geopolymer concrete

The central performance of all concrete is hardened compressive strength. Depending on differebt condition, results for compressive strength of Geopolymer concrete depends on the type

of aluminosilicate, activators, and the Molarity of hydroxide, the percentage of binders or aggregates, and the curing method [Farooq et al., 2021]. Geopolymer concrete has higher compressive strength performance than other types of concrete at early ages.

The performance of concrete at 28 days in the structural design and construction field is crucial. Regarding existing studies, most results of Geopolymer concrete the strength increase until 28 days and then drop. On the other hand, depending on the investigation of the Molarity of NaOH, the compressive strength of concrete shows different performance. Hydroxide plays a prominent role in the polymerization process, where it breaks aluminum and silicon particles. The strength of GPC, which was investigated in the Ghafoor et al. (2021) study, where cconcrete samples was cured at room temperature (23^0C) and was significantly influenced by the Molarity of the NaOH. The Molarity of NaOH was increased from 8 M to 14 M, increasing the compressive strength of GPC between mixtures by about 106%. In contrast, the Molarity of NaOH was increased from 8 M to 16 M, increasing the flexural strength of GPC by approximately 59%.

Durability properties of geopolymer concrete

The properties of engineering structures of concrete and the intended structural lifespan by preventing deterioration, chemical attack, abrasion, and degradation process of concrete. Durability is one of the most critical factors in maintaining concrete performance for a long time. Commonly the durability performance of geopolymer concrete is dominated mainly by two factors: the production technique with the material used and resilience to harsh environmental factors.

The durability performance of geopolymer concrete can depend on the proportion of binder, alkaline activator, aggregate, the phase of calcium silicate hydrate, the degree of compaction of samples, and the curing time of it. The content of alkali-activated binders creates the stabilization of geopolymer concrete after blending with AAS. These binders are rich in aluminum and silicate minerals. The 3D aluminosilicate hydrate (N-A-S-H) gel matrix evolves the form, which can improve the mechanical properties of concrete. If OPC shows good durability performance in temperate environmental conditions, on the other hand, geopolymer concrete resists even in a risky environment.

Durability properties are related to swelling reaction, which reacts into a concrete matrix between hydroxyl ions and definite silica form. The protuberance reaction, also called concrete cancer, can cause expansion by water and alkali silicon reaction, cracking of the concrete, and

strength loss of it. The study of Lodeiro et al. shows that FA-based geopolymer concrete shows decreased ASR expansion, less than 0.1%, because of low calcium concentration. The involvement of AAS in geopolymerization process formation of bonds in a complicated polymeric sequence of Si-O-Al-O is as functional as the concentration of the alkaline activator effect. According to a previous study, the proportion of AAS between 0.25 and 3.0 is the most optimum.

2.2. Fly Ash (FA)

2.2.1. Background

During the cooling process, the thermal power plant generates coal-fired products such as fly ash (FA). The dust is collected by the dust collector after the raw coal is burnt at a high temperature in the coal-fired boiler. Commonly, FA calls a pozzolanic material containing silicates and aluminosilicates [Chen et al., 2022]. According to Lee et al. (2002), during a mix of concrete with FA, the volume of the mixture increases because of the lower specific gravity of FA (cement has higher specific gravity). On the other hand, using FA may inhibit the blocks by cement particles and slow down the reaction of cement hydration by FA. Another benefit of using FA is the ball-bearing effect of this material because of its spherical shape.

These days rather than just dumping the wastes such as FA, coal burning is used in the construction field, using for manufacturing cement or replacement of cement during concrete manufacturing. This recycling method may solve environmental problems such as polluting soil and groundwater by FA. Especially FA, which can be an alternative to an alkali activator binder-based geopolymer concrete, are become more popular in the construction industry because of follows feasibility: using FA in the manufacturing of GPC reduces global warming potential; reduces virgin materials usage; remarkable life cycle cost saving; recycled industrial waste; longer service life; low carbon emission; and as final sustainable construction product [Amran et al., 2021].

SiO_2 and Al_2O_3 contained in FA may react as silicon aluminum for polymerization or geopolymerization. The aluminosilicate geopolymer gel and calcium oxide are thought to combine to generate calcium silicate hydrate (CSH). To involve this reaction, FA requires a high dosage of alkaline solution, more than 10M of sodium or potassium hydroxide [Law et al., 2013]. Also, it is predominated by chemical composition and cool down curing method of its source [Bellum et al., 2022].

As stated earlier, the significant elements of silicon, aluminum, and crystalloid graphics composites, such as quartz, mullite, and magnetizes, can be used for reusing and recycling this material [Yaping et al., 2008].

As mentioned earlier, FA sometimes calls as a pozzolan material, which can mitigate concrete expansion. Partial cement replacement with FA reduces the ASR expansion by 30% [Multon et al. 2008; Ostertag et al. 2007]. The limestone, dolomite, cherts, or flints can be formed by non or poorly-crystallized silica or silicon dioxide, which causes the ASR reaction expansion of concrete. FA contains elements with low alkali index [Kupwade-Patil et al., 2013]. The opposite hand, replacing 30% of FA binder with GGBFS may improve the mechanical performance, as compacting by itself of geopolymer concrete [Karthik et al., 2017].

Usually, the properties such as physical, chemical, and mechanical of FA depend on the type of raw material for coal, level of pulverization, ash collection, combustion conditions, and handling and disposal techniques at the plan. Regarding F class FA, this type is after altering the bituminous coal kinds, and burning circumstances gathered from a hopper linked to an electrostatic precipitator [Lee et al., 2002].

2.2.2. Properties of FA

Hardened properties

The interaction between CaO and SO_3 content in FA affects the mechanical characteristics of geopolymers, which is mainly connected to ettringite production. The optimal CaO and SO_3 values in fly ash-based geopolymers at standard temperature (20°C) are 11% and 4%, respectively. The 28-day flexural and compressive strength may be increased by 17.91% and 15.56%, respectively, when compared to materials with low CaO and SO3 concentrations (FlyAsh has a CaO content of 9% and a SO_3 content of 3.0%) [Chen et al., (2021)].

Durability properties

The study of Chen et al. (2021) aimed of this study was to see how calcium and sulfur levels affected FA-based geopolymer concrete.. The chemical composition of FA is based on 2.32% of calcium and 0.18% of sulfur. The use of CaO and SO_3 on fly ash-based geopolymers' mechanical characteristics and dimensional stability is constrained due to the unclear mechanism behind this effect. On the flexural strength, compressive strength, water immersion expansion rate, and drying shrinkage rate of fly ash-based geopolymer, the effects of CaO and SO_3 content were

investigated. To modify the behavior of calcium and sulfur, during the mix of concrete reagents as $CaSO_4$ and $Ca(OH)_2$ were added. For FA-based geopolymer concrete, hardened characteristics by compressive and flexural strength, as well as durability performance by expansion test and shrinkage examination, were investigated. Geopolymers' water immersion expansion rate increases gradually as CaO and SO_3 concentration rises, whereas SO_3 content substantially affects fly ash-based geopolymers' expansion rate. The drying shrinkage of geopolymer may be efficiently decreased by adding more CaO and SO_3, and the drying shrinkage is lowest at 11% CaO and 4% SO_3 when compared to unmodified fly ash-based geopolymer, which is 60.65% lower.

2.3. Ground Granulated Blast Furnace slag (GGBFS)

2.3.1. Background

One of the most useful waste by-products of the steel and iron-making process - is the industry by-product Ground Granulated Blast Furnace slag (GGBFS). GGBFS type of furnace that melts under at 1500^0C. As a raw material for this furnace, use limestone, iron ore combinations [Ahmad et al., 2022]. According to the making process of GGBFS, it usually contains molten calcium of silicate and aluminosilicate, which occurs from blast furnaces. These elements help GGBFS to be an excellent binder and a replacement material for cement. In the construction field, GGBFS perceives as a cementitious material. The reason for using GGBFS as a binder material and replacement for cement is that this material improves the strength of concrete, increases the boundary of aggregates to each other, increases the ITZ, and can show lower penetrability. All the pozzolanic characteristics regarding ASTM can be found in GGBFS.

Physical properties of GGBFS related to the cool-down process of molted steel. According to many research works, ordinary specific gravity of this material between 2.5 and 3, where absorption capacity is about 1.2%, significantly affects concrete workability compared to cement [Ahmad et al., 2022].

The chemical makeup of the slag is required for it to have a hydraulic impact. Usually, from 100% consistency, Calcite, Silicate, and Aluminosilicate minerals consist of 36.56%, 39.41%, and 11.63%, respectively. Based on their chemical makeup, the basicity index of slags can be used to categorize them. Calcium must be added to siliceous oxide in quantity greater than one for it to be effective. In the presence of alkaline activators, slag's hydraulic activity rises with basicity; hence, the more basic the slag, the higher its hydraulic activity. To compensate for the shortage of calcium oxide, increase the quantity of alumina used in the production of magnesia oxide while retaining

basicity, increase the concentration of alumina trioxide, and improve the strength [Ahmad et al., 2022]. Calcium silicate hydrate is the result of the hydration process of GGBFS when it react with liquid.

2.3.2. Properties of GGBFS

Fresh properties

As mentioned earlier, using GGBFS instead of ordinary cement improve the workability of concrete, which make concrete self-compact concrete. Ganesh et al., 2019, shows that 40% of GGBFS in the binder portion is the most optimum consistency. The more higher percentage can negatively reacts to concrete performance. The workability of concrete is one of the essential aspects of the construction field. Generally, GGBFS has a smooth and dense surface, thus making concrete more flowable than Portland cement-based concrete. Duos and Eggers, 1999 proved that concrete with GGBFS shows more extraordinary slump test results by 20-50%, compared to cement based concrete.

Hadi et al. (2017) research on geopolymer concrete based on GGBFS and constructed with the Taguchi technique was undertaken, as well as fresh performance, setting time, and workability. For variables, the ratio of Binder (0.35, 0.45, and 0.55), the ratio of alkaline activators (1.5, 2, 2.5), and the Molarity of NaOH (10, 12, 14) with different proportions of binder (400, 450, 500) were used to find optimum mix proportion by Taguchi. The geopolymer paste's initial and ultimate setting times are lengthened when the GGBFS is replaced with FA, MetaKaolin, and SilicaFume. The slump of freshly cast concrete is also lengthened. Combining GGBFS and FA could extend the setting time of geopolymer concrete when ambient curing is being used, as this mix had a longer setting time than GGBFS and MK, and SF combined.

The setting periods were not considerably impacted by the GGBFS replacement levels, according to Duos and Eggers (1999), if the temperature was 23^0C, the room temperature. Slag might expect a significant delay in setting time compared to control concrete at temperatures lower than 23^0C, which has substantial implications for winter concrete (Malhotra, 2008).

Hardened properties

Shahmansouri et al., 2021, this study shows geopolymer concrete performance by using the response surface method. The response surface method (RSM) was utilized to optimize the compressive, flexural, and tensile strengths of the pozzolanic GGBFS-based GPC. There as values were used, NaOH, silica fume, and natural zeolite. Overall, the results demonstrated that the

compressive strength dropped as the concentration of NaOH increased. In contrast, the greatest flexural and tensile strengths were attained at a concentration of 6 M instead of 4 and 8 M. Furthermore, a 10% substitution of sodium silicate raised the compressive, flexural, and tensile strengths of GGBFS-based GPC by around 4%, 6%, and 20%, respectively. At a 30% replacement rate, substituting GGBFS with SF might boost GPC's compressive, flexural, and tensile strengths by 30%, 20%, and 25%, respectively.

The results of Hadi et al. (2017) show that geopolymer concrete with the highest 7-day compressive strength (60.4 MPa) under ambient curing conditions had a binder content of 450 kg/m3, an AAS/Bi ratio of 0.35, an SS/SH ratio of 2.5, and an sodium hydroxide concentration of 14 M. The compressive strength of geopolymer concrete is decreased by using FA, MK, and SF as partial replacements for GGBFS.

Durability properties

As stated earlier, Alkali silica is a chemical reaction that forms a hydrophilic gel. A chemical reaction occurs between alkaline pore fluids and the silicious aggregate particles of concrete. The kind and quantity of reactive silica, as well as the concentration of alkali hydroxide in the concrete pore solution, all affect how much gel forms. Moisture has a strong affinity for ASR reaction products. It expands in volume as it takes in moisture, creating strong forces to rip the concrete's structure apart. Cracks develop as the pressure exceeds the concrete's tensile strength, allowing more water penetration through migration and gel swelling. The idealized Equations (10) and (11) below can be used to determine how the reaction is progressing [Hansen, 1944]:

$$4SiO_2+2NaOH = Na_2SiO_4O_9+H_2O \quad (10)$$

$$SiO_2+2NaOH = Na_2Si_3O_9+H_2O \quad (11)$$

GGBFS limits and controls the expansion of the ASR of concrete. GGBFS can quench alkalis, bind alkali hydrates with slag, and also affect the behavior and speed of water and alkali ions on the structure of the hydrate. [Maeda, 2015; Siddique and Khan, 2011].

A drying shrinkage test is one of the types for testing concrete for durability. Shrinkage occurs due to water evaporation internally, which also means independent deformation by stress. Wei et al. (2011) investigated autogenous shrinkage development for cement paste and concrete hydration under sealed circumstances at room temperature as a function of time. They employed GGBFS content as a proportion of the total cementitious material at 0%, 30%, and 50% by mass with

various water-cementitious material ratios (0.35, 0.40, and 0.45). Their findings demonstrated that GGBFS initially decreased shrinkage due to its filler-like behavior, boosting the good water-cementitious material ratios. Shrinkage was accelerated over time. They concluded that the leading cause of the increase in shrinkage was a decrease in pore humidity brought on by pozzolanic processes.

2.4. Basic oxygen furnace slag (BOFS)

2.4.1. Background

Basic oxygen furnace slag is a waste product from the steel-making process. BOF (Basic Oxygen Furnace) manufactures crude steel or molten iron from pig iron and blast furnace, respectively. There are several steel-making methods, but 71% of the world uses the BOF process to produce steel. All the components, including liquid metals and fluxing agents like dolomite or limestone, are loaded into a furnace to create steel. The next step is injecting oxygen into the mixture while taking off all the contamination (Carbon monoxide, slags et al.) [Brand and Fanijo, 2020]. Also, dolomitic lime adds to the mix to keep the ovenproof properties of the material [Martins et al., 2021], which forms slags. Usually, after removing the slag from a furnace, it should be cooled by natural air, quenching, spraying water to slags, or chilling in a shallow box. All central performances of BOFS, such as physical, mineralogical, or chemical, rely on the cooling method and could differ [Piemonti et al., 2021]. Each cooling effect is different on slags, but the most suitable cooling method, if the material is planned to reuse is recycling steel wastes for construction applications, is naturally atmospheric cooling. This is because natural air cooling improves slag material's hardened properties and density [Naidu et al., 2020].

Steel and iron waste products have possibilities for recycling in the construction of roads, bridges, or various building areas and also to stabilize the soil. Based on other research work in the last few decades, the construction field is more focused on using steel wastes. BOFS wisely used as a coarse aggregate for asphalt concrete. In building construction research, BOFS was used as a cementitious binder materials and coarse and fine aggregate replacement [Piemonti et al., 2021]. The usage of slag in the construction industry is about replacing natural sand, gravel, or crushed stones with slags. The main benefit of it is that this replacement can reduce natural resource extraction [Carvalho et al., 2017].

BOFS used in Carvalho et al., the study was collected from Companhia Siderurgica Nacional (CSN). It shows the existence of particles with rough surface roughness, a somewhat rounded shape, and irregular morphology visible through the micrographs and is caused by the crystalline

material's limited friability. These morphological characteristic scans enhance the cement paste's workability and promote interaction with the concrete aggregates, improving the mechanical characteristics of concrete and increasing the mass's fluidity.

2.4.2. Properties of BOFS

Fresh properties

Kabay et al. (2021) characterized the behavior and optimized the BOFS and GGBFS-based concrete mix. Mix proportion designed from BOFS (0, 20, 40, 50, 60, 70%), GGBFS (100, 80, 60, 50, 40, 30%), and NaOH (6, 8, 10, 12 M) by using Response Surface Methodology. A fresh performance of the workability and initial and setting time were conducted. While the setting time increased dramatically for the mixes having more than 40% of BOFS, the setting time for the mixes with 20% of BOFS was only slightly higher than that of the reference mixes (8, 10, and 12 M of NaOH).

In another study [Omur et al., (2022)], BOFS were used under two conditions: unweathered, which means slag came right after steel manufacturing, and weathered, which is air-cooled for five years or more. The comparison of two types of BOFS-based mortar gave different workability. The mix design includes 0, 50, and 100% BOFS substitution of natural sand. The flow values for the mortars having 50% and 100% of unweathered BOFS were 119% and 99%, respectively, while these values were 87% and 38% for the replacement weathered BOFS. The integration of weathered BOFS produced a lesser flow than unweathered BOFS, which can also be attributed to weathered BOFS's higher water absorption rate and more porous and uneven surface structure.

Hardened properties

XRD and Thermogravimetric analyses confirmed the development of reaction products due to hydration processes. At 28 days and 90 days for 6, 8, and 10 M, the compressive strength of the mixes containing 20% and 40% of the BOFS reached comparable values. However, additional BOFS inclusion considerably decreased the compressive strength. Also, it was noted that BOFS did not fully engage in the reactions; traces of $Ca(OH)_2$ were found, which limits its ability to contribute to the strength of the reaction at higher BOFS ratios.

In Kuo et al. (2019) study, BOFS was used to make eco-friendly porous concrete material. GGBFS were added as a binder bonding material. The size of BOFS aggregate, which is used in

this research, is coarse 4.75–9.5 (#4 - 3/8in) mm and 9.5–19.00 mm (3/8in – 3/4in). According to hardened performance, the compressive strength at 28 days shows that the smaller aggregate mixture has a higher strength. The reason is that increasing porosity with coarser aggregate decreases the strength, because it makes pores, and concrete get weaker.

Depends on Mastali et al. (2019) research used carbonated BOFS as a replacement for natural aggregate in alkali-activated concrete and additionally reinforced it with various types of fiber. The conclusion of this study shows that using carbonated BOFS aggregate hardened and durability properties were higher than regular concrete, about 55 MPa, which is higher than standard strength. On the other hand, the increasing ratio of aggregates to a binder, from 3 to 5, decreases the performance of concrete specimens. This is because morphology analysis shows that BOFS, which has a high percentage of free lime (CaO), provides a tight matrix between solid materials.

The study of Lee et al., 2020, the use of cutting-edge geopolymer technology to stabilize the basic oxygen furnace slag has been investigated; the slag expansion problem can be avoided because the geopolymer matrix contains a large amount of free silicon, which can combine with free CaO and free MgO to produce stable silicate compounds. Pilot-scale research and ready-mixed plant findings revealed that the fine BOFS-based geopolymer mortar had improved compressive strength after 28 days, reaching 30-40 MPa. Furthermore, after ASTM C151 autoclave testing, the expansion may be kept to less than 0.5%.

Slag cement mortars made with BOF-A perform similarly to sand and cement. The investigation of Ding et al. (2017) related to the treatment of BOFS with scrubbing attrition and chelating reagent method. This method is for removing the expansion problems from BOFS-based concrete. After treatment of BOFS, the samples were cured under autoclaved conditions. The results showed that the free lime and other minerals in BOFS removed by chelated oxalic acid reduced mortar expansion and improved the hardened properties, such as compressive and flexural strength. This is because the calcium oxalate monohydrate that developed on the surface of the slag following the oxalic acid chelating treatment can substitute the water that generally fills the micropores of cement mortar, increasing its densification and strength.

According to the RSM, the ideal mix ratio was 25.5% BOFS and 6 M NaOH, which predicted a compressive strength of 36.83 MPa after 28 days. Using the best mix design, the produced mix proportion was experimentally studied and shown to have a calm and dependable

compressive strength of 36.87 MPa. Considering the ideal mix design discovered by RSM, between 20% and 40% of BOFS can be applied effectively without significantly lowering compressive strength. As a result, this strategy may be an alternative to currently used BOFS utilization techniques, which may reduce related environmental issues [Kabay et al., (2021)].

Durability properties

Ozkan et al.'s (2011) study conducted the ASR expansion for 14 days, where clinker and gypsum were cementitious materials and BFS and BOFS aggregates. The expansion values show 0.2%, which means reactive aggregate by ASTM C 1260. The high volume of CaO and MgO in BOFS causes this expansion. The formation of ettringite occurs through expansion and then the crack of materials. According to XRD examination, the sample is mainly distinguished by Al minerals and Fe, FeO, and Mg minerals. Even if the separated BOFS is used, XRD research revealed that the mineralogy still contains a sizable amount of Fe minerals. The volume of ASR expansion is increased by the mineralogy's high Al and MgO minerals concentrations. This allegation is strongly supported by the SEM image demonstrating cracks in the C-S-H gel.

According to Omur et al. (2022) study of the ARS expansion results, replacing unweathered BOFS with natural sand dramatically enhanced volume expansion and caused mortar specimens to shatter and disintegrate. Weathered BOFS, on the other hand, consistently reduced volume expansion and improved the structural integrity of mortar samples. The mortar mixture of Weathered BOFS 50 % the lower limit of expansion (0.01%), whereas Weathered BOFS 100 % the higher limit of expansion (0.02%) by further reducing the volume expansion of the mortars.

The volume stability test in lime-saturated water revealed that after 14 days, the mortar specimen containing 100% unweathered BOFS had substantial swelling behavior and exceeded the expansion limit of 0.02%. Contrarily, the unweathered BOFS 50%, Weathered BOFS 50%, Weathered BOFS 100%, and Control 100 % mixtures had good stability in water and met the limit.

According to the results of physical and mineralogy tests done on aggregates, storing BOFS aggregates outside led to carbonation and a considerable decrease in the particle density of aggregates. The SEM examination also revealed that the aging of BOFS aggregates resulted in a more porous surface roughness, which accounts for increased water absorption.

2.5. RSM

Response surface methodology (RSM) is an effective statistical method for designing experiments, developing models, evaluating the influence of various elements, and finding the best

conditions. RSM fits a quadratic function to several factors that change at the same time. Compared to the time-consuming and inefficient element-by-element method, which also ignores component interactions, RSM has several advantages for optimization. In RSM, the materials of the components are distributed in such a way as to create an optimal mixture for mathematically predicting the required qualities. [Awolusi et al., 2018].

RSM is a statistical technique that employs regression analysis for the collective data. Tools such as STATISTICA, Design Expert, Minitab, etc., help design experiments and analyze the data. The whole flow of the RSM study starts from the design of the experiment (DOE), including variable selection, DOE spreadsheet, and experiment. After the Analysis of Data, the mathematical model, validity of the data, and find relationship. The final step is the optimization of a design. The main objectives of RSM are shown in Figure 3 [Sarabia et al., 2009].

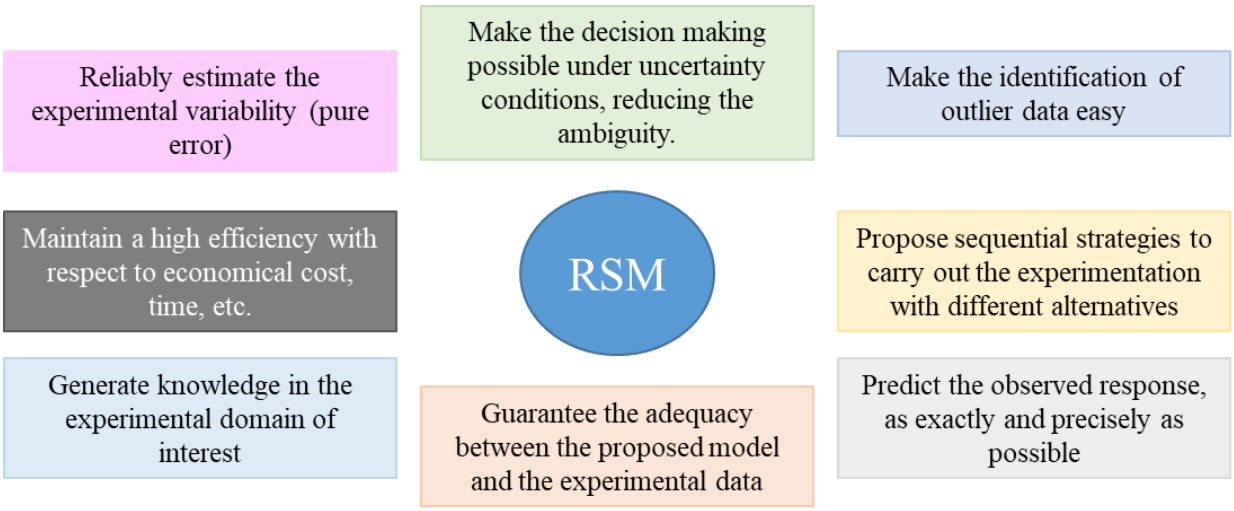

Figure 2.3. The objective of RSM

RSM provides statistically proven prediction models that may be changed to discover the optimum process configurations. RSM is often useful when multiple variables affect one or more characteristics or responses. Moreover, it can refine the response or response to fit a specific set of requirements. In addition, RSM offers an adequate experimental interpretation of the nonlinear response surfaces of experimental results.

Chandra Prakash et al. (2022) investigated the influence of recycled construction waste (RCA) and Bone China fine (BCA) aggregate-based normal strength eco-friendly concrete. Through the mathematical analysis and analysis of variance test (ANOVA) with the fresh

properties and hardened performance used to create the RSM. As variables content of aggregates was considered. For hardened performance, all mixtures show 95% satisfied results. For workability, it shows that this concrete requires more water since the slump test results decrease with increasing aggregate content.

Dinh et al . 2020 study used RSM for GGBFS and FA-based geopolymer concrete. The main variables were sodium hydroxide proportion, sodium silicate proportion, and the ratio of GGBFS, how their interactions affect the desired 28-days compressive strength responses, and the price per ton of binder. According to the study, compared to sodium hydroxide and GGBFS, sodium silicate has a negligible impact on the strength of mortar. Using the multi-objective optimization approach, the optimum mixture proportions were evaluated. With the objectives of achieving the highest compressive strength, the tremendous volume of fly ash, and an affordable price per ton of binder, the ideal values were found to be percentage of sodium hydroxide=5.18%, percent of sodium silicate=1.16, and GGBFS=50%. According to the experimental findings, the samples' compressive strength varied between 62.95 and 63.54 MPa and agreed with the optimization results.

Chapter 3 . Experimental program

3.1. Materials

3.1.1. Characterization of binders

ASTM Class F fly ash (FFA) and ground granulated blast furnace slag (GGBFS) (Fig.1), were binding materials to make GPM. A fixed binder containing 60% FA and 40% GGBFS was employed in a prior study to increase the workability and adhesive strength of the binder. The specific gravity (SG) of F-FA and GGBFS is conducted using the standard method for density of hydraulic cement ASTM C188 – 17, and results showed about 1.91 and 2.92, respectively.

(a) **(b)**

Figure 3.1. F-Fly Ash (a) and GGBFS (b)

3.1.2. Characterization of aggregates

The RS and BOFS aggregate gradation was fixed with the specification suggested by the ASTM C 1260 Standard Test Method for Potential Alkali Reactivity of Aggregates (Mortar-Bar Method). The chemical composition and gradation of aggregate are also shown in Table 1.

Table 3.1. Gradation of fine aggregate by ASTM C 1260

Aggregate Gradation										
	Passing	Retained	Passing	Retained	Passing	Retained	Passing	Retained	Passing	Retained
Sieve size	4.75 mm	2.36 mm	2.36 mm	1.18 mm	1.18 mm	600 µm	600 µm	300 µm	300 µm	150 µm
Mass (%)	10		25		25		25		15	

To examine the effect of BOFS aggregate content on properties of GPM mixture, various combinations of RS and BOFS aggregate (100% RS, 75% RS+25% BOFS, 50% RS+50% BOFS, 25% RS+75% BOFS, and 100% BOFS) were used. The Table 3 shows the physical properties of aggregates, and these tests were conducted depending on ASTM C 1260, where aggregates were sieved into five groups of gradation, (Fig.2), as shown in Table 2. ASTM C128 was used to determine the physical properties of aggregate, which is mentioned above, and gravimetric

(pycnometer) procedures were used. W_{SSD} = saturated surface–dry specimen mass in g, W_{OD} = oven-dry specimen mass in the air in g, $W_{pyc+water}$ = water-filled pycnometer mass in g, and $W_{pyc+water+SSD}$ = water and specimen-filled pycnometer mass in g. Regard to standard Eq. (12) and (13) was used to calculate the properties.

$$AC\ (\%) = 100 * \frac{W_{SSD} - W_{OD}}{W_{OD}} \quad (12)$$

$$G_{SSD} = \frac{W_{SSD}}{W_{pyc+water} + W_{SSD} - W_{pyc+water+SSD}} \quad (13)$$

Whereas the SG of RS and BOFS aggregate were 2.77 and 3.16, (Fig.3) and from the data, it was also possible to obtain the absorption capacity (AC) of RS and BOFS aggregate, which was 2.67 and 5.12, respectively (Table 3).

Figure 3.2.. Sieve machine

Table 3.2. Gradation of fine aggregate by ASTM C 1260

Aggregate Gradation										
	Passing	Retained	Passing	Retained	Passing	Retained	Passing	Retained	Passing	Retained
Sieve size	4.75 mm	2.36 mm	2.36 mm	1.18 mm	1.18 mm	600 µm	600 µm	300 µm	300 µm	150 µm
			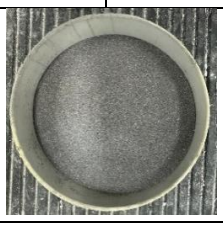							
Fresh BOFS										

River sand

(a) (b) (c)

Figure 3.3. (a) and (b) testing SSD condition and (c) pycnometer

Table 3.3. Fine aggregate specific gravity and absorption capacity

Aggregates	Specific gravity (%)	Absorption capacity (%)
BOFS	3.16	5.12
River sand	2.77	2.67

3.2. Experimental Program

As illustrated in Figure 4, the Characterization of binders (FA and GGBFS) and fine aggregates (Natural River sand and BOFS) will be conducted as the first step in the experimental program. The following properties will be investigated: mineralogy by X-ray diffraction (XRD), chemical composition analysis using X-ray fluorescence (XRF), morphology by scanning electron microscope (SEM), particle size distribution (PSD) by laser particle analyzer, and specific gravity and basic aggregate properties by various American Society for Testing and Materials (ASTM) test methods.

Following the conclusion of the material characterization tests, 15 mixes are produced to investigate the influence of different proportionate combinations of river sand BOFS aggregate,

alkali activator concentration, and CO2 curing on the characteristics of the GPCThe BOFS-based GPC mix design is based on a set binder composition of 60% FA and 40% GGBFS, an alkali-activated solution of 10 Molarities of NaOH and 1, 1.5, and 2 ratios of Na_2SiO_3 to NaOH, and different combinations of river sand and BOFS aggregate. (100% sand, 75% sand+25% BOFS, 50% sand+50% BOFS, 25% sand+75% BOFS, and 100% BOFS). All mixtures with different proportions of the materials are presented in Table 4.

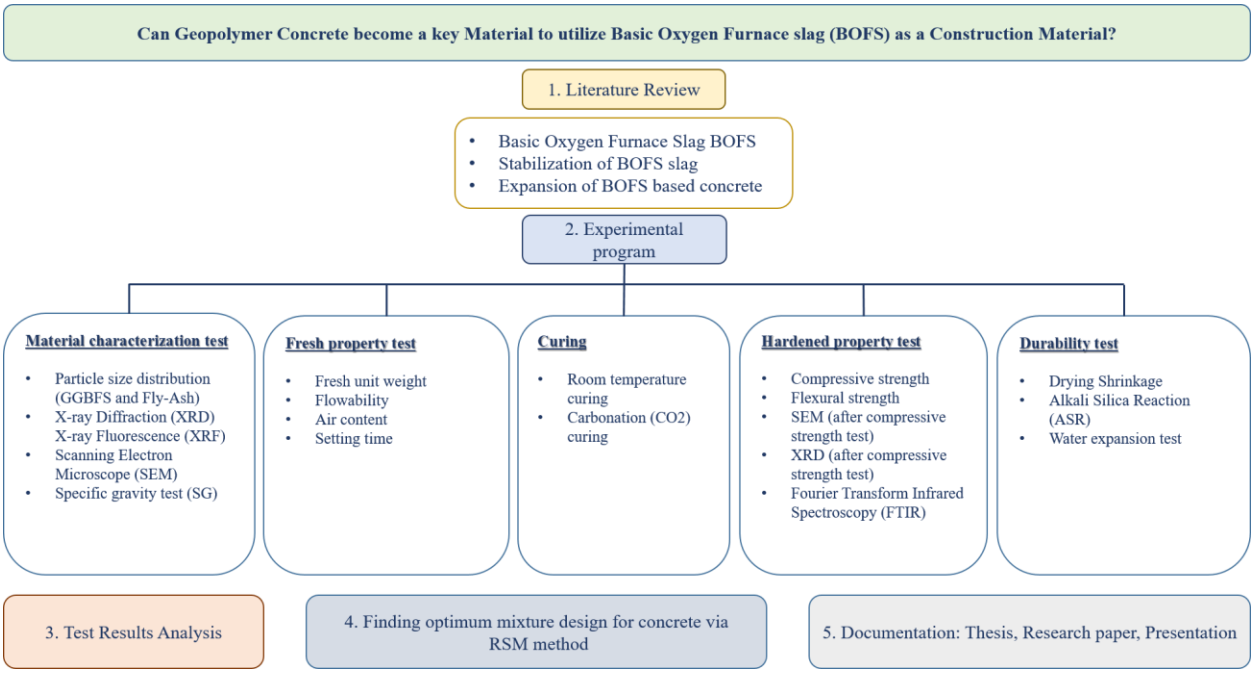

Figure 3.4.. The experimental program of research

Table 3.4. Mixture proportions

Mixture	Fly ash (kg/m^3)	GGBFS (kg/m^3)	BOFS (kg/m^3)	River sand (kg/m^3)	AAS (kg/m^3)	Water (kg/m^3)
1NS+0%BOFS	545.01	363.34	-	605.57	363.34	106.41
1.5NS+0%BOFS	545.01	363.34	-	605.57	363.34	111.58
2NS+0%BOFS	545.01	363.34	-	605.57	363.34	115.03
1NS+25%BOFS	548.72	365.81	152.42	457.26	365.81	110.86
1.5NS+25%BOFS	548.72	365.81	152.42	457.26	365.81	116.06
2NS+25%BOFS	548.72	365.81	152.42	457.26	365.81	119.53
1NS+50%BOFS	552.47	368.31	306.93	306.93	368.31	115.37
1.5NS+50%BOFS	552.47	368.31	306.93	306.93	368.31	120.61
2NS+50%BOFS	552.47	368.31	306.93	306.93	368.31	124.1
1NS+75%BOFS	556.24	370.83	463.53	154.51	370.85	119.94
1.5NS+75%BOFS	556.24	370.83	463.53	154.51	370.85	125.22
2NS+75%BOFS	556.24	370.83	463.53	154.51	370.85	128.74
1NS+100%BOFS	560.13	343.42	622.36	-	373.42	124.58
1.5NS+100%BOFS	560.13	343.42	622.36	-	373.42	129.89
2NS+100%BOFS	560.13	343.42	622.36	-	373.42	133.43

Fresh attributes of GPC, including as setting time, workability, air content, and fresh unit weight, are investigated after GPC samples are cast. GPC toughened characteristics are also tested. These properties include compressive strength (ASTM C109), flexural strength (ASTM D790), expansion based on water and 1 M NaOH solution (ASTM C 1260), drying shrinkage (ASTM C806), and dielectric constant. The compressive strength test was conducted at four different testing periods (3, 7, 28, and 56 days) on four cube samples with the dimension of 50x50x50 mm for each testing date. The flexural strength test is performed during the same testing periods as the compressive strength (3, 7, 28, and 56 days) on four beam samples with the dimension of 40x40x160 mm. Four bar samples with the dimension of 25x25x285 mm were used for water expansion, ASR expansion, and drying shrinkage tests, and test data are recorded periodically. Finally, dielectric constant tests were performed to evaluate the hydration process of GPC using the cube specimen with the dimension of 70x70x70 mm.

3.3. Mixing procedure. Casting method. Curing method of specimen

As stated previously, five combinations of RS and BOFS aggregate were used to examine the impact on the properties of GPM as the BOFS aggregate content increases, and 15 mixtures were prepared to analyze the effect of aggregates. As presented in Table 4, a total of 15 GPM mixtures were produced, and the proportion of each material is represented. The water-to-binder (w/b) ratio of 0.32 was used for all mixtures. The BOFS-based GPM mix design is based on a fixed binder content mixed with 60% FA and 40% GGBFS, and an alkali activator solution to binder ratio (AAS/b) of 40% and 1, 1.5, and 2 ratios of Na_2SiO_3 to NaOH (called 1, 1.5, or 2 AAS content) with 10 Molarities of NaOH.

First, AAS was prepared 24 hours before starting mixing. Binding materials (F-FA and GGBFS) were mixed in the Hobart mixer at a slow speed for 30 seconds. Then, water and AAS were added to the bowl and mixed slowly for 60 seconds. After that, both RS and BOFS aggregate were added and continuously mixed at a slow speed or another 60 seconds. After scraping and collecting materials on the sides of the bowl for 90 seconds, all materials were remixed at medium speed for additional 120 seconds (Fig.5). After mixing, the plastic state GPM mixtures were placed into molds of different sizes for each test requirement shown in Table 5. After 3 hours, each test sample was de-molded and air-cured at room temperature and under carbonation curing condition until the testing day.

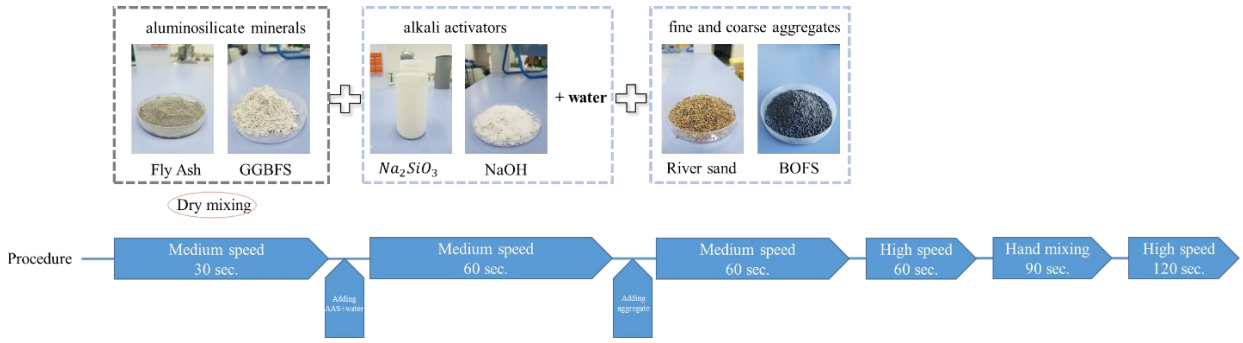

Figure 3.5. Mixing procedure of Geopolymer mortar

The Table indicates all test methods, the number of samples conducted in each test, sample size, and test age. Tests to evaluate the fresh properties of the GPM mixture include workability, air content, and setting time. In contrast, tests to assess the hardened properties of the GPM mixture contain include compressive strength, flexural strength, and an expansion test submersed in water and 1 M NaOH solution, and drying shrinkage. A two-layer filling technique was used throughout the casting process to maintain proper compaction of the mortar mixes in the molds. A steel tapping rod was utilized for drying shrinkage, sulfate attack, and ASR test samples, whereas a rubber tamper was used for compressive strength test samples (as required by ASTM C109 (2000)). Fresh mortar was compacted by tamping and shaking it before superfluous material was screed off the mold surface to make the top surface level with the specimen's surface. After casting, a plastic cover was put over the specimen to stop the mixture's water from evaporating, and it was left to cure for a day at room temperature. Mortar specimens were tagged with the product name and batch code after the samples had been de-molded, and they were then placed for curing under the predetermined circumstances for each test technique. Both compressive and flexural strength tests were performed using four specimens for each mixture at the specified ages (3, 7, 28, and 56 days). Finally, measuring drying shrinkage and expansion data using four samples of 25x25x285 mm were periodically obtained.

Table 3.5. Test methods

Test method	Test specification code	Specimen dimension	No. of the test specimen or trial	Testing age (day)
Workability	ASTM C 1437 / C 230	A high of 50 ± 0.5 mm, inside bottom Ø of 100 ± 0.5 mm, and at the bottom, inside top Ø of 70 ± 0.5 mm.	3	Immediately after mixing
Air content	ASTM C 185	400 ± 1 mL	3	Immediately after mixing
Setting time	ASTM C 191	A high of 40 ± 1 mm, inside bottom Ø of 70 ± 3 mm, and at the bottom, inside top Ø of 60 ± 3 mm.	3	Immediately after mixing
Compressive strength	ASTM C 109	50 x 50 x 50 mm	4	3, 7, 28, 56 days
Flexural strength	ASTM C 348	40 x 40 x 160 mm	4	3, 7, 28, 56 days
Drying shrinkage	ASTM C 157	25 x 25 x 285 mm	4	3- and 4-day intervals (6 months)
Expansion*	ASTM C 1260	25 x 25 x 285 mm	4	3- and 4-day intervals (28 days)
Dielectric constant	-	70x70x70 mm	2	3- and 4-day intervals (6 months)

*Note: The expansion test was conducted using the modified ASTM C 1260 test method: water and 1 M NaOH solution submersion for up to 28 days.

For the first curing condition, geopolymer mortars, after demolding mortars from molds, were cured at ambient curing condition, at 23^0C. The curing period for each sample depends on each test. Tables 5 show the testing ages by day where the hardened performance of samples was 3, 7, 28, and 56 days, which means the curing duration follows the days for the test.

Carbonation (CO_2) curing techniques were employed to describe the behavior of BOFS with fluctuating or poor expansion outcomes. The CO_2 Concrete Carbonation Testing Cabinet was set up with a CO_2 concentration of 20%, a relative humidity (RH) of 65% 5%, and a temperature of 23^0C (Fig.6).

Figure 3.6. Concrete Carbonation Testing Cabinet and CO_2 gas cylinder

3.4. Test methods

3.4.1. Material characterization

Chemical composition of binder

The AxiosmAX X-ray fluorescence spectrometer by PANalytical equipment requires a tablet for conducting the test. To obtain rugged tablets, 20% of binders of a defined weight of binder and binder materials (FA or GGBFS) should be mixed and compressed by machine, as shown in Figure 7. The Figure 7 shows the procedure for making the tablet specimens for XRF.

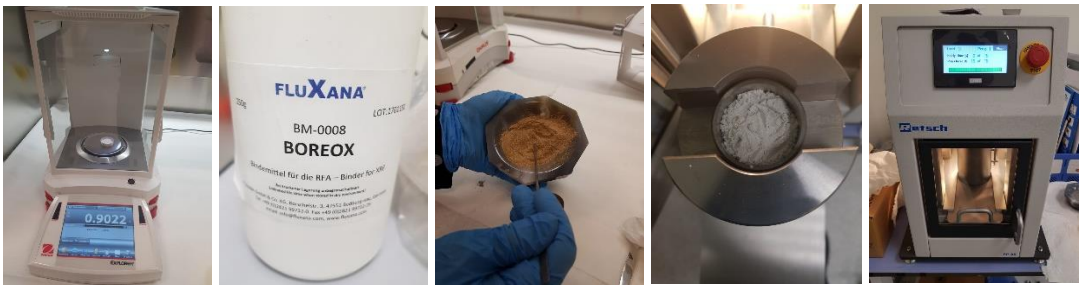

Figure 3.7. The procedure for making the tablet for the XRF test

Particle size analysis of binder

The size of particles is one of the crucial aspects of pozzolanic (siliceous) and calcium-based cementitious materials. According to ASTM C 618, to achieve high strength and durable concrete, it is significant to keep the amount retained less than or equal to 34% on the #325 sieve. A laser scattering analyzer, Mastersizer 3000, was used to determine the mean particle size D_{50} and cumulative percent passing.

Mineralogical analysis of binder

The fly ash and GGBFS were examined by Rigaku Smart Lab X-Ray Diffractometer (Fig.8). The condition for this test was the fine particles of binders which were passed #325 (45µm) sieve, and running degree for a 2theta range from 5 to 70, by duration time 3 counts per second speed.

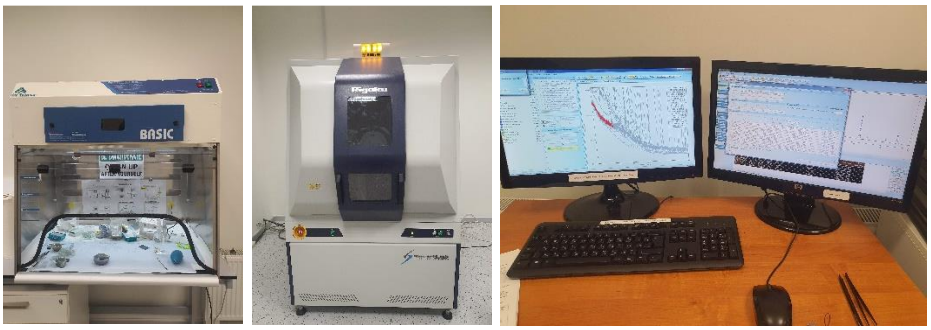

Figure 3.8. The procedure of testing the XRD test

Mineralogy analysis of binder

The morphology and mineralogy of FA were studied using a JEOL JSM-IT200 (LA) scanning electron microscope. For this test, all materials were sieved #325 and placed on the plate (Fig.9).

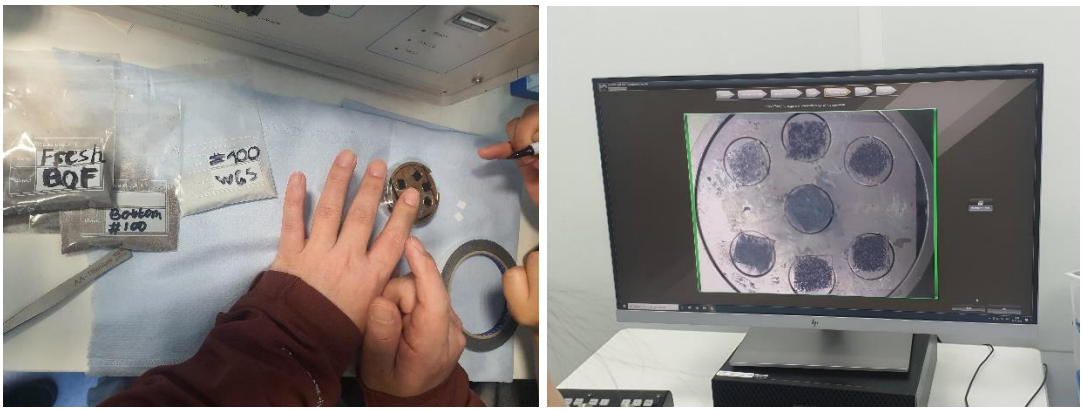

(a) **(b)**

Figure 3.9. Preparing samples for SEM

3.4.2. Fresh properties

Workability

The Figure 10 presents the flow cone set up to measure GPM's relative flowability (Γ_m). Flow cone test measures the deformability related to the diameter of the test specimen after a collapse has been obtained. The relative flow area is calculated using Eq (14). A larger Γ_m indicates higher deformability and more flowable.

$$\Gamma_m = \frac{\left(D_1 \times D_2 - D_0^2\right)}{D_0^2} \qquad \textbf{(14)}$$

Where, D_1 and D_2 are flow diameters measured and D_0 is flow cone diameter (bottom)

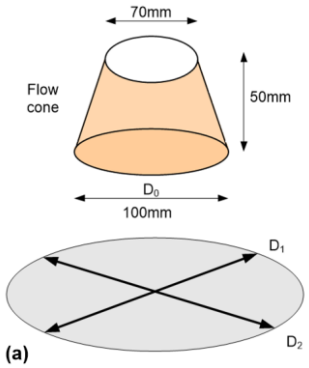

Figure 3.10. Relative flowability (Γ_m) test setup

Air content & Fresh unit weight

To conduct Air content and Fresh unit weight (Fresh density), ASTM C185 was used. According to this standard, the Eq (15) is calculated in volume %.

$$\textbf{Air content, volume } \% = 100 * \left[1 - \left(\frac{W_a}{W_c}\right)\right] \quad \textbf{(15)}$$

The first step of this test is filling the cylindrical cone with geopolymer mortar for two layers and hitting it after tamping them by 20 times to remove all bubbles or air, which can occur due to the mixing process. W_a = (W/400 g/mL) is the actual mass per unit of volume, and W is the mass in grams of the given 400 mL of mortar. Using the values for material quantities and specific gravities, W_c is the theoretical mass per unit of volume, which is computed on an air-free basis as follows.

Setting time

Using the Vicatronic test in accordance with ASTM C191-19 Standard Test Methods for Time of Setting of Hydraulic Cement by Vicatronic, the initial and ultimate setting times of mortar mixtures were determined. The initial setting time was calculated using the measurement data below using Eq (16), and the final setting time was calculated as the amount of time between the first cement-water contact and the needle, leaving a complete circular imprint on the paste's surface. As shown in Figure 11, the Vicatronic was calibrated before the test to have a maximum penetration of 40 mm depending on the height of the conical ring. The device was attached to an ASTM configuration, which automatically records penetration measurements at predetermined intervals of 30 minutes at least 5 mm away from previous penetrations and 10 mm away from the inner side of the mold.

$$\boldsymbol{Initial\ setting} = \frac{(\boldsymbol{H}-\boldsymbol{E})}{(\boldsymbol{C}-\boldsymbol{D})} * (\boldsymbol{C}-\mathbf{25}) + \boldsymbol{E} \qquad \textbf{(16)}$$

E = time in minutes of last penetration<25mm, H = time in minutes of first penetration>25mm, C= penetration reading at time E, D = penetration reading at time H.

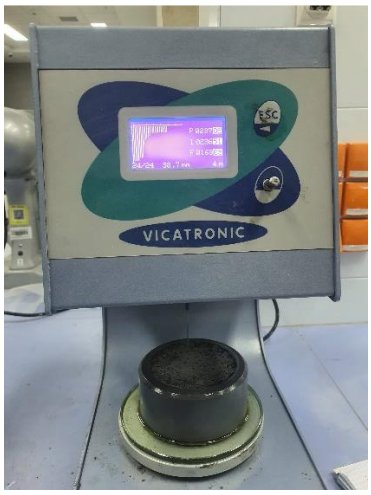

Figure 3.11. Vicatronic setting time apparatus

3.4.3. Hardened properties

Compressive strength

The compressive strength of BOFS-based geopolymer mortar samples was determined using the standard testing procedure described in ASTM C 109. The geopolymer mortar was then cast into 50x50x50 mm cubic molds. After 3 hours of de-molding, the samples were cured at room temperature under plastic wrap until particular testing days. The volume change rate of the cubic specimen was estimated for hardened density prior to compressive strength testing (Fig.12).

The result of compressive strength may effect by mixture proportion, curing method, and testing method. The mixture proportion is dominated by water to cement ratio (w/c), where the strength of concrete is governed by its porosity. The porosity depends on the water/cement ratio and concrete hydration degree. The ITZ porosity and the matrix porosity w/c compressive strength of low- and medium-strength concrete prepared with normal aggregate are equal.

The strength of concrete and porosity directly affect the hydration effect. Another effect comes from the cement type. Portland cement ASTM Type III: Early ages of hydration due to its higher fineness and C3A & C3S a higher strength; at a given w/c, production of a lower porosity

a higher strength. Slower strength growth up to 28 days for ASTM Type IV and Type V cement types, including Portland slag and portland-pozzolan types of cement.

The size of the aggregate, the shape, the texture of the surface, and the mineralogy of aggregate particles impact the ITZ characteristic. Aggregates also influence the compressive strength of concrete. Due to the increase in aggregate concentration producing a more significant number of secondary cracks prior to failure, which requires more energy, i.e., higher stress, to reach fracture, the volumetric proportion of aggregate in the mix at constant water-to-cement ratio results in a relatively small increase in concrete strength. The minimum effect may come from mixing water, air-entraining, water-reducing admixture, retarding, or supplementary cementitious material admixtures.

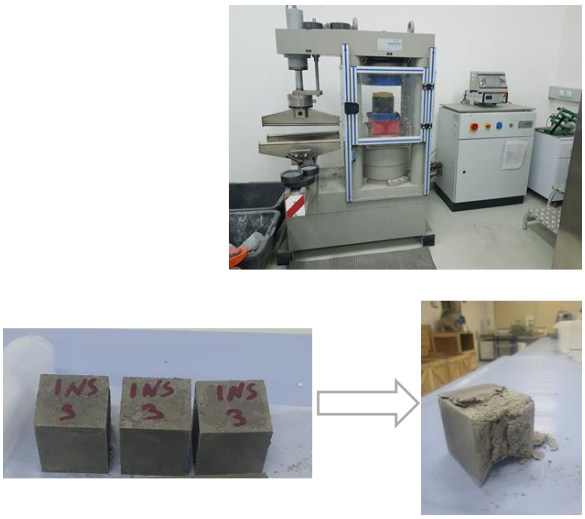

Figure 3.12. Compressive strength device and samples before and after testing

Flexural strength

Flexural strength testing was carried out in the same manner as compressive strength testing. The use of ASTM C 348, with 40x40x160mm Beams-MoR bar samples (Fig.13).

Figure 3.13. Flexural strength device and samples before and after testing

Dielectric constant

k (dielectric constant) value to determine the capacitance of GPM. As shown in Figure 14, the apparatus should be correlated by a silicon cube with a 2.5 k value before testing the samples.

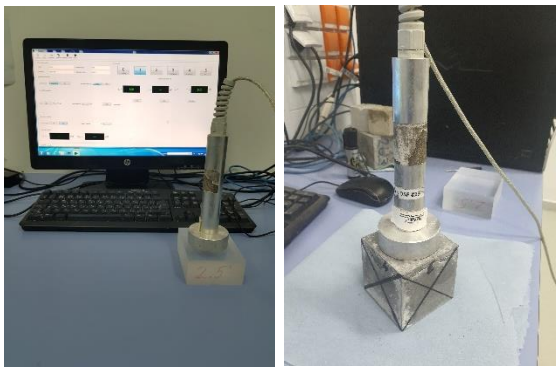

Figure 3.14.. Dielectric constant device and sample for test

3.4.4. Durability properties

Water & ASR expansion

Finally, the volumetric expansion behaviors of different GPM mixtures are presented in Figure 15. Two test conditions are applied to evaluate the expansion potential related to BOFS aggregate: the expansion in water and 1 M NaOH solution at 80 °C for 28 days. The length change and weight loss of mortar bars was monitored for up to 28 days. Despite the fact that the expansion value is based on the ASTM C 1260 criterion, the threshold value (0.1% expansion: potentially

reactive aggregate at 14-day) is sufficient to determine whether the aggregate used in the GPM mixture has the expansion potential due to the formation of $Ca(OH)_2$ or $Mg(OH)_2$ that causes cracks in the GPM matrix.

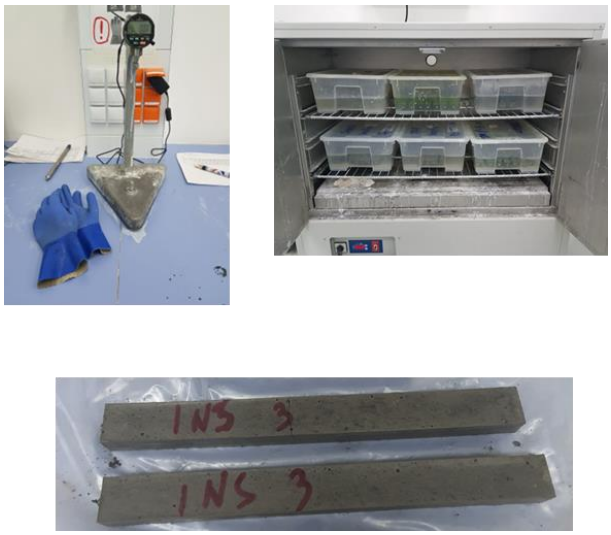

Figure 3.15. Device for expansion test and champer to keep samples in the container

Drying shrinkage

The Figure 16 presents the shrinkage behavior of the GPM mixture. During the polymerization process, binders, AAS, and water react to form geopolymerization products. This reaction causes chemical shrinkage in the GPM matrix. Also, the volume changes due to autogenous shrinkage (self-desiccation) and the volume change through capillary pores (drying shrinkage) dominate the overall shrinkage behavior of GPM.

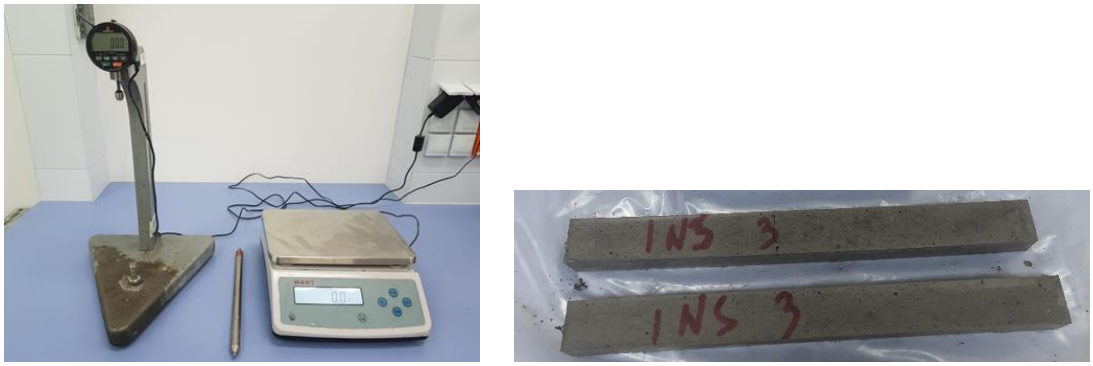

Figure 3.16. Device for conducting shrinkage and weight change of sample

3.5. Test Result Analysis and Finding Optimum Mix Design Using RSM Method

The most important part of the project is the analysis of all obtained test results. As stated earlier, then the quality of these materials is evaluated; the most relevant characteristics of the material for use in construction applications such as aggregate and binder materials are gradation, particle size distribution, adsorption/specific surface area, chemical composition, mineralogy, unburned carbon content, and morphology. These properties will be identified by different techniques mentioned in the previous section. For example, the chemical composition, PSD, and mineralogy of binders (FA and GGBFS) used in this study are interconnected with each other. The binder's crystalline and amorphous phases and PSD influence the early-age reactivity and later-age mechanical properties and durability of GPC. As a consequence, the findings of the fundamental material characterization tests will be utilized to interpret and anticipate the performance of GPC in terms of fresh and hardened qualities, as well as durability.

The primary goal of this research is to create a BOFS-based GPC with high mechanical qualities and durability while avoiding expansion issues. To achieve this purpose, the fresh and hardened characteristics, as well as the durability of BOFS-based GPC, will be investigated. River sand to BOFS aggregate combination ratio and AAS concentration will be variables to influence these properties. These parameters will be used to determine the optimum mixture proportion of GPC via response surface methodology (RSM) by using statistical software (Minitab). For the best-optimized mixture, CO_2 curing with three different concentrations will be applied, and this mixture's hardened properties and durability will be evaluated.

Chapter 4 . Test results and Discussion

4.1. Material characterization

4.1.1. Chemical composition of binders

According to ASTM, F class FA means composition with a lower calcium (Ca) percentage and the highest silicate (Si) percentage. The chemical composition of FA and GGBFS presented in Table 1 shows that FA mostly contains aluminosilicate glasses such as SiO_2 (65.34%) and Al_2O_3 (24.85%). To stabilize the geopolymer concrete with F-FA, the content of SO_3 is important. According to Law et al., 2015, the percentage of sulfur trioxide should be less than 1%, and the XRF chemical composition test results show only 0.31% of SO_3. This means that a desirable GPM with good durability is guaranteed with this F-FA. According to previous studies F clas FA conten CaO less than 10%, and in this study FA has only 1.86& of it mineral.

The chemical composition of GGBFS commonly depends on the material used during the steel-making process because GGBFS is a by-product of the steel-making process—also, the cooling process of molten material affects the material's physical properties. The Table 1 shows that GGBFS is hydraulic material and its response to the hardened performance of concrete/mortar. Apart from F-FA, GGBFS is glassy and also crystalline-phased materials. The tabulated chemical composition of GGBFS shows that combine of SiO_2 and Al_2O_3 is about 48.27%. One of the highest content elements is CaO (33.06%), after silicon dioxide, due to the use of limestone in the production of slag to remove impurities by reducing iron ore.

The hydration products, such as the calcium silicate hydrate (C-S-H) and calcium aluminum silicate hydrate (C-A-S-H) crystals, are created when $Ca(OH)_2$ react with enough SiO_2 and Al_2O_3 from BOFS and GGBFS (Tsai et al., 2014).

Table 4.1. Chemical composition of binders (F-FA and GGBFS)

Chemical Composition (W_t %)											
	Na_2O	MgO	Al_2O_3	SiO_2	SO_3	K_2O	CaO	TiO_2	MnO	Fe_2O_3	ZnO
FA	1.03	0.53	24.85	65.34	0.31	0.68	1.86	1.10	0.07	4.01	0.04
GGBFS	1.08	12.07	12.43	35.84	2.67	0.69	33.06	1.34	0.37	0.34	-

4.1.2. Particle size distribution (PSD)

The Particle Size Distribution (PSD) of materials is specified in Figure 1; it is significant to note that the mean particle sizes of GGBFS for 100% passed sieve #325. On the other hand,

only 47% of F-FA passed 45µm. This is because, according to ASTM C 618, FA, which is used for this study, is low-quality F class FA. Since the cumulative percent passed, the PSD of this material conforms to the ASTM C 618 limitation for pozzolanic material. The mean particle sizes (D50) of F-FA and GGBFS are 55.73 µm and 2.60 µm, respectively.

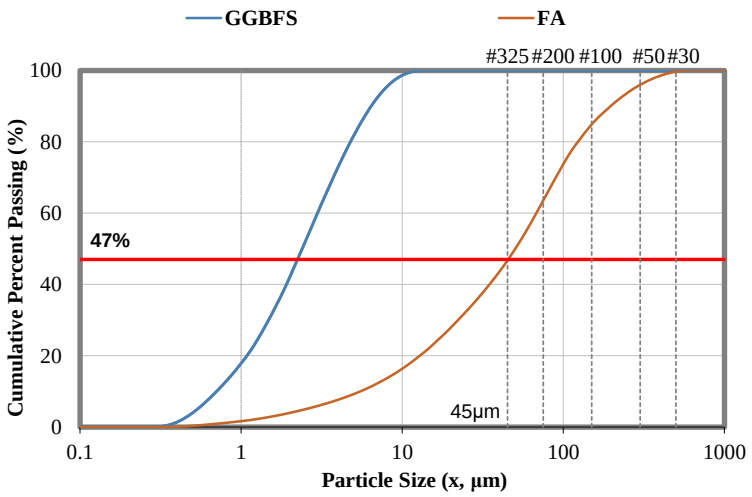

Figure 4.1. Particle size Distribution test result

4.1.3. Mineralogical analysis of binders

The Figure 2 below displays the chemical formula for each symbol for minerals. Apostolidou et al., 2018, FA is composed primarily of crystalline minerals, unburned lignite, and alumino-silicate amorphous. A study presented in other papers, Fly Ash in this study shows similar XRD patterns, such as crystalline phased mullite ($3Al_2O_3 \cdot 2SiO_2$) and sillimanite (Al_2SiO_5) at 28^0, 42^0, and 60^0 points, where various metallic oxides show a peak at 20^0. At 20^0, titanium oxide (TiO_2) shows a peak. Regardless of F-FA, GGBFS shows a high concentration of $CaCO_3$ (Calcite) and Ni_3C (Nickel Carbide) at 30^0 and 50^0 2theta, which effect on hardened properties of the material, which is the mineral gypsum, except for gypsum minerals, titanium hydride (TiH_2) and sulfide mineral stibnite (Sb_2S_3) at 25^0, 35^0 and 42^0 shows peaks in GGBFS.

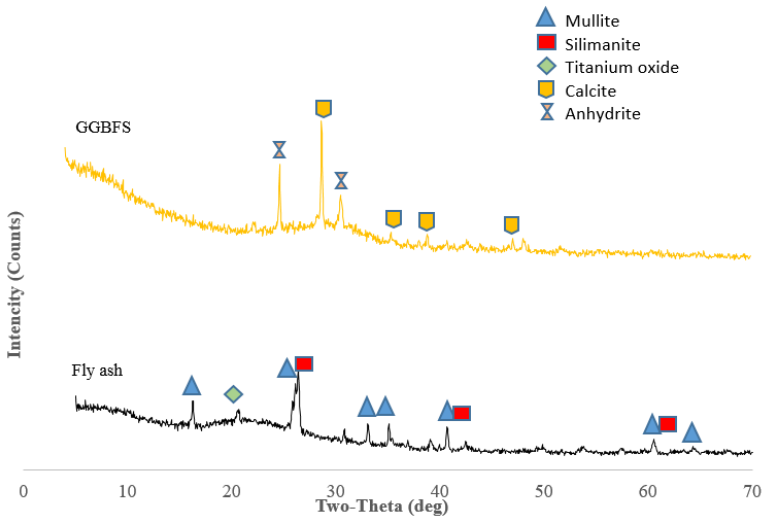

Figure 4.2. Morphology structure of binder materials

4.1.4. Mineralogy analysis of binders

F class FA, which is used in this study, has value as a pozzolanic material because it is a by-product of burning coal. The Figure 3 shows the spherical particles of FA by SEM test with hollow cenospheres. The cracks on the surface of balls may be related to a drop in the elasticity of the relative dynamics of the material [Amran et al., 2021]. According to Styszko-Grochowiak et al., FA balls contain calcium (Ca) and aluminosilicate (Al_2SiO_5) minerals. SEM results show high Si, Al, and C content by mass, 24.67%, 9.52%, and 7.08%, respectively, except Au (10.71%), which is the plate where the samples were fixed (Fig.4).

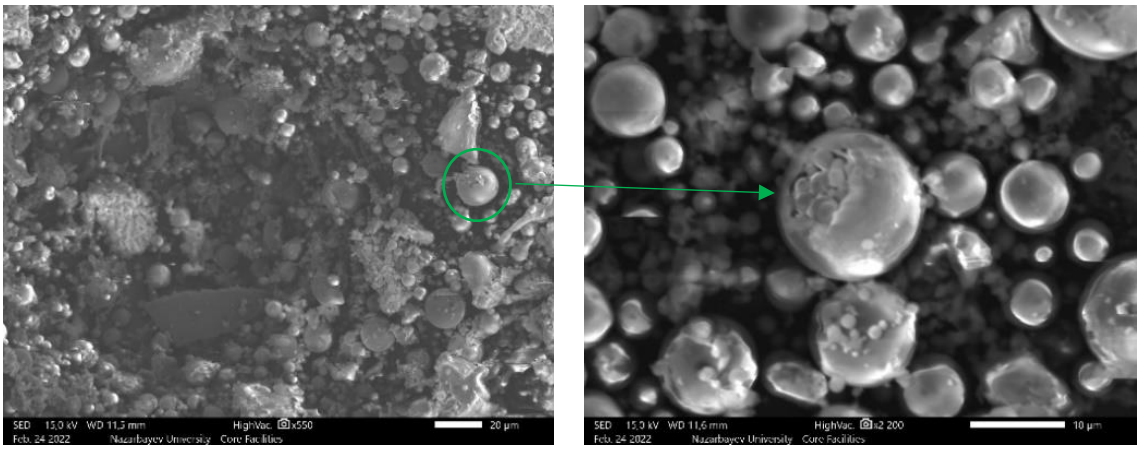

Figure 4.3. Scanning Electron microscope result of FA

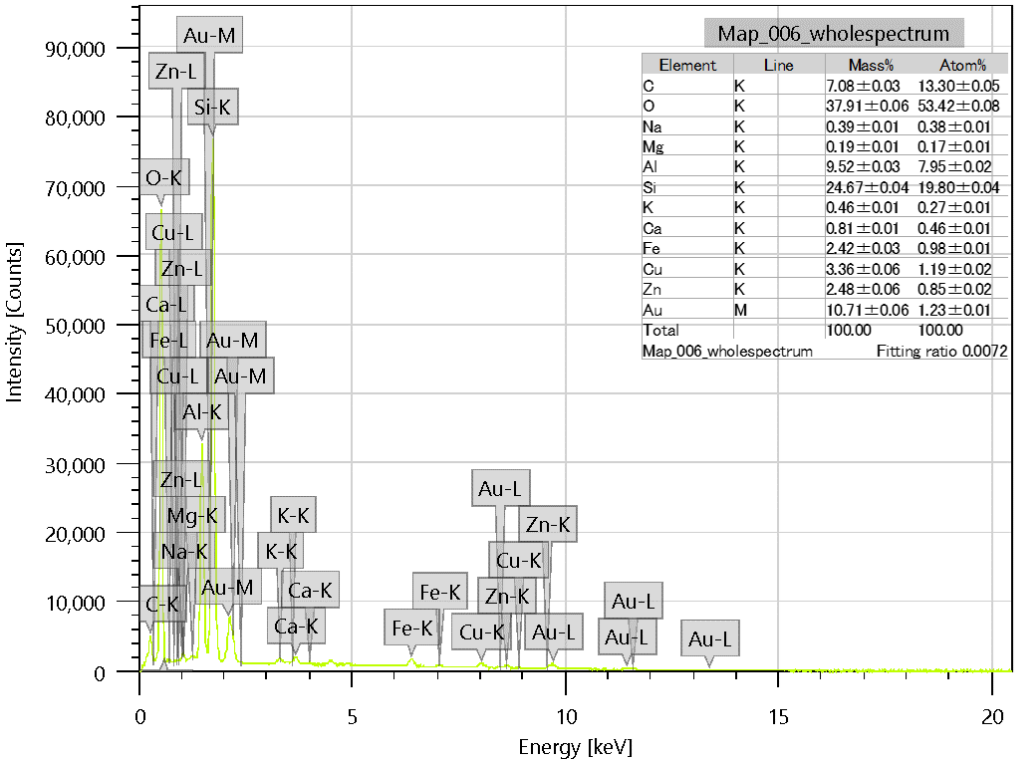

Figure 4.4. EDS result of SEM of FA

4.1.5. Chemical composition of aggregates

The particle sizes of aggregates for conducting chemical properties were under 45μm and shown in Table 2. Free lime concentration (f-CaO) in BOFS, as previously mentioned, restricts the usage of BOFS in building applications, mainly when BOFS is employed as an aggregate. As anticipated, the f-CaO concentration of fresh BOFS is more extensive, which is 47.95%. These f-CaO concentrations in the BOFS materials might affect the mortar mixture's qualities, such as setting time or early age compressive strength. Substantially, BOFS contains Fe_2O_3 and MgO, 24.82% and 11.26%, respectively, whereas RS mainly contains SiO_2 and CaO (55.85% and 16.13%).

Table 4.2. Chemical composition of fine aggregates

Chemical Composition (W_t %)											
	Na_2O	MgO	Al_2O_3	SiO_2	SO_3	K_2O	CaO	TiO_2	MnO	Fe_2O_3	ZnO
BOFS*	0.00	11.26	1.66	8.73	1.65	0.11	47.95	0.38	1.88	24.82	0.82
RS	2.97	2.29	11.83	55.85	0.67	1.88	16.13	0.77	0.85	6.53	-
*Note: free CaO content: 4.47%											

4.1.6. Mineralogical analysis of aggregates

Similar to binders, aggregates were examined by Rigaku Smart Lab X-Ray Diffractometer (Fig.5) under the same condition. The Figure shows that the BOFS used in this study were naturally air-carbonated materials. Regarding XRD results, BOFS is dominated by calcite ($CaCO_3$), which shows a hump at 30^0 and an iron oxide (FeO) peak at 43^0 and 63^0 2theta. Compared to RS results, the spectrum of BOFS is not fully shown the materials' mineralogy. The RS shows high quartz and silicon oxide contents at approximately 28^0, which play an essential role in geopolymerization.

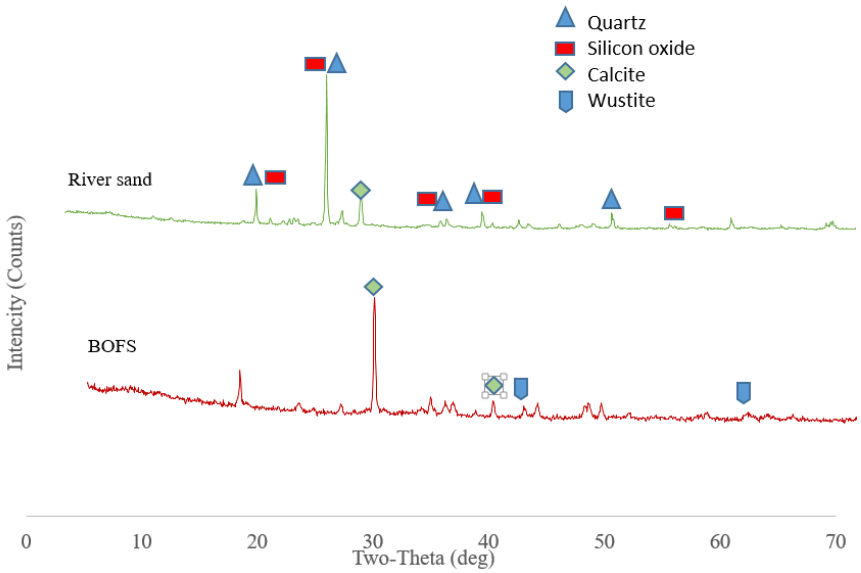

Figure 4.5. Mineralogical XRD analysis of aggregates

4.1.7. Mineralogy analysis of aggregates

The Figure 6 and 7 the findings of the scanning electron microscope investigation of BOFS are presented. The size of BOFS was fine #325 passed particles for SEM, along with other material characterization tests. The results show a rich surface of aggregates with porous. It can cause high water to absorb and slag's mineral long-term leaching. Additionally, on the surface, the tiny dust covers the particles, which can be a reason for the alkaline hydration of slag. Mix with bigger rectangular shape particles; there are other specific fractions.

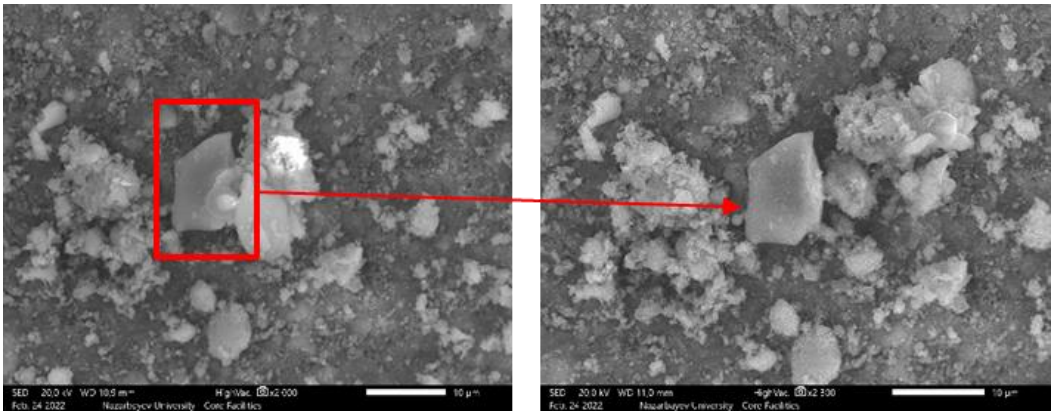

Figure 4.6. Mineralogy analysis of BOFS

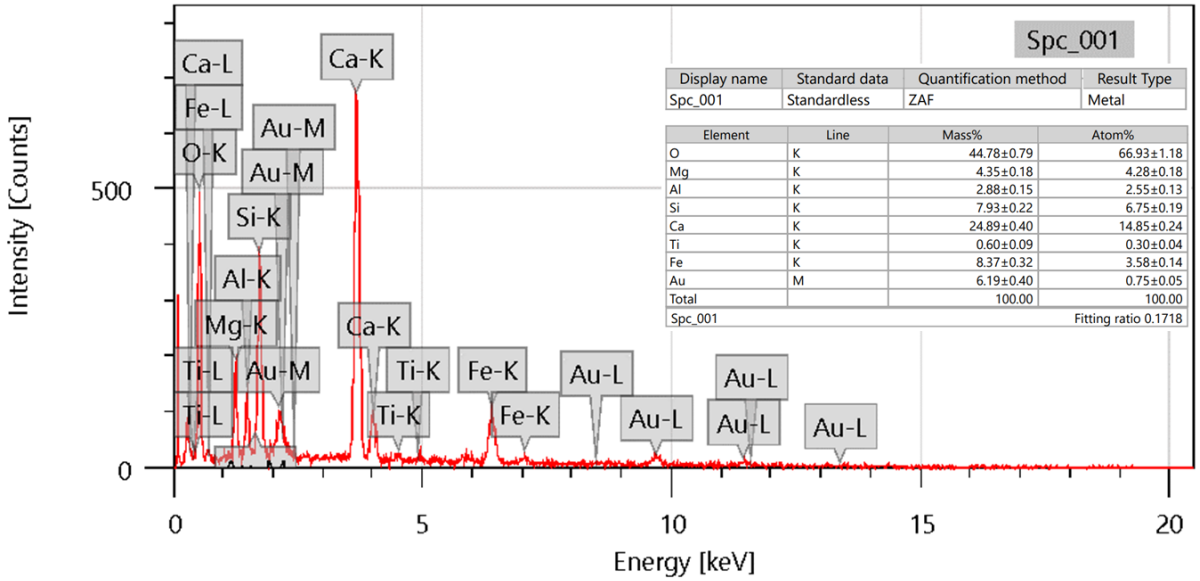

Figure 4.7. EDS results of SEM analyze

4.2. Fresh properties

4.2.1. Flowability

Flow cone test measures the deformability related to the diameter of the test specimen after a collapse has been obtained. Figures 8 -(a), (b), (c), (d), and (e) presents the flow cone set up to measure and test results of the relative flowability (Γ_m) of GPM. The relative flow area is calculated using Eq (14). A larger Γ_m indicates higher deformability and more flowability.

Regarding Figure 8, the intended five graphs show any trend. In the control mixture, where 100% river sand, Figure 8 (a) illustrates that the flowability declines when the sodium silicate ratio to NaOH increases. Because the high concentration of sodium silicate with NaOH concentration

rise degrades the flowability and workability of fresh mortar and concrete, geopolymer mortar/concrete requires water and superplasticizer to enhance workability. However, applying a superplasticizer reduces the strength of the geopolymer mortar. As the slag and sodium silicate doses in the GPC mix rise, the matrix gets denser, and the porosity and mesoporous volume decrease [Verma et al., 2022].

Mixture with 50% and 75% of BOFS replacement, Figure 8 (c) and (d) shows their high relative flowability at 1.5 ratios of sodium silicate, 4.8 Γ_m, and 4.9 Γ_m, respectively. On the other hand, a 1.5 ratio of Na_2SiO_3 to NaOH with 25% and 100% of BOFS replacement, Figure 8 (b) and (e) shows lower slump test results than the 1 and 2 ratios of Na_2SiO_3. The highest workability result for all 15 mixtures is 100% of BOFS with a two ratio of sodium silicate to sodium hydroxide, by 5.2 Γ_m. At the same time, the GPM mixture containing a 1.5 ratio of sodium silicate with 100% BOFS aggregate had the lowest Γm (approximately 3.7). Every second of delaying the flowability test reacts to the results of this test. This fluctuation of results may be related to human factors. Because of the AAS, the geopolymerization reaction is fast, and measuring the slump test should also be urgent right after the mix.

As BOFS aggregate is more angular than RS, the increasing BOFS aggregate content in the mixture must have lower Γ_m. However, except for the mixture having 100% BOFS aggregate, the obtained test results show the opposite trend. This result may be attributed to the BOFS aggregate to binder ratio (BOFS/b) [Harini et al., 2012], which is 30/70. As presented in Figure 8, increasing the amount of BOFS aggregate leads to increasing the total binder content due to the higher specific gravity of BOFS aggregate. This means that F-FA and GGBFS paste content that surrounds and coats aggregates combined with BOFS aggregate and RS increases. The increased paste may work as a lubricant to increase the flowability of GPM. The binding paste content for the GPM mixture containing 100% BOFS aggregate does not seem to improve the flowability because more porous BOFS aggregate than RS absorbed the paste instead of coating the BOFS aggregate.

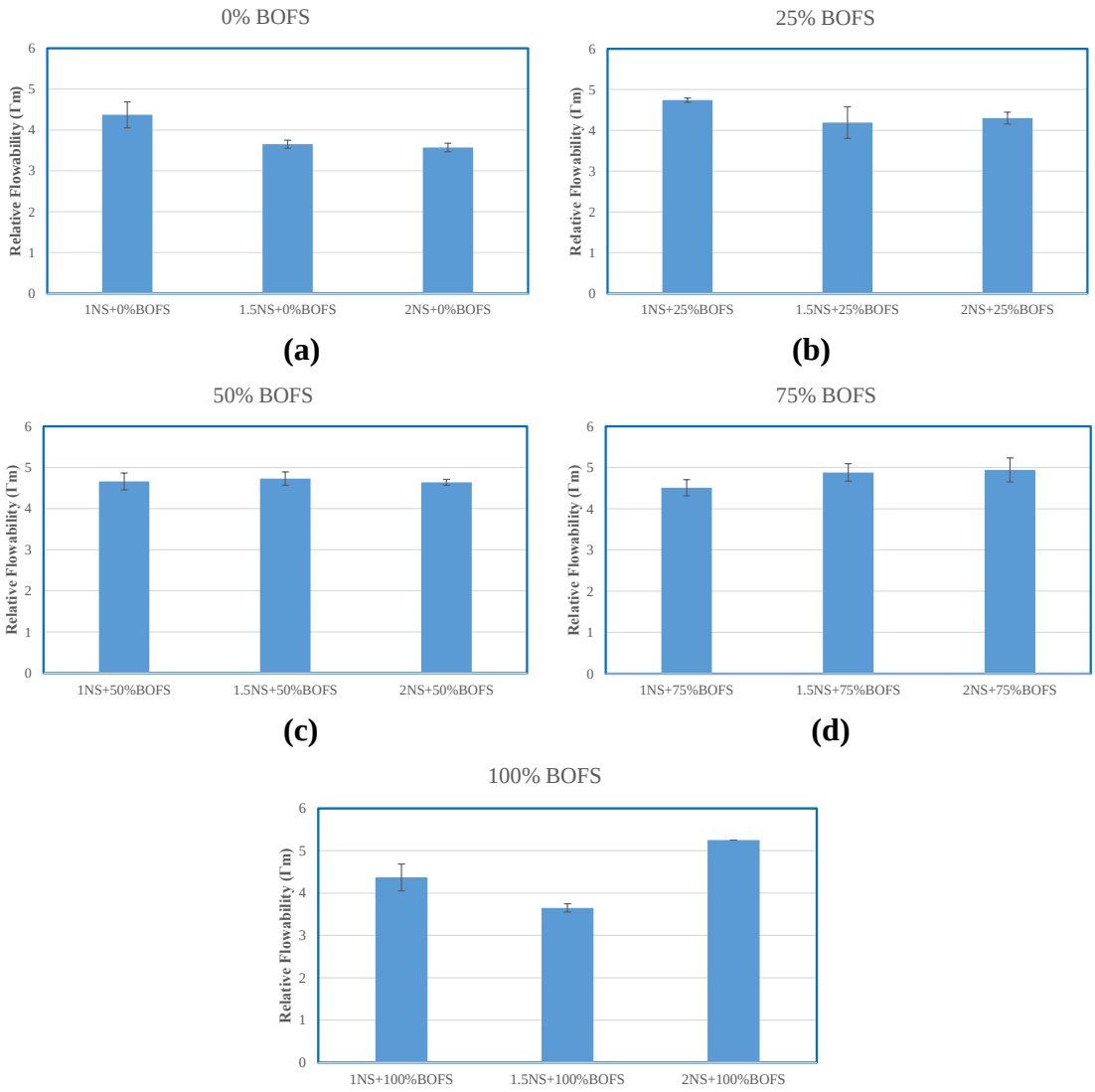

Figure 4.8. Relative Flowability (Γ_m) test results of GPM mixture

4.2.2. Air content

Figure 9 (a), (b), (c), (d), and (e) illustrates the air content of GPM. The graphs show that air content increases with increasing the AAS ratio in a mixture with 0%, 50%, and 75% of BOFS-based GPM. Alternatively, 100% BOFS GPM shows a decrease in air content results with an increased solution ratio. The highest score shows 1.5NS+25% BOFS GPM, at 24% of air content, whereas the lowest is 1NS+50% BOFS-based GPM, the same as the workability test results. The fresh condition test is conducted when GPM is in paste form, so controlling its behavior is impossible and depends significantly on human factors.

Besides the mixture having 100% BOFS aggregate, increasing BOFS aggregate content leads to decreasing air content. Although BOFS is used as an aggregate in this study, BOFS contains f-CaO. In such a high 1, 1.5, and 2 AAS content, f-CaO can easily dissolve and participate in geopolymerization and hydration. The chemically formed products fill the voids in OPM and are hardened. As a result, air content is reduced.

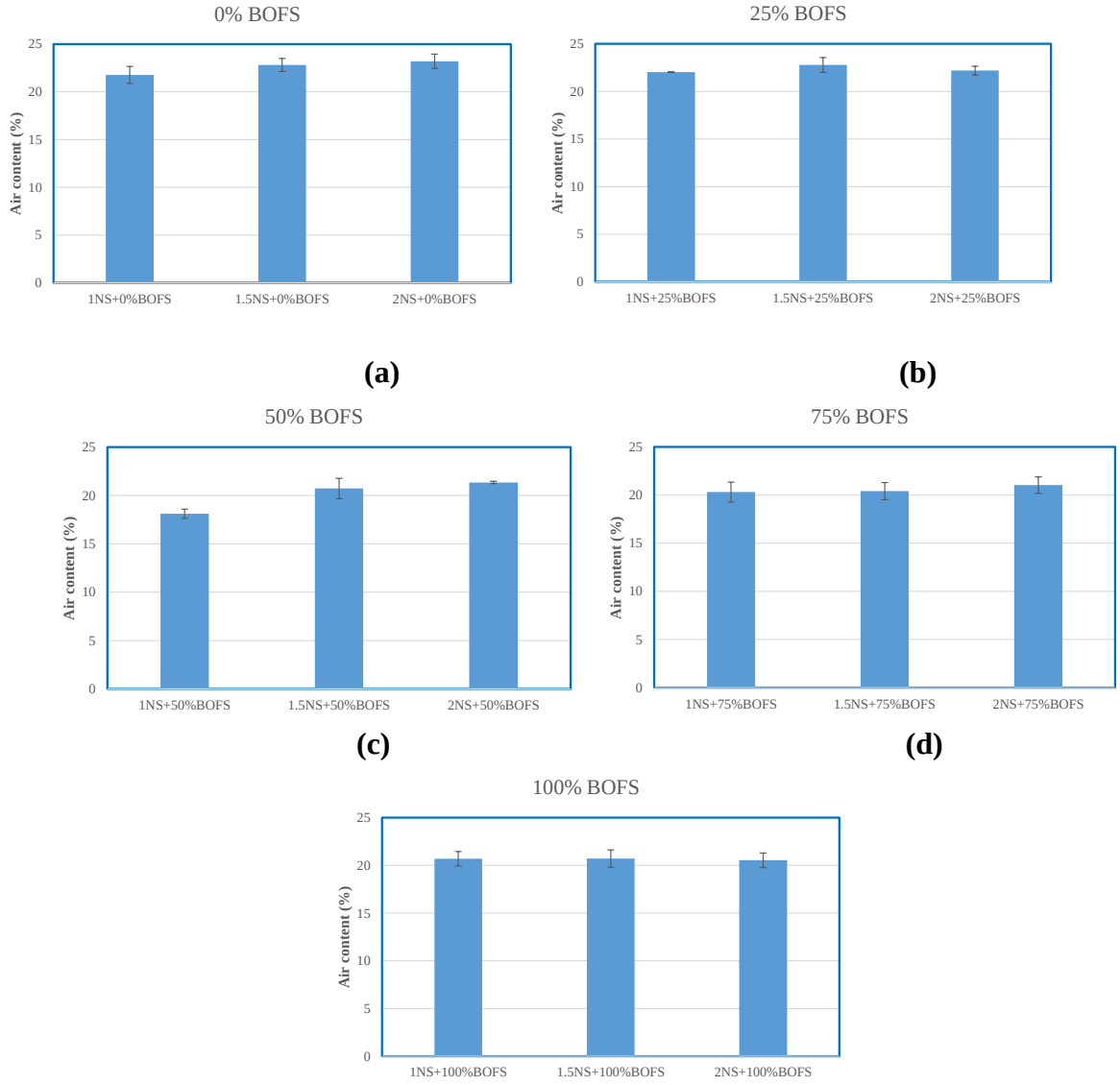

Figure 4.9. Air content of GPM mixture

4.2.3. Setting time

The Vicat instrument was used to gauge how long the geopolymer mortar took to solidify. Figure 10 list the start and ultimate setup times. The control geopolymer mortar samples had beginning and ultimate setting times of 70 and 180 minutes, respectively. For all the mixtures, the final setting time is significantly reduced by raising the sodium silicate ratio (1, 1.5, and 2 ratio AAS) to sodium hydroxide. Clearly, an increased percentage of BOFS sped up the geopolymer mortar setting process. Besides the mixture having 100% BOFS aggregate, increasing BOFS aggregate content leads to decreasing setting. BOFS, while being employed as an aggregate in this work, contains f-CaO. With such high sodium silicate to sodium hydroxide AAS content ratios as 1, 1.5, and 2, f-CaO dissolves quickly and participates in geopolymerization and hydration. The chemically formed products fill the voids in OPM and are hardened. As a result, setting times are reduced. The GPM mixture with 100% BOFS aggregate slightly increases setting time than the GPM mixture having 75% BOFS aggregate and 25% RS. Nevertheless, both properties in that GPM mixture are lower than those in the GMP mixture containing 100% RS.

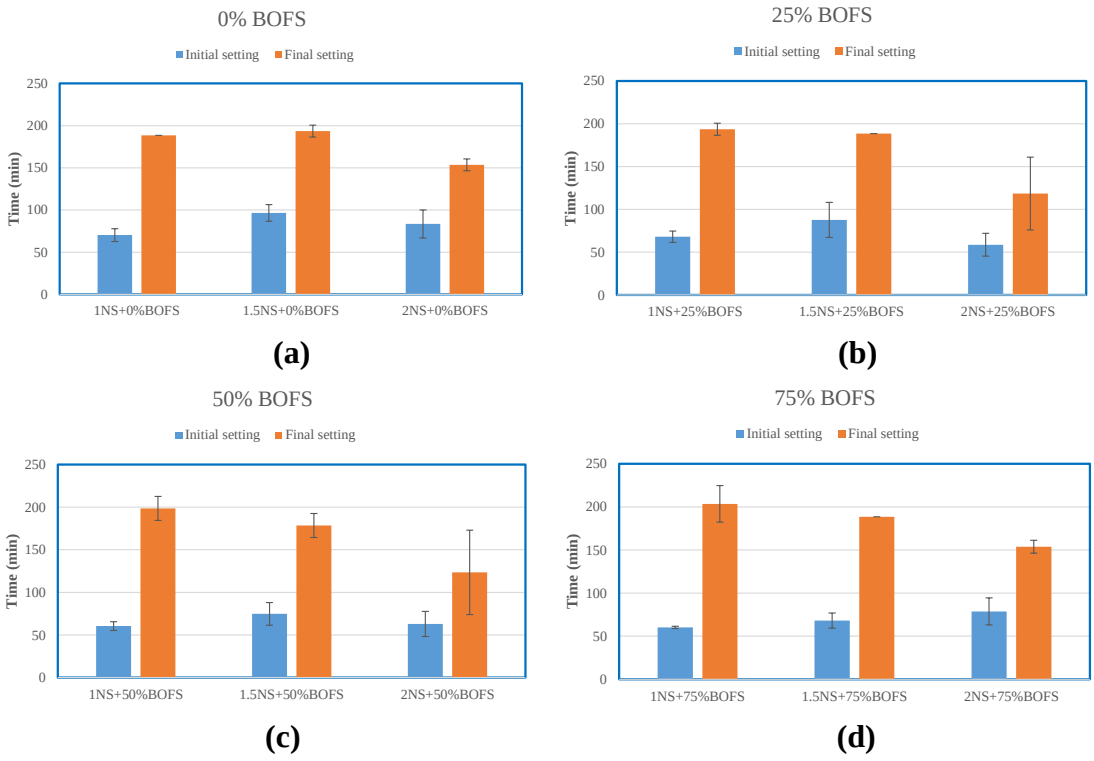

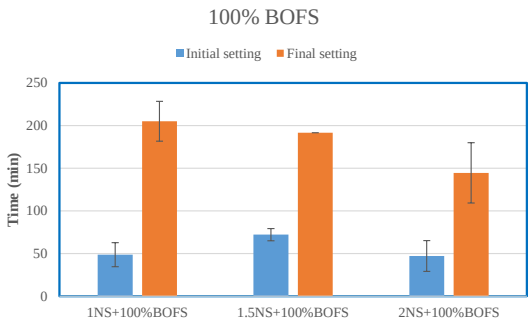

(e)

Figure 4.10. Setting time of GPM mixture

4.3. Hardened properties

4.3.1. Compressive strength

The compressive strength results obtained at 3, 7, 28, and 56 days, are illustrated in Figure 11-(a), (b), (c), (d), and (e) concerning the BOFS aggregate replacement ratios under the ambient curing condition (room temperature 23^0). Additionally, 75% of BOFS replacement to RS GPM carbonation curing was conducted. This is because, by all results, this mixture was the most optimal option for a user-friendly mix design of geopolymer mortar to the carbonation treatment. As expected, all GPM mixtures' compressive strength increases throughout up to 28 days but decreases at 56 days, irrespective of mixture type. However, all GMP mixtures almost reach 30 MPa after 7-day curing, longer ages exceed 30 MPA at both 28-day, despite dropping compressive strength at 56-day, except 25% BOFS with 75% River sand with 2 ratios of sodium silicate to sodium hydroxide, which show only 19 MPa and 23 MPa, respectively. The strength drop at 56 days may be caused by dropping the density of GPM, which is supported by Figure 12. Also, this strength drop may be attributed to a poor dissolution of the aluminosilicates. Tian et al.2020 reported that silicon and aluminum components were well dispersed and dissolved in the geopolymer matrix at a high temperature (80^oC), while the appearance of silicon and aluminum with cracks was observed in the geopolymer system at a low temperature (20^oC), resulting in less formation of sodium-alumina-silicate-hydrate (N-A-S-H) gel to contribute the strength development.

In this study, the compressive strength due to enough aluminosilicates continues to increase with a curing time of up to 28 days. Since fewer amounts of silicon and aluminum are remained with curing after 28 days, the compressive strength can stay the same. It should be noted that GPM

mixture specimens which showed in Figures 11- (a), (b), (c), (d), and (e) were air-cured at room temperature.

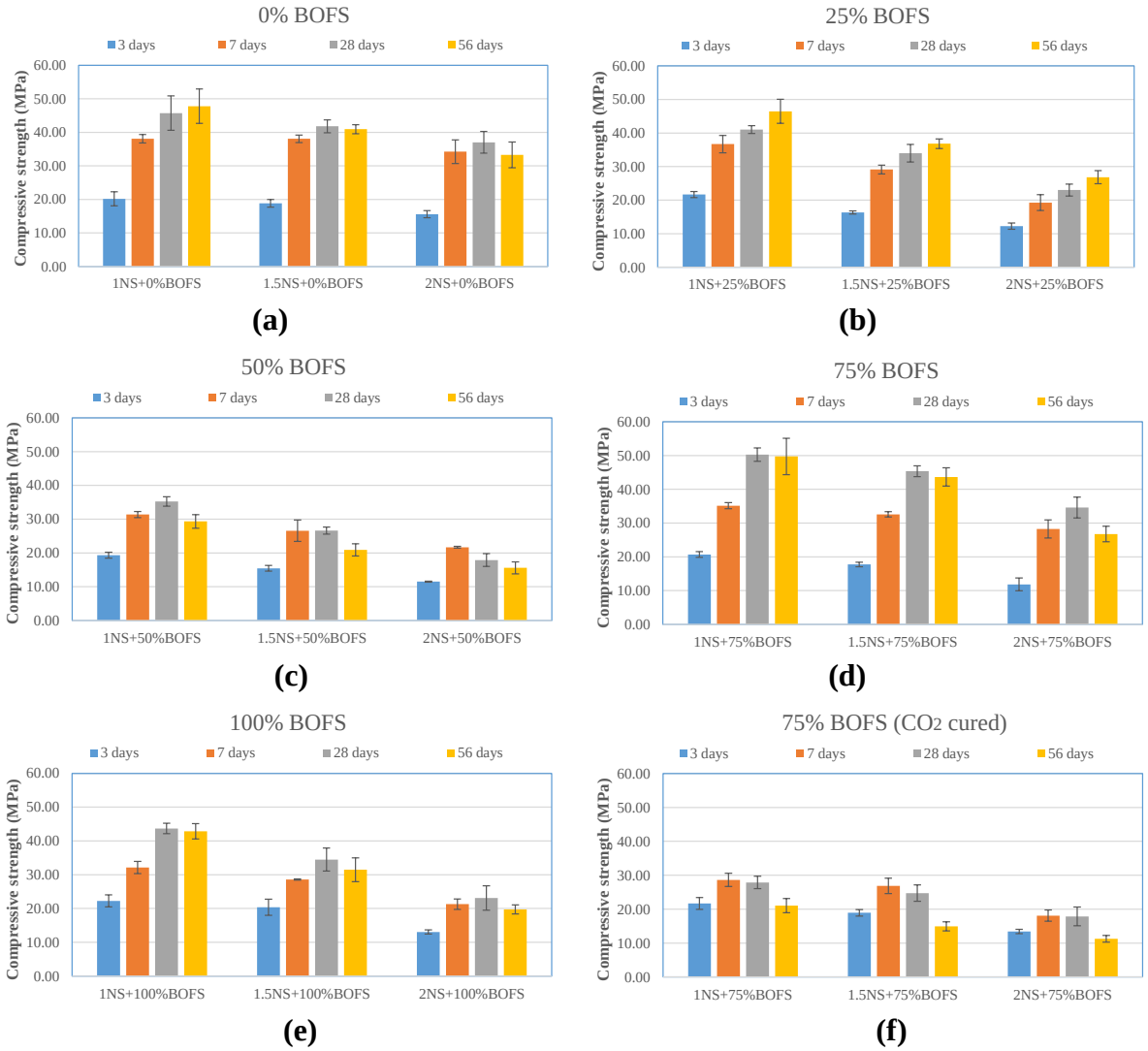

Figure 4.11. Compressive strength of GPM mixture. (a), (b), (c), (d), and (e) ambient cured samples; (f) CO_2 cured sample

The Figure 11 also presents the effect of the BOFS aggregate replacement ratio on the compressive strength. Up to 7 days, the compressive strength of the GPM mixture is lower than control mixture that of 100% RS GPM mixture, regardless of the replacement ratio of BOFS aggregate. However, at both 28- and 56-day, the GPM mixture combined 25% RS and 75% BOFS, 75% RS and 25 % BOFS, and 100 % BOFS aggregate had higher compressive strength than 50% BOFS with 50% RS-based GPM mixtures. The increase in compressive strength of those mixtures may be due to the combined effect of the formation of N-A-S-H and calcite ($CaCO_3$). The f-CaO

in BOFS aggregate reacts with CO_2 and produces subsequent precipitation of $CaCO_3$. The formation of $CaCO_3$ decreases void contents in BOFS aggregate (pore-filling effect), eventually increasing strength [Solomon et al., 2010].

The mixture containing 100% BOFS aggregate may generate too much $CaCO_3$, and the dissolution of $CaCO_3$ leads to the leaching of calcium from the GPM matrix. Moreover, from the results in Figure 11, there is a minimum ratio of RS to BOFS aggregate for the compressive strength of the GPM mixture. As a result of the poor compressive strength, the GPC matrix has a high degree of porosity and lacks structural integrity.

Another curing method was used in this study to characterize the behavior of BOFS in geopolymer mortar. The curing method Carbonation was conducted only for 75% BOFS with 25% RS-based GPM for all ratios of Na_2SiO_3 (1, 1.5, and 2 ratio AAS). To compare the effect of carbonation curing for different mixture this study used a similar condition for carbonation curing, to Han et al., 2020, study where 20% of CO_2 were used, with 23^0C and 75% of humidity. That study with cement mortar shows 33MPa of strength at three days, with W/C=0.35. In contrast, this study at the same age compressive strength shows only 22MPa where the ratio was 1 ratio of sodium silicate to sodium hydroxide, and this strength decreased with increasing AAS to 13MPa. Overall, from the comparison of Figure 11 (d) and (f), the strength of GPM decreased for all ratios two times.

According to Cai et al., 2019 findings make it clear that CO_2 curing had no beneficial effect on the compressive strength of Alkali Activated Slag Concrete (AASC). That study focused on the The influence of early age-curing methods on the drying shrinkage of alkali-activated slag concrete (AASC) hydration products reacting with CO_2 in a CO_2 curing environment to produce $CaCO_3$, which is exceedingly insoluble in water. Besides, concrete became denser due to $CaCO_3$ precipitating in the material's pores. This is advantageous for AASC's growth of compressive strength [Shi et al., 2012]. The decalcification of C-(A)-S-H gel, on the other hand, was brought on by carbonation, which led to a partial loss of strength [Shi et al., 2018; Li et al., 2017]. Consequently, considering these two factors, CO_2 curing has no good impact on geopolymer concrete/mortar compressive strength. Similar to this study, the carbonation treatment method's impact could have been more positive.

4.3.2. Hardened density

The density of samples was examined and calculated by the dimension and weight of the samples. All results of the compressive strength of GPM samples are directly related to the hardened density of it. With the decreasing density of the samples, the compressive decreases together. This is because samples' hydration is lost, and samples become weaker. According to Figure 12, the hardened density of GPM decreases with age, and increasing of AAS ratio from 1 to 2.

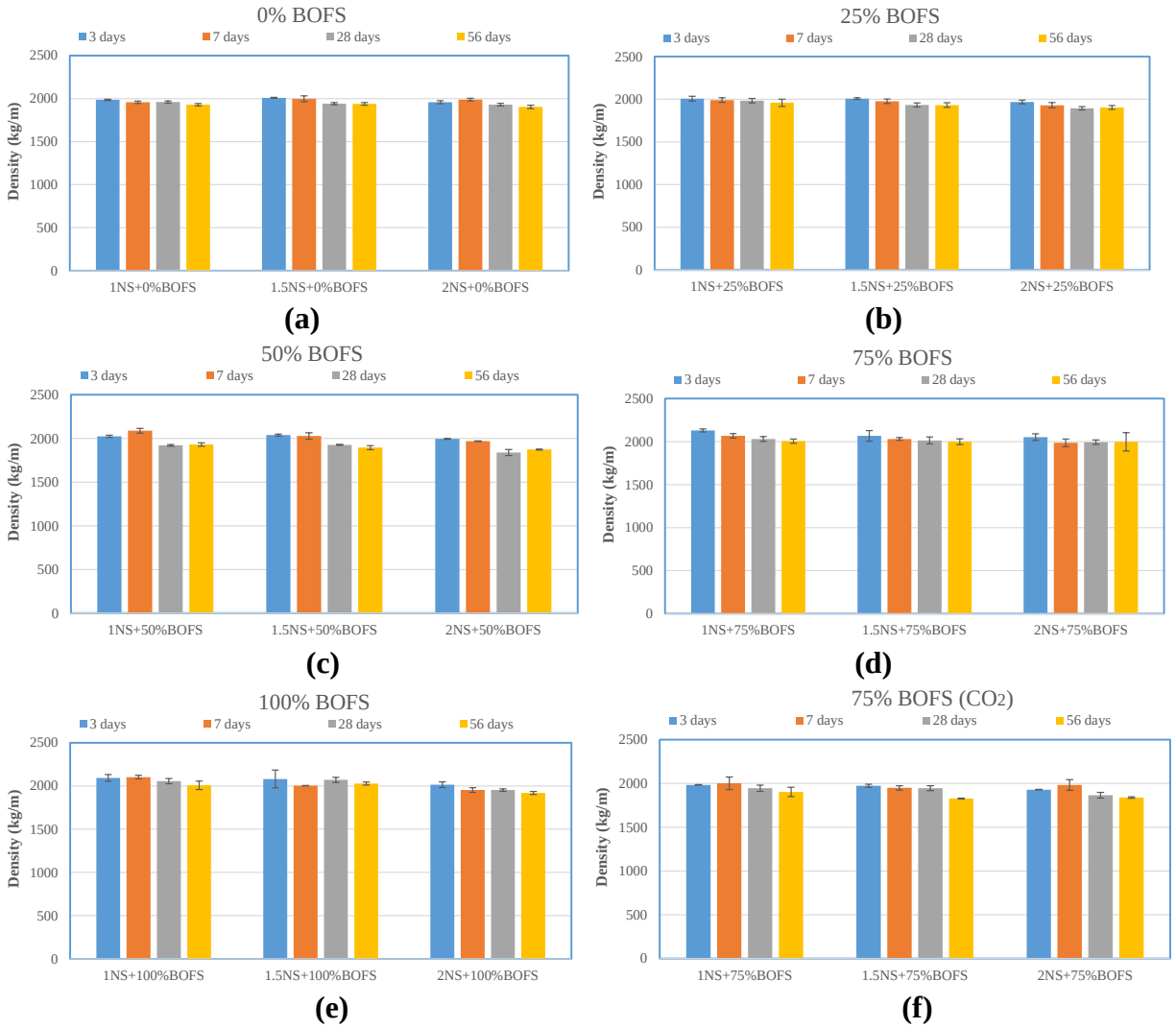

Figure 4.12. The hardened density of the GPM mixture. (a), (b), (c), (d), and (e) ambient cured samples; (f) CO_2 cured sample

4.3.3. XRD (broken compressive strength test samples)

The Figure 13 shows the X-ray diffraction analysis results after the compressive strength test. Scans were performed over 0 to 75° 2θ range at 0.01° 2θ steps and integrated at the rate of 3 seconds step. To compare 3 age and 28 age-broken GPM samples, 1NS+75% BOFS, 1.5NS+75% BOFS, and 2NS+75% BOFS were selected under ambient and carbonation curing conditions. The reason for selecting these examples is that the early age strength of GPM may be demonstrated using three days of broken models. The geopolymer's findings from the previous three days are the most important and definitive markers of the geopolymer's performance. The 28-day compressive strength samples are chosen because the highest and normal performance geopolymer concrete might be at this age.

The strength of these samples at 3 days under ambient curing conditions were 1NS+75% BOFS 20.71MPa, 1.5NS+75% BOFS 17.77MPa, and 2NS+75% BOFS 11.85 MPa. At 28 days 1NS+75% BOFS 50.29MPa, 1.5NS+75% BOFS 45.37 MPa and 2NS+75% BOFS 34.59 MPa. After carbonation treatment, the strength shows results such as 1NS+75% BOFS 21.66 MPa, 1.5NS+75% BOFS 18.92 MPa, and 2NS+75% BOFS 13.42 MPa (at 3 days), and 1NS+75% BOFS 27.88 MPa, 1.5NS+75% BOFS 24.72 MPa, and 2NS+75% BOFS 17.85 MPa at 28 days.

As mentioned earlier, for each curing condition, it shows that with the increasing ratio of AAS, the strength decreases. The mechanical point of view in previous papers shows that a high amount of sodium silicate does not dissolve, and there is no reaction between aluminosilicate minerals and solution. On the other hand, the Figure 13 shows the mineralogical content of these samples and many chemical minerals.

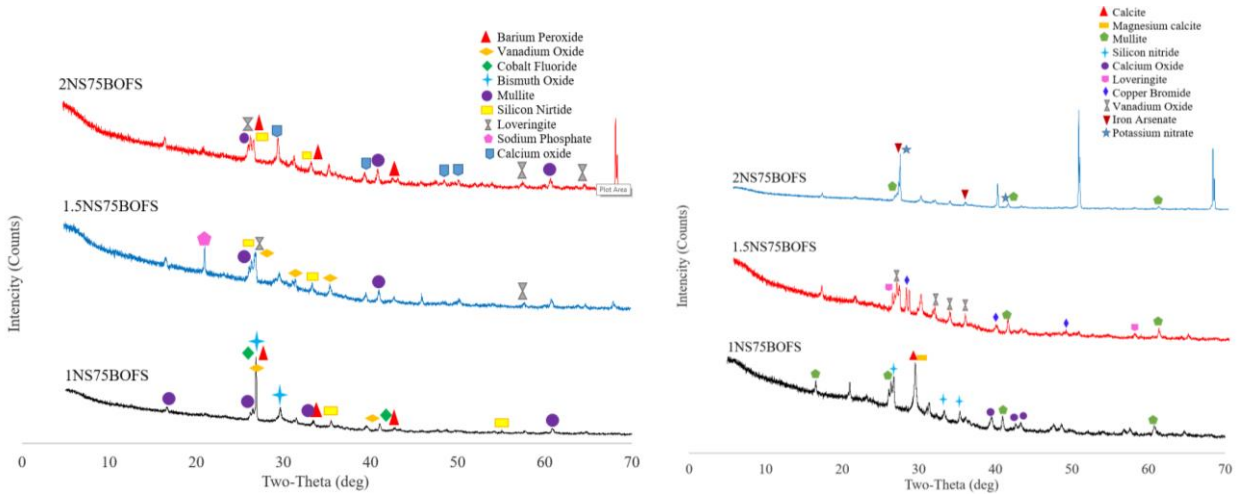

(a) **(b)**

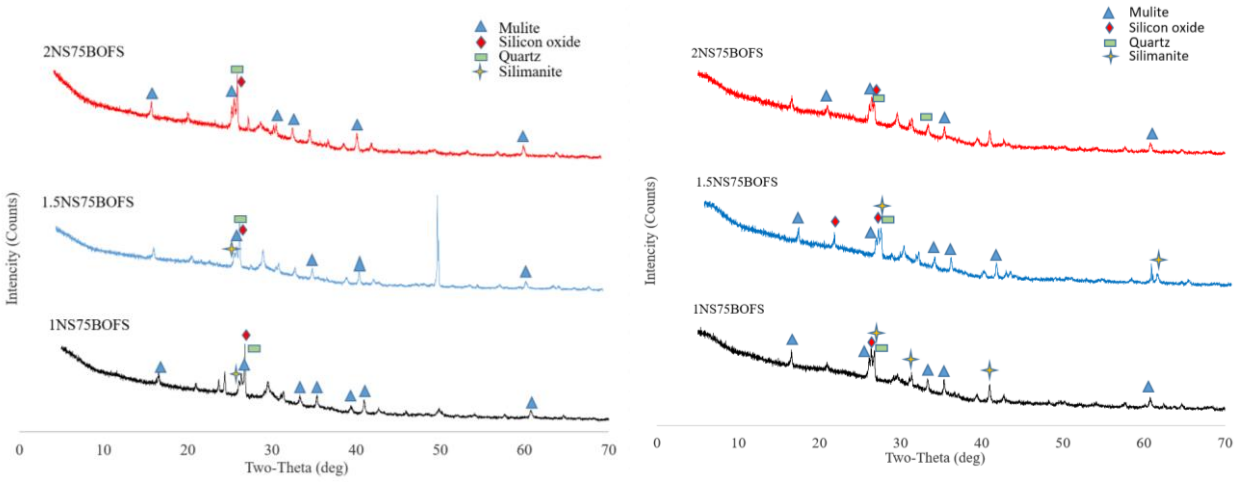

(c) **(d)**

Figure 4.13. XRD analysis after compressive strength; (a) 3 days compressive strength samples under ambient curing condition; (b) 3 days compressive strength samples under CO2 curing condition; (c) 28 days compressive strength samples under ambient curing condition; (d) 28 days compressive strength samples under CO2 curing condition

Figure 13 (a) and (b) results of 3-day broken samples. The ambient cured samples show Barium peroxide (BaO_2), Vanadium oxide (V_2O_5), Cobalt fluoride (CoF_2), Bismuth oxide (Bi_2O_3), Mullite ($Al_6Si_2O_{13}$), Silicon nitride (Si_3N_4), Loveringate, Sodium phosphate (Na_3PO_4), Calcium oxide (CaO), while the carbonation cured samples follows next chemical composition: Calcite ($CaCO_3$), Magnesium calcite, Silicon nitride (Si3N4), Loveringite, Copper bromide (CuBr), Vanadium oxide (V2O5), Iron arsenate (AsFeO4), Potassium nitrate (KNO3).

The characterization and behavior of several elements: BaO_2 - a highly oxidizing agent. The solid resembles calcium carbide, or CaC2, isomorphically. Organic compounds can fire at temperatures and oxygen concentrations brought on by contact with water. Due to the creation of acetyl peroxide, it reacts violently with acetic anhydride. It ignites when combined with powdered calcium-silicon alloys, powdered magnesium, or powdered aluminum. The components of the fuel type create highly reactive combinations. V_2O_5 - the synthesis of ferrovanadium and vanadium metal requires technical grade, which is generated as a black powder. Making sodium metavanadate, or $NaVO_3$ involves treating a vanadium ore or residue with sodium carbonate and an ammonium salt. When vanadium metal is heated with excessive oxygen, vanadium (V) oxide is generated. However, this material is also polluted with other, lesser oxides. CoF_2 - the manufacture of metal is one area where it is exploited since it is oxygen-sensitive. Metal alloys can be created using cobalt (II) fluoride as a catalyst. Bi_2O_3 - a very insoluble and thermally stable

source of bismuth, bismuth oxide is ideal for use in ceramic, glass, and optical applications. In addition to being a naturally occurring mineral known as bismite and sphaerobismoite, bismuth oxide may also be produced as a by-product of the smelting of copper and lead ores. An essential component of bismuth for the industry is bismuth oxide. These mixtures include a metallic cation and at least one oxygen anion.

CSH(S) was found in small peaks suggestive of an amorphous calcium silicate hydrate matrix in samples containing either slag or a combination of fly ash and slag as a precursor. These findings are congruent with those of other studies [Skvara et al., 2006; Sakulich, 2009]. Peaks of calcium oxide were seen in the XRD data in Fig. 13(a)-(e), which matches to the condition with GPM mixes cured at 23°C. This event demonstrates that slag hydration resulted in the production of calcium silicate hydrate [CSH(S)] in the polymer product's mineralogy. The hydration of the slag was assumed to be similar to that of Portland cement. This results in the formation of a matrix similar to calcium silicate. As a result, a matrix similar to calcium silicate is formed. This results in the production of a calcium silicate hydrate matrix with a different Ca/Si ratio than PC. This hydration happens concurrently with the polymerization activities involved with alkaline activation of the fly ash.

The creation of sodim phosphate, which exhibits three peaks at 22° with the maximum strength at 24.50°, 2 theta, is depicted in the diffractogram specifically for sample 1.5NS+75BOFS at 3 days under room temperature curing. Such a zeolite-specific phase's appearance shows that a mesoporous material of a semi-crystalline character has formed. The cation exchangeability of the raw material and activation solution is directly inversely related to the produced sodim phosphate content.

Figure 13 (c) and (d) results of 28-day broken samples. The ambient cured, and CO_2 cured samples show the same and less amount of chemical results as Mullite ($Al_6Si_2O_{13}$), Quartz (SiO_2) or silicon dioxide, and sillimanite (Al_2SiO_5). All samples show that mullite and quartz crystals form a phase in crystal growth. The high pH causes fly ash to dissolve and geopolymer, mostly the X-ray amorphous (glassy) phases. Amorphous silica is distinguished by having a hump in the 28^0 after-room curing method and carbonation curing range. This suggested that there could be some fly ash that has not yet reacted in the system.

According to Alvarez-Ayuso et al., greater crystallinity fly ash-based geopolymers demonstrated greater compressive strengths. Furthermore, fly ash-based geopolymers with 12 M NaOH showed the highest compressive strengths. According to XRD measurements, the greatest compressive strengths were caused by the intensity of the visible crystallinity.

The tetrahedral structure of the silicon-oxygen-silicate mineral known as quartz, or silicon dioxide, which crystallizes in the hexagonal system, is a mineral that may be discovered. Because quartz particles can operate as barriers against fracture propagation, their concentration improves the mechanical properties of geopolymers.

Mullite is a less frequent compound that develops between aluminum, silicon, and oxygen, and it crystallizes in the orthorhombic system. This mineral's presence causes the geopolymers' refractivity to rise because of its extremely high melting temperature (1840 °C).

4.3.4. Flexural strength

The flexural strength of the GPM mixture is shown in Figure 14. Despite a small quantity of variation, the flexural strength of GPM also increases over time. At early 3 days, all mixtures have a minimum of 3 MPa strength. Except for the GPM control and having 100% BOFS aggregate, all GPM mixtures have 6 MPa at 28- and 56-day, at all ratios of sodium silicate. Moreover, up to 3-day, replacing RS with BOFS aggregate increases flexural strength regardless of the replacement ratio. At a later 28 age, only the GPM mixture containing 25% RS and 75% BOFS aggregate, or 50% RS and 50% BOFS aggregate with 1 ratio of AAS, had higher flexural strength than the 100% RS GPM mixture 8.9MPa and 7.8MPa, respectively.

Overall, all the mixture shows a rising trend from 3 to 28 days, and in 56 days, all indicators dropped. This is because GPM has good strength at early age to 28days performance. Additionally, all results for 1 ratio of sodium silicate to sodium hydroxide show higher strength than 1.5 or 2 ratios of AAS. It means that increasing of sodium silicate amount effect negatively to geopolymer mortar, because high amount of silicate cannot dissolve and it results of low strength performance.

On the other hand, compared to Ghafoor et al., 2020, the results at 28 days show better flexural strength. In the previous study, strength was 4.2 and 2.6 MPa, where 10 M of NaOH was used with w/binder 0.4 and 1.5 and 2.0 ratio of Na_2SiO_3/NaOH. This decrease might be the decrease in hydroxide in the solution caused a decrease in the development of the three-

dimensional network of sodium aluminosilicates hydrate [N- A-S-H] gel, which resulted in a drop in flexural strengths when the Na_2SiO_3/NaOH ratio was increased. In this study, the lowest strength at 28 days is 5.9 MPa. In both studies, samples were cured under the ambient curing condition.

The formation gel by AAS has been affected by carbonation curing. Flexural strength values following carbonation curing are similar to compressive strength results, Figure 14 (f), dropped 1.5 times. This is because CO_2 gas, where samples were exposed, influenced the bond of binders, AAS, and aggregates.

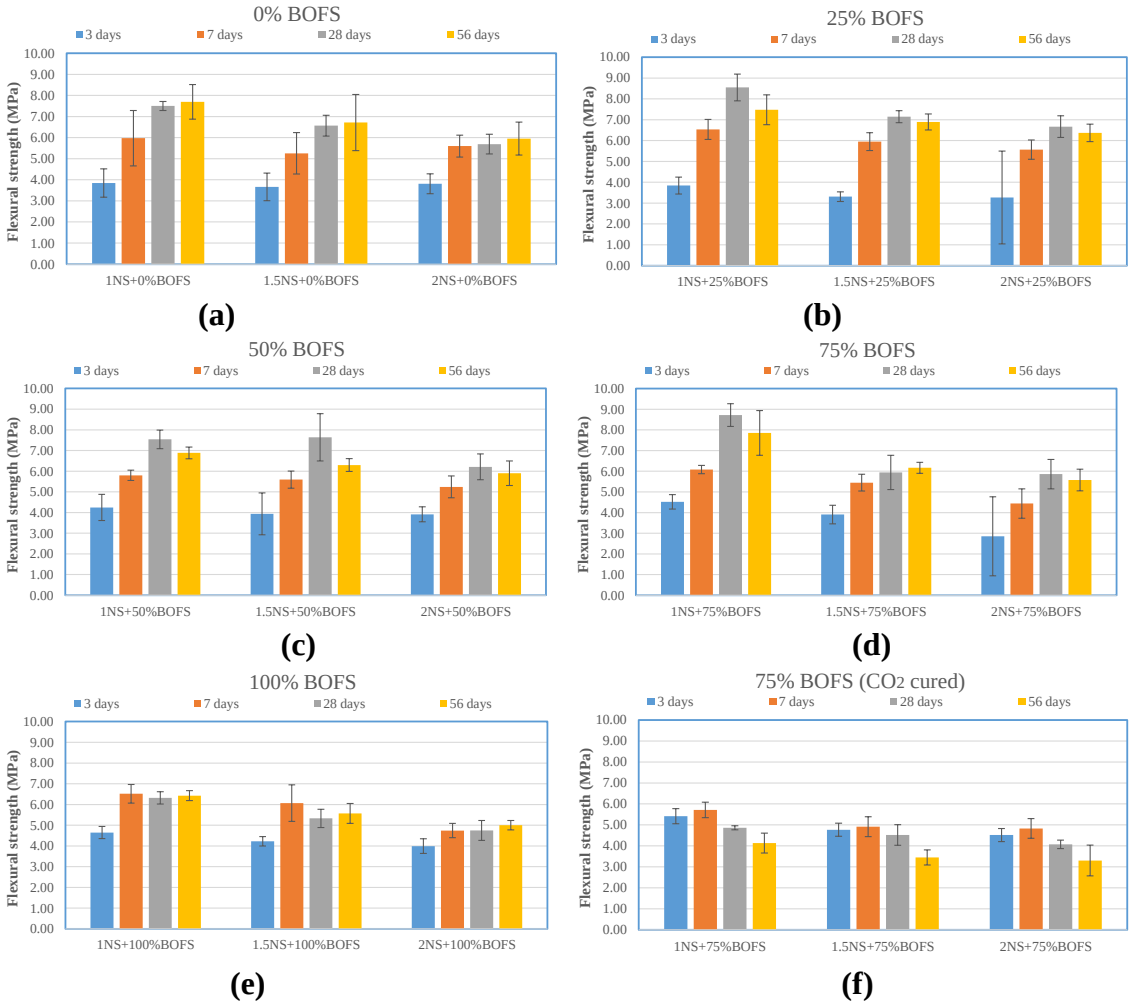

Figure 4.14. Flexural strength of GPM mixture. (a), (b), (c), (d), and (e) ambient cured samples; (f) CO_2 cured sample

4.3.5. Dielectric constant

The permittivity of the material should improve as the concentration of BOFS increases. Because of its high silica concentration, BOFS can function as a dielectric material. A dielectric material is an electrical insulator that may polarize when an electric field is applied. When exposed

to an electric field, dielectric materials do not carry electricity like electrical conductors do. Instead of a minor variation from their normal equilibrium position, the result is dielectric polarization [Schmitt et al., 2002] rather than a minor deviation from their typical equilibrium locations. Many research on the dielectric performance of geopolymers have recently been published [Hanjitsuwan et al., 2014, Topark-Ngarm et al., 2015, Nuruddin et al., 2016, Kantakam et al., 2013, Aradoaei et al., 2016]. Geopolymers are inorganic crosslinked long chain polymers of AlO_4 and SiO_4 that require alkali cations such as Na+ and K+ for charge balancing. The dielectric constants of the geopolymer paste and solution were determined to be 3.5 and 7-10 hours after mixing [Vlasceanu et al., 2013 Jumrat et al., 2011]. The most important elements influencing the electrical conductivity and dielectric characteristics of geopolymers at room temperature are water molecules and hydroxide [Hanjitsuwan et al., 2011].

The Figure 15 shows the permittivity results by the dielectric constant test. The dielectric constant demonstrates a sizable change depending on its moisture level, mineral content, bulk density, temperature, and the frequency of the electromagnetic signal passing through it. Over time the permittivity of samples drops; this is related to the hydration of GPM. The samples show better the electromagnetic wave passing at early ages and dropping with increasing ages because the hydrated material penetrates the signals better than dried-out solid materials. The severe fluctuation of GPM results in room conditions. Sometimes when the temperature or humidity of the room where samples were cured, the indications of samples change.

The fluctuation showed in Figure 15 results of the changed temperature and humidity of the room where the GPM specimens were cured.

The Figure 16 shows the weight change of samples. Similar to the permittivity of sample results, all samples lost their hydration over time, and the weight also dropped. These results were expected. Over the six months, all GPM samples lost about ±100 g of weight overall.

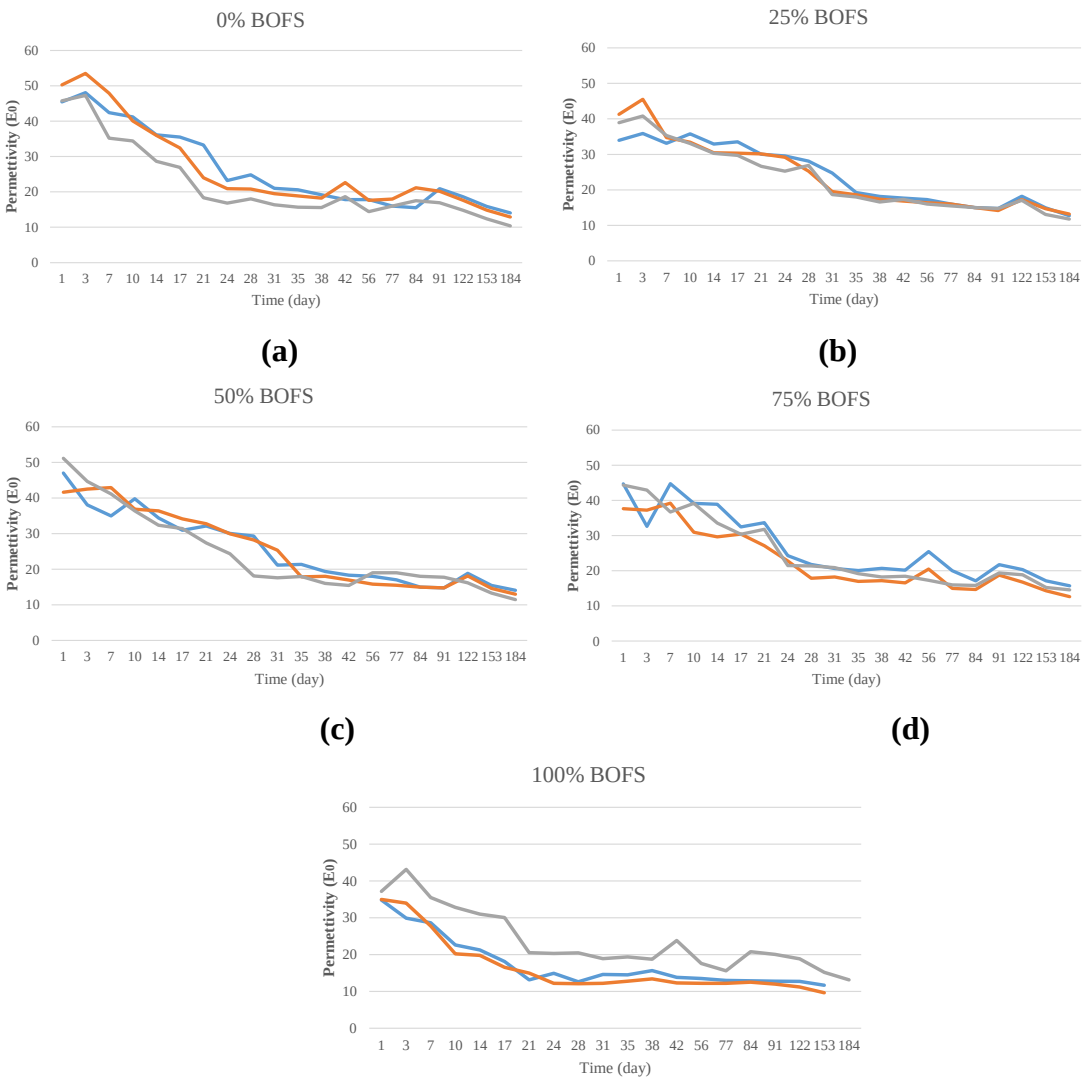

Figure 4.15. The permittivity of GPM mixture. (a), (b), (c), (d), and (e) ambient cured samples

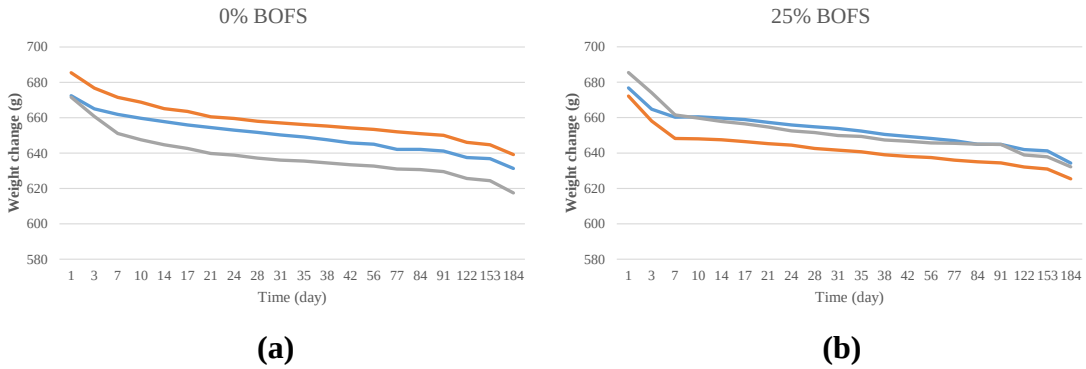

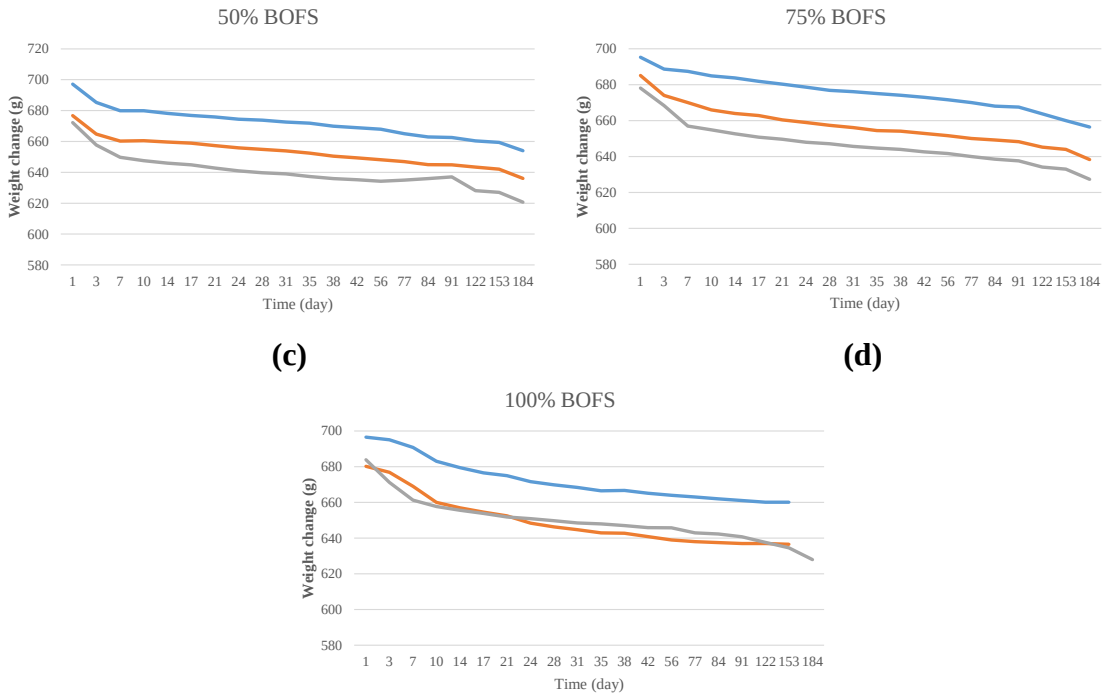

Figure 4.16. Weight change of GPM mixture. (a), (b), (c), (d), and (e) ambient cured samples

4.4. Durability properties

4.4.1. Expansion

The volumetric expansion behaviors of different GPM mixtures are presented in Figure 17 and 18. Two test conditions are applied to evaluate the expansion potential related to BOFS aggregate: the expansion in water (Figure 17) and 1 M NaOH solution (Figure 18) at 80 °C. The length change of mortar bars was monitored for up to 28 days. Though the expansion value is based on the criterion of the ASTM C 1260, the threshold value (0%<0.1% expansion: Non-reactive aggregate criterion at 14-day, 0.1%<0.2%: potentially reactive aggregate at 14-day, 0.2%< : reactive aggregate criterion) is good enough to judge whether aggregate used in the GPM mixture has the expansion potential due to the formation of $Ca(OH)_2$ that causes the cracks in the GPM matrix.

All GPM mixtures submerged in the water had less than 0.1 % expansion at 14- and 28-days, irrespective of mixture type. For example, the GPM with 25% RS and 75% BOFS had expansions of 0.011% at 14 days and 0.070% at 28 days, respectively. As stated earlier, these results indicate that f-CaO or f-MgO in the BOFS aggregate may react with f-Si in the GPM matrix and is converted to stable $CaSiO_3$ or $MgSiO_3$ form, which mitigates the volumetric expansion of BOFS

aggregate. It should be stated that the author's previous work [Tukaziban et al., 2022] presented that the standard specimen containing 100% BOFS aggregate had 0.882% expansion and was broken at 8-day.

When the GPM mixtures were submerged in 1 M NaOH solution it satisfy the ASTM C 1260 criterion at 14 days expansion. The expansion of all mixtures except for the mixture with 25% RS and 75% was less than 0.1% at 14 days. However, the GPM mixture containing 25% RS and 75% had 0.034% expansion at 14 days but exceeded 0.1% of the expansion threshold at 28-day. It is still being determined why only this mixture had higher expansion at 28 days. It can be explained that $Ca(OH)_2$ produced by extra-remaining f-CaO in BOFS aggregate reacts with highly concentrated dissolved silica and produces alkali-silica reaction (ASR) gel, which results in the higher expansion [Qiu et al., 2022]. However, more investigation to identify the actual reason is required. Overall, all the expansion results for the water expansion test do not expand over 0.1%, except the 1NS+100% BOFS sample. 1 sample from 3 was broken after 14 days, and the average expansion seems higher because of the reduced quantity of samples.

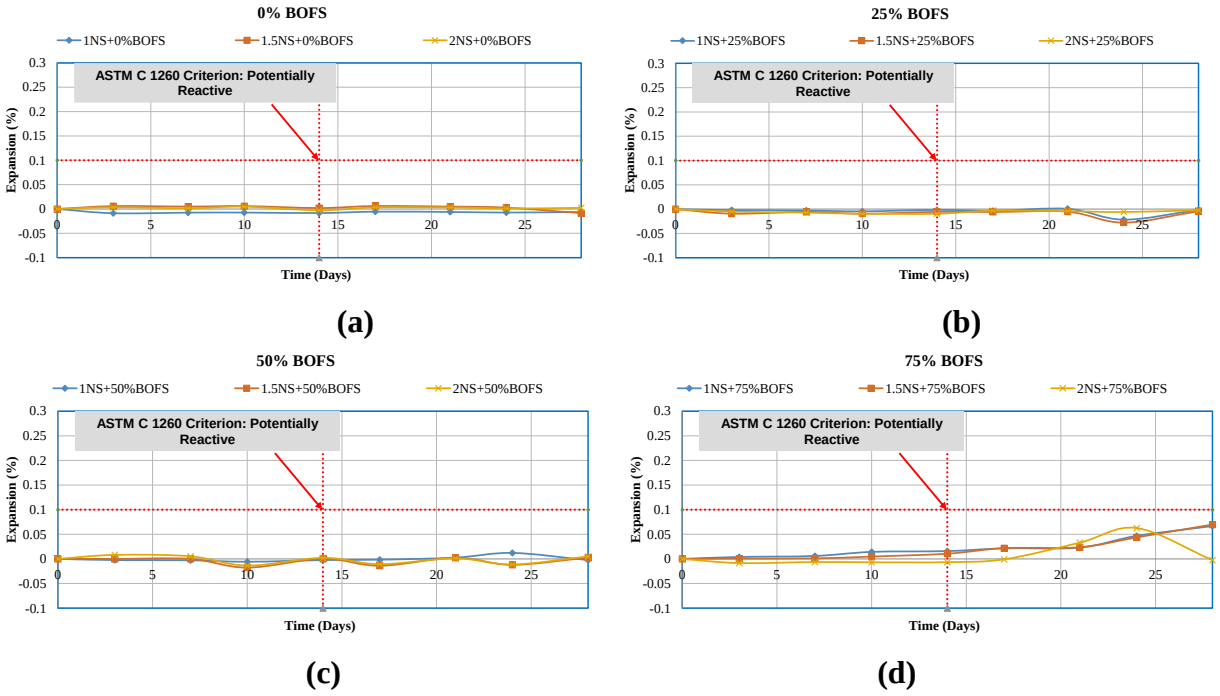

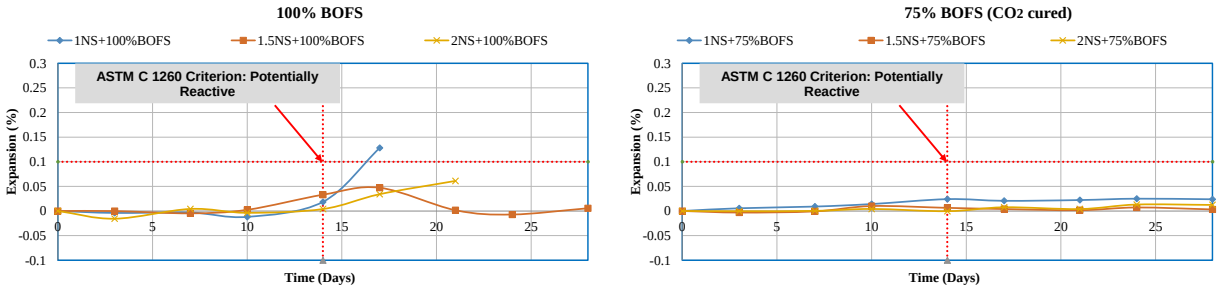

(e) **(f)**

Figure 4.17. Water expansion of GPM. (a), (b), (c), (d), and (e) ambient cured samples; (f) CO_2 cured sample

By ASTM C 1260 criterion, the samples exposed to water and conducted water expansion test show satisfied results. Compared to previous research, where BOFS was used as an aggregate to make OPC concrete, in this study via geopolymerization process with the AAS solution the behavior of BOFS stabilized. The GPM specimens did not expand even in the water bath. As illustrated in Eq. (1) and (2), when BOFS reacts with water, it occurs free lime hydroxide, and the dimension of samples increases and even can be broken. The silicate could restrict these behaviors.

The exact mix design samples but under different curing conditions show different results. 75% BOFS aggregate-based GPM shows that carbonation treatment expands less than ambient cured samples. As shown in Eq (8) and (9), when the geopolymerization process reacts with CO_2 gives stabilization results.

Figures show the increasing expansion with the increasing percentage of the BOFS from control 0% to 100%. 0%, 25%, and 50% BOFS-based GPM samples show some increase but under 0.1%. On the other hand, the GPM with 1NS and 1.5NS+75% and 2NS+100% of BOFS content expand to 0.12% and 0.25%.

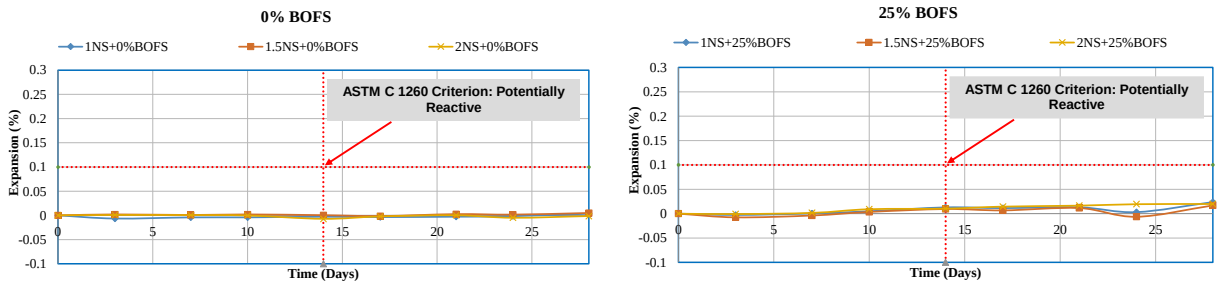

(a) **(b)**

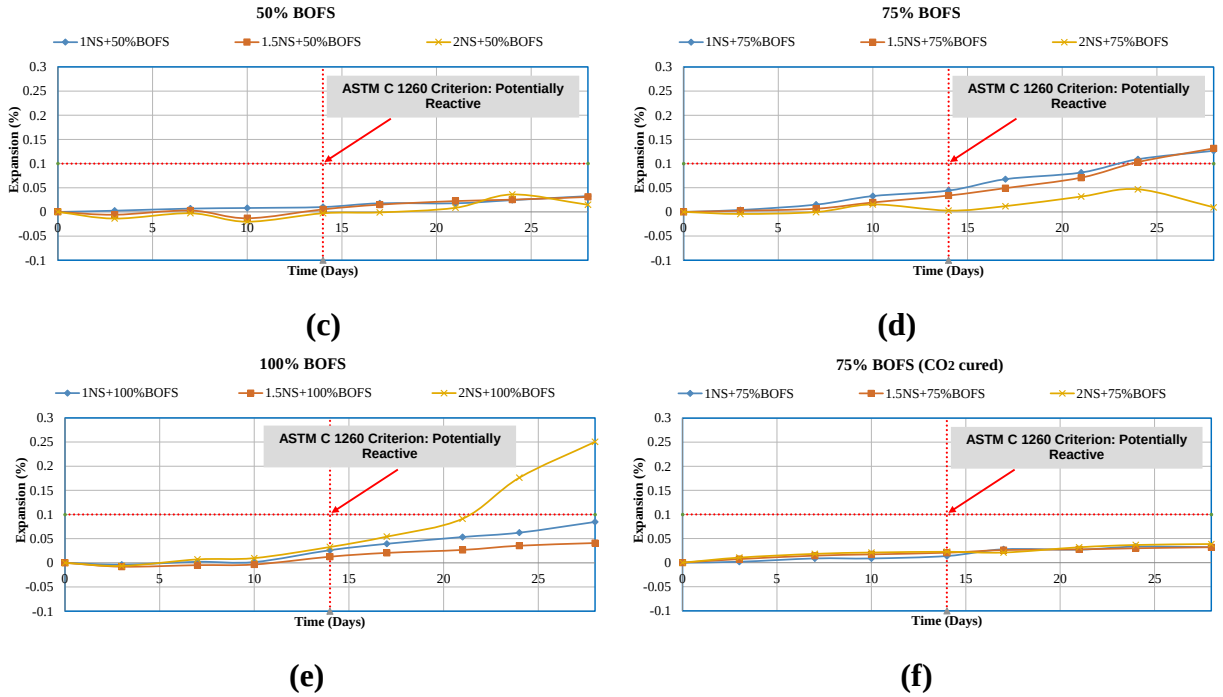

Figure 4.18. ASR expansion of GPM. (a), (b), (c), (d), and (e) ambient cured samples; (f) CO_2 cured sample

4.4.2. SEM (broken ASR test samples)

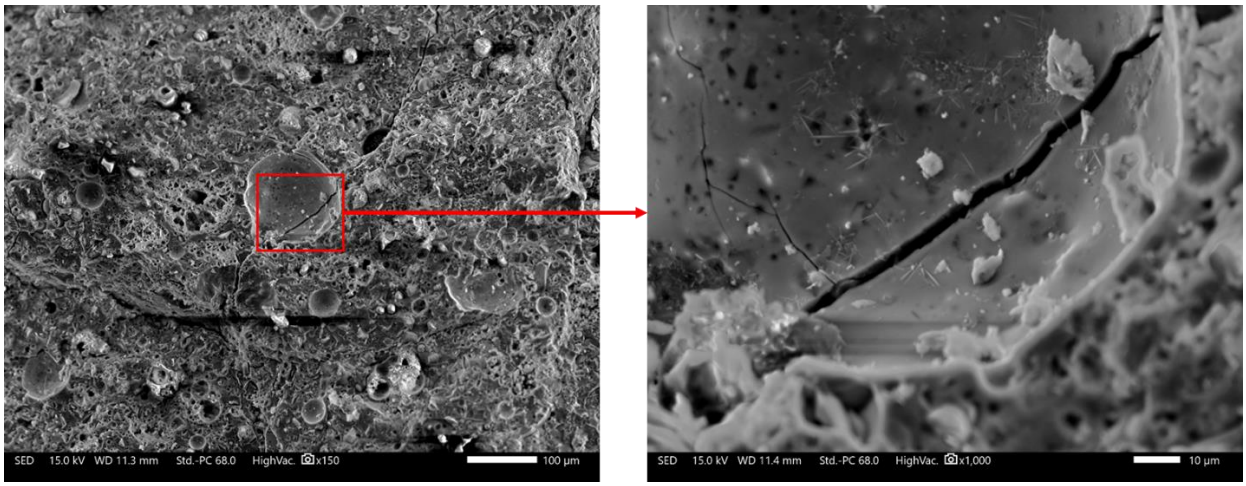

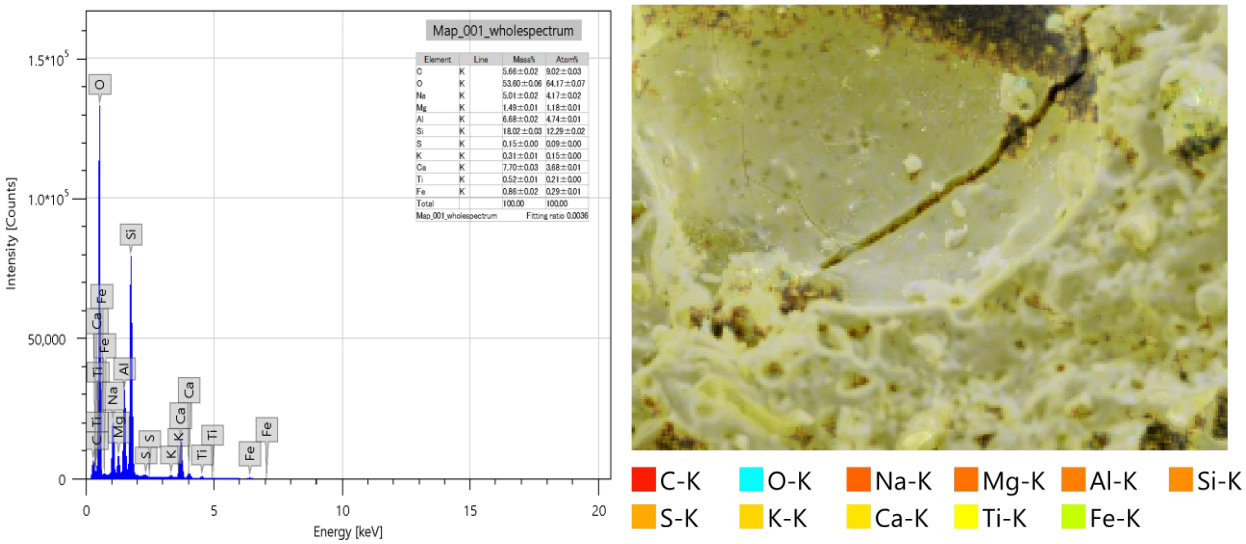

Figure 4.19. 1NS+75% BOFS (ambient curing)

The ASR expansion test samples after 28 curing were used for the SEM test. The collection of samples focused on the expansion percentage. The most expansion was of the GPM samples, BOFS 75% based, under ambient curing. The Figure 19 demonstrated the material's crystallization and the appearance of many voids that might heighten the exposition. The EDS results show (C), Sodium (Na), Magnesium (Mg), Aluminum (Al), Silicate (Si), Sulfur (S), Potassium (K), Calcium (Ca), Titanium (Ti), and Iron (Fe). The quantity of crystalline silica in the 1NS+75% BOFS (ambient curing) sample was visible in the SEM images in Figure 19. It can be deduced from the EDS analysis. When there is a high silicon concentration in a solution, condensation begins with the creation of oligomeric silicates and progresses to 3-D stiff polymeric structures. Since poly-sialate polymer structures are produced when Si low concentrations are available, the high Si percent at one months old was due to polymerization rather than crystalline silica initially present in the exact Figure 22. Moreover, the Si/Al ratio might be used as a second sign of decreased expansion.

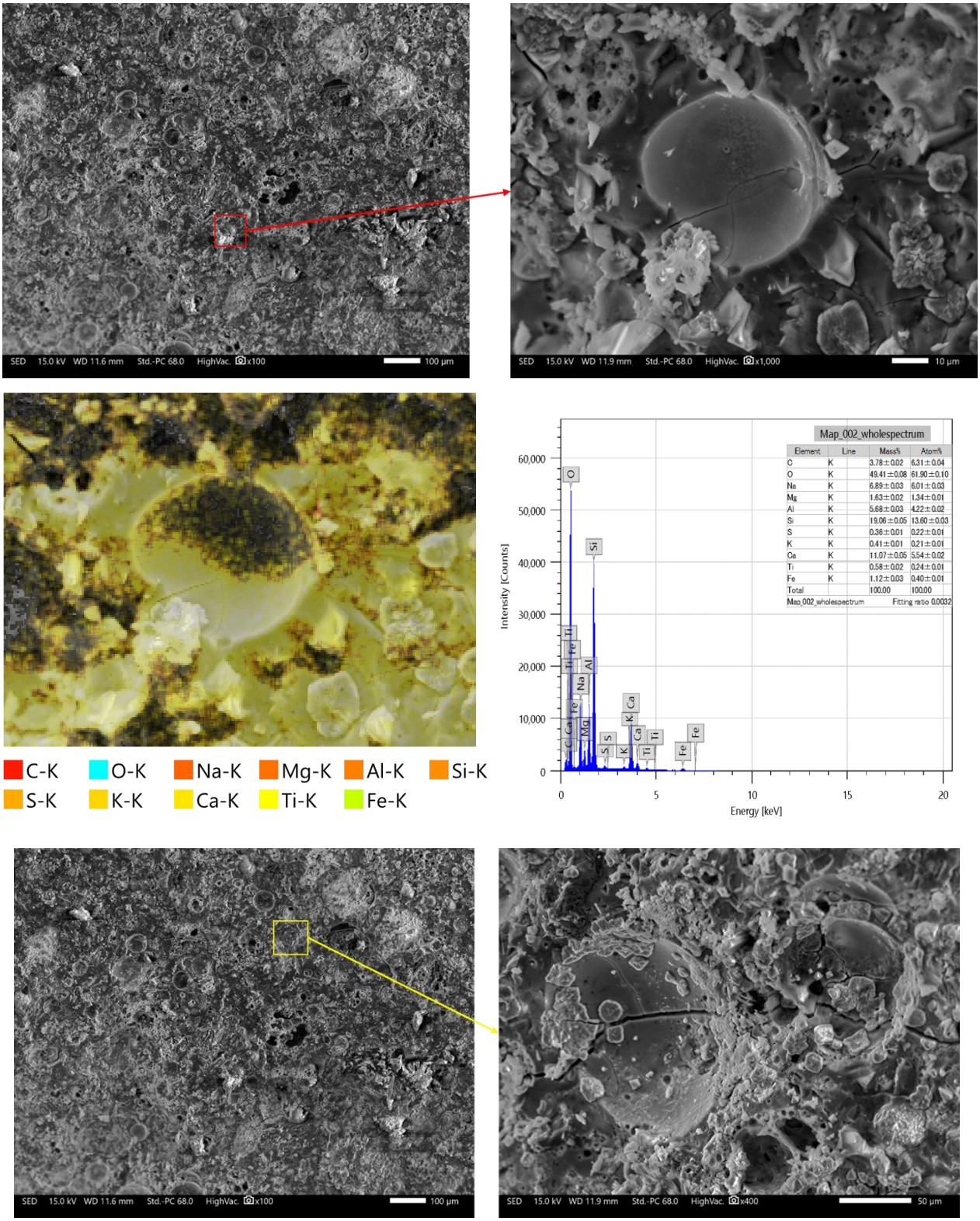

Figure 4.20. 1.5NS+75% BOFS (ambient curing)

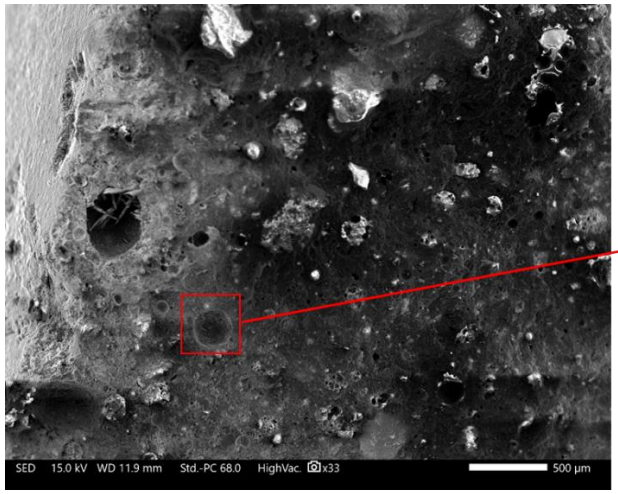
SED 15.0 kV WD 11.9 mm Std.-PC 68.0 HighVac. x33 500 µm

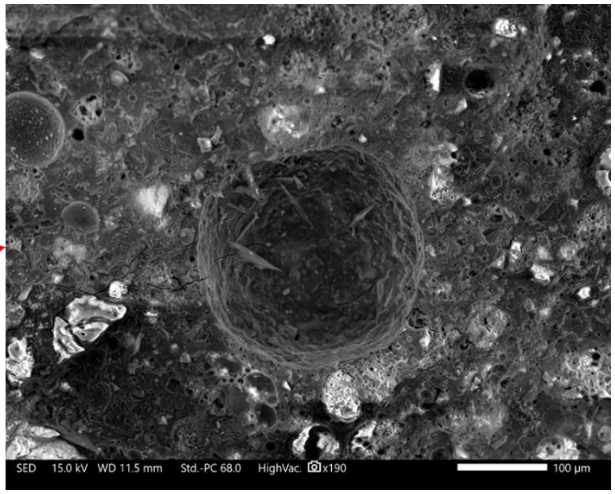
SED 15.0 kV WD 11.5 mm Std.-PC 68.0 HighVac. x190 100 µm

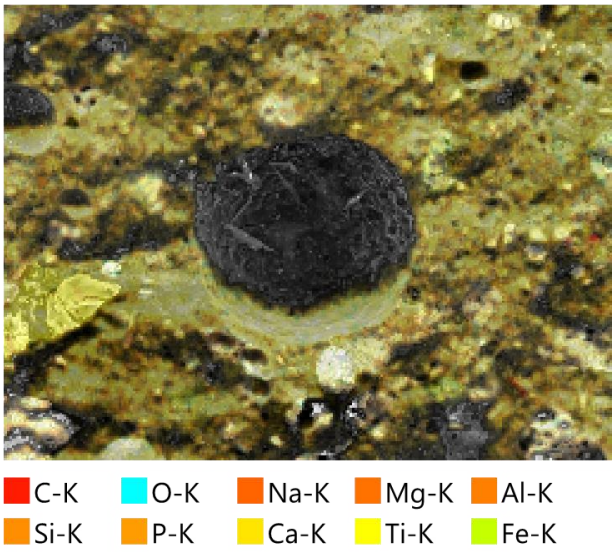
C-K
O-K
Na-K
Mg-K
Al-K
Si-K
P-K
Ca-K
Ti-K
Fe-K

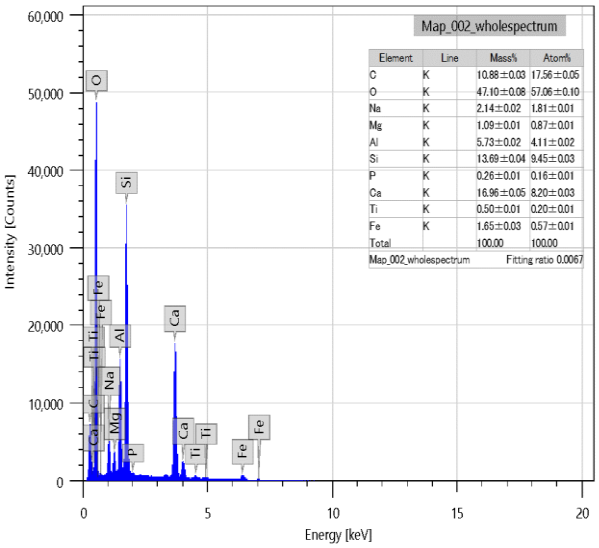
Map_002_wholespectrum
Element Line Mass% Atom%
C K 10.88±0.03 17.56±0.05
O K 47.10±0.08 57.06±0.10
Na K 2.14±0.02 1.81±0.01
Mg K 1.09±0.01 0.87±0.01
Al K 5.73±0.02 4.11±0.02
Si K 13.69±0.04 9.45±0.03
P K 0.26±0.01 0.16±0.01
Ca K 16.96±0.05 8.20±0.03
Ti K 0.50±0.01 0.20±0.01
Fe K 1.65±0.03 0.57±0.01
Total 100.00 100.00
Map_002_wholespectrum Fitting ratio 0.0067
Intensity [Counts]
Energy [keV]

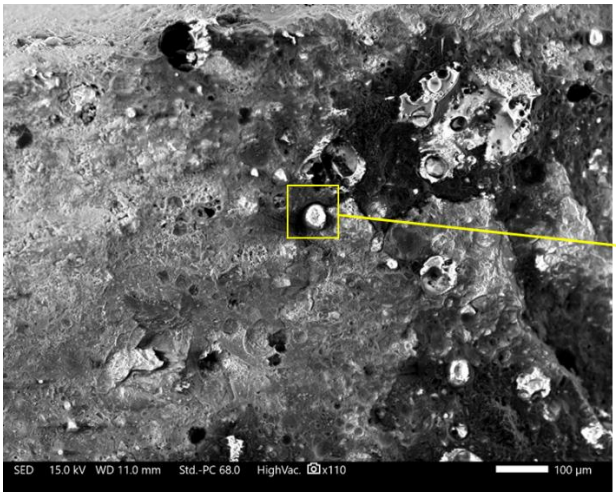
SED 15.0 kV WD 11.0 mm Std.-PC 68.0 HighVac. x110 100 µm


SED 15.0 kV WD 11.0 mm Std.-PC 68.0 HighVac. x500 50 µm

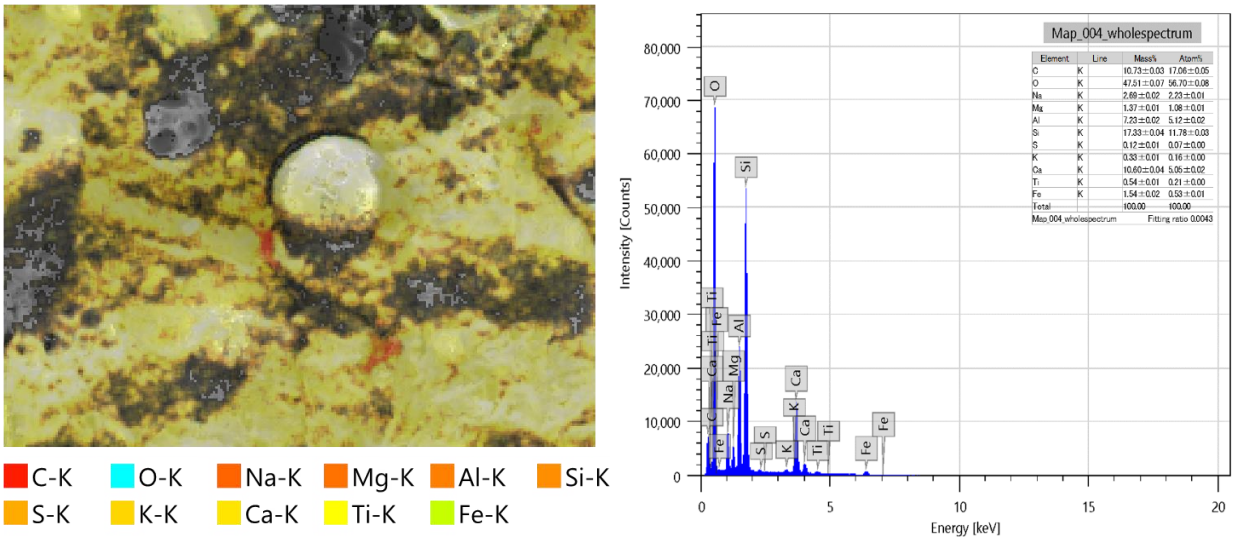

Figure 4.20. 2NS+75%BOFS (ambient curing)

When compared to the other samples, the 2NS+75%BOFS (ambient curing) samples showed the highest homogeneity and the fewest holes, with the least unreacted F-FA, GGBFS, and BOFS from the alkaline activator. 1.5NS+75% BOFS (ambient curing) indicates that aluminosilicate dissolution in the geopolymerization process in the sample resulted in the greatest ASR expansion.

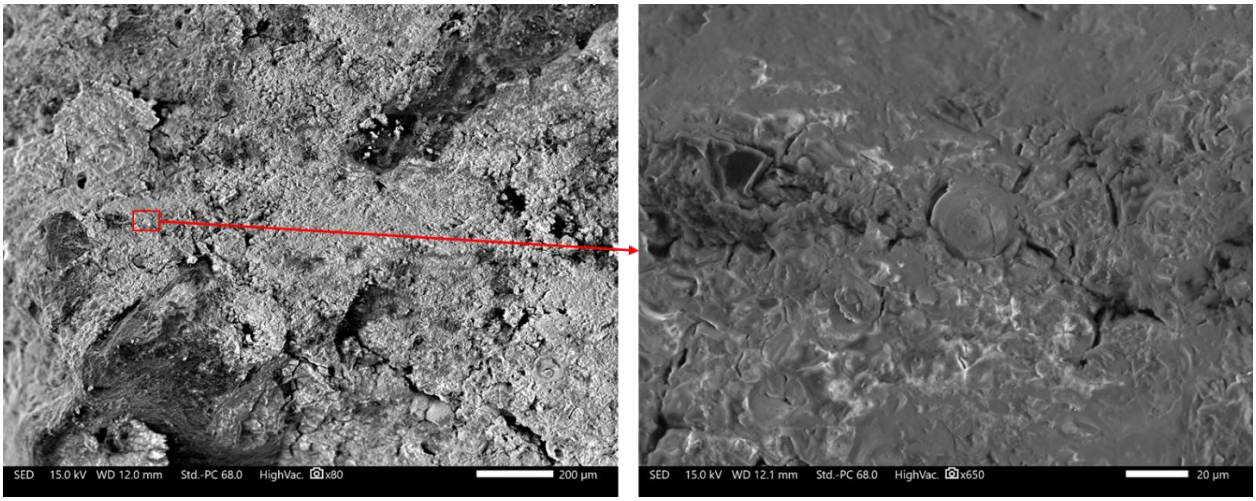

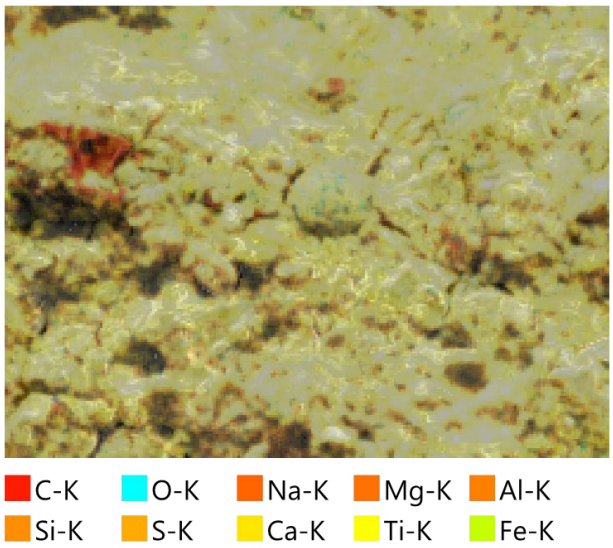

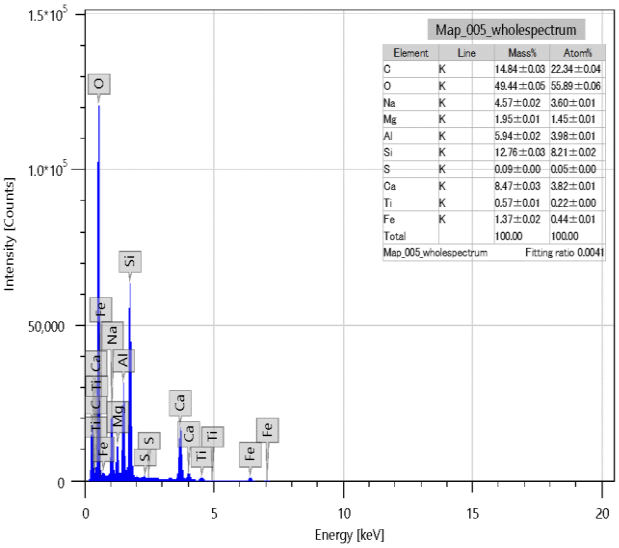

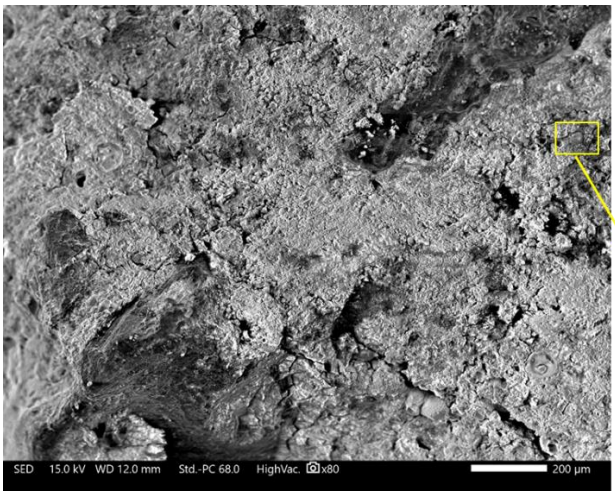

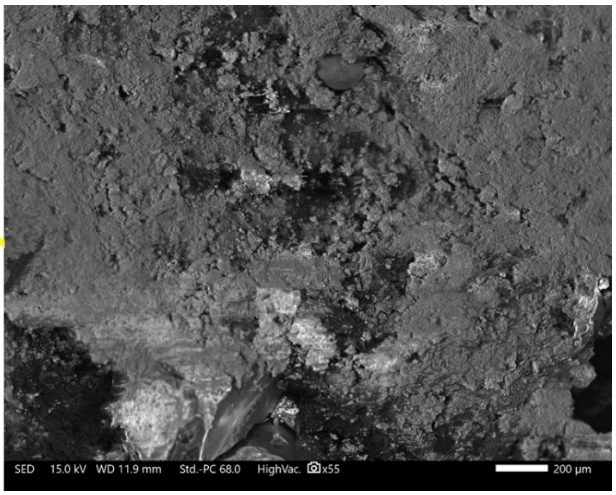

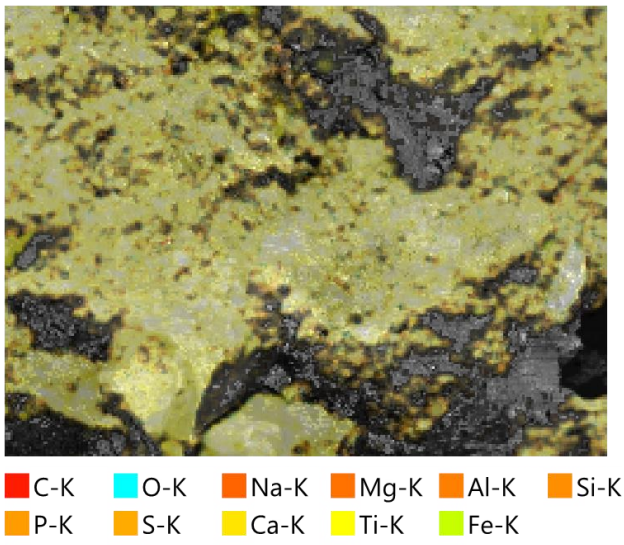

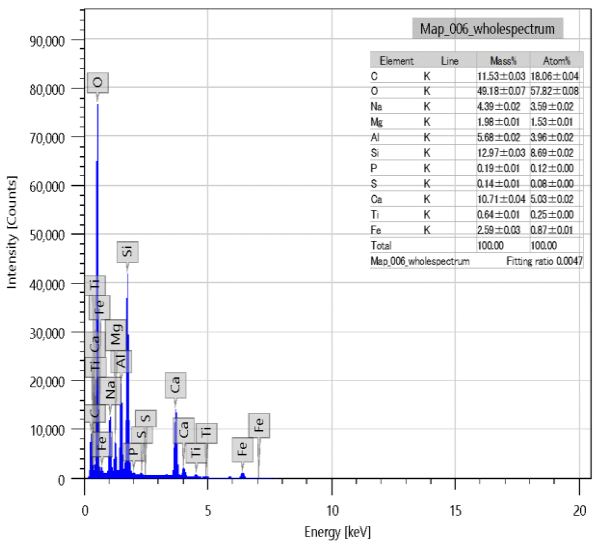

Figure 4.21. 1NS+75% BOFS (CO_2 curing)

The mineralogy of the BOFS-based geopolymer comprising varying amounts of sodium silicate ratio exhibited different proportions of unreacted raw materials as F-FA after carbonation curing, as can be seen in Figures 22. As seen in the images, all samples were coated in unreacted raw materials that had developed on their crust, and they had less holes in the matrix than the ambient cured samples.by arrows. Despite this, the matrix was homogenous with a dense-compact mineralogy and a smaller fraction of unreacted raw materials in the 1NS+75% BOFS (CO_2 curing), 1.5NS+75% BOFS (CO_2 curing), and 2NS+75% BOFS (CO_2 curing). This is consistent with the observation that GPM samples had lower ASR expansion findings than room temperature cured bar samples.

CSH formation exemplifies this: The EDS analysis confirms the presence of calcium in the BOFS and Na2SiO3, showing that increasing the quantity of BOFS and adding carbonation curing significantly increases the calcium content in the mixture, resulting in the production of a calcium silicate hydrate (CSH) gel (Figure 22, 23 and 24). As a result, incorporating BOFS introduces more calcium, which bears compounds and leads to more binding products. This also improves the expansion, decreases porosity, and affects the setting behavior of geopolymeric gels at an early stage, allowing it to preserve and stable its behavior. The presence of fly ash particles in the cement matrix allows for the production of a more compact gel structure and, as a result, enhances mechanical qualities. The fly ash particles react with the GGBFS (due to the tiny particle size of GGBFS in comparison to other solid materials), fill the gap, and begin interacting with GGBFS, hence improving the characteristics. The inclusion of fly ash particles reduces the region of fracture start on the surface of geopolymer concrete. (F). The dissociation of fly ash particles from the polymerization matrix is observed in fly ash particles of porous character. On a scale of 100 microns, the random dispersion of fly ash particles is seen. Partially reacted fly ash particles are visible, as are some fully reacted ones randomly in Figure 22, 23. Higher magnification reveals reacted and unreacted fly ash particles. The porous structure of the material is also plainly evident.

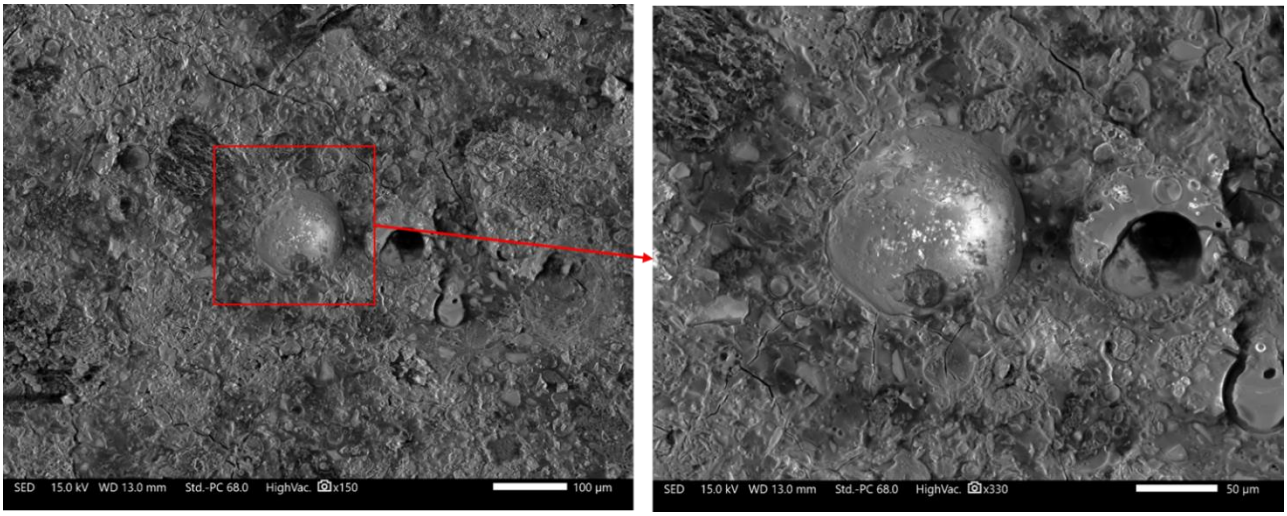

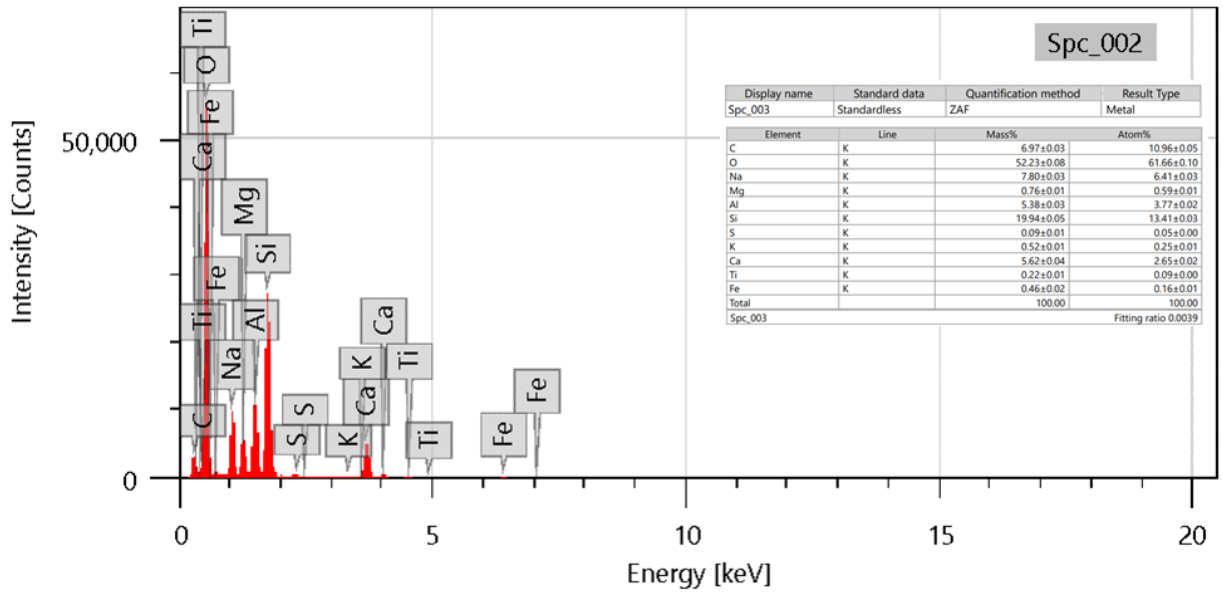

Figure 4.22. 1.5NS+75% BOFS (CO_2 curing)

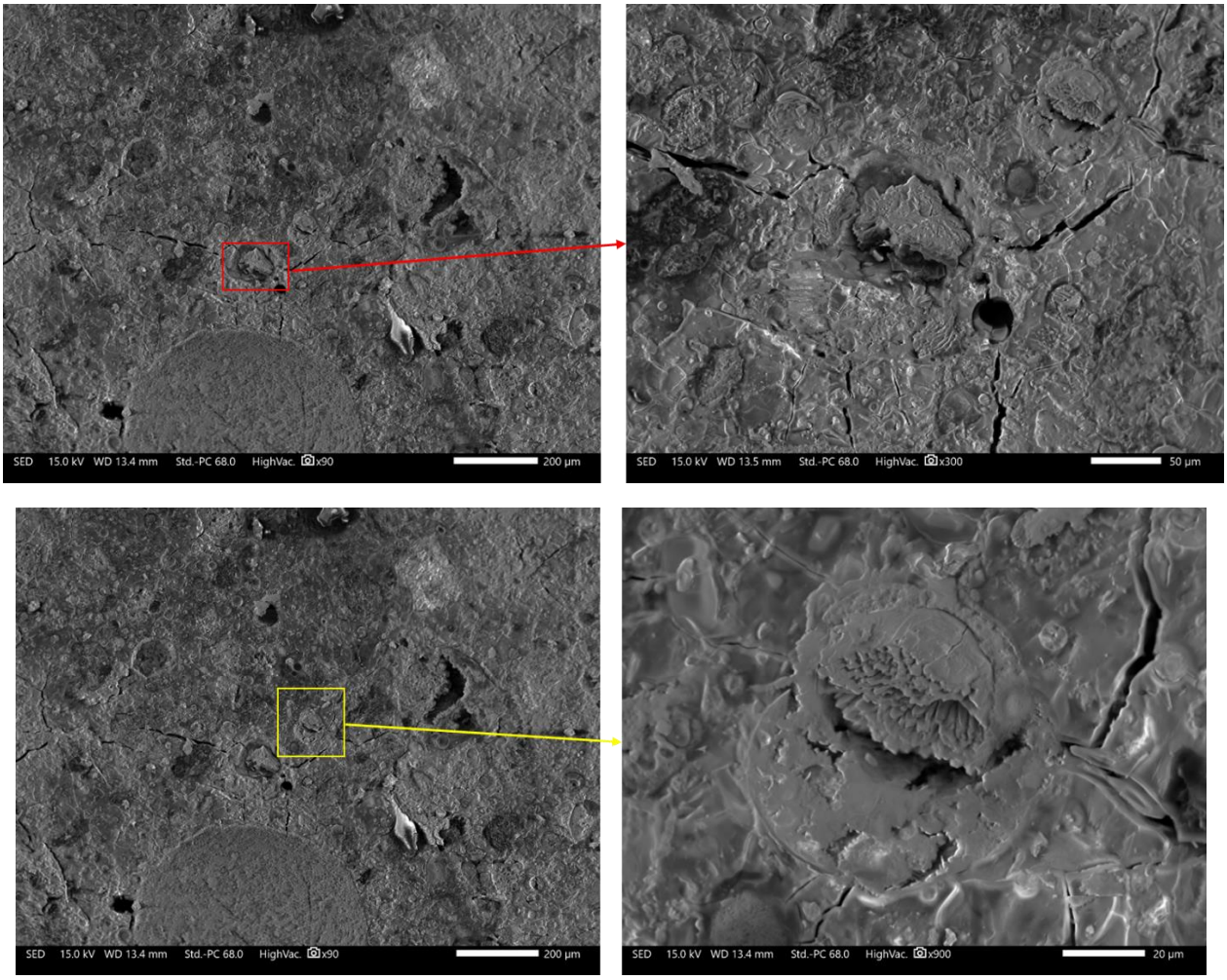

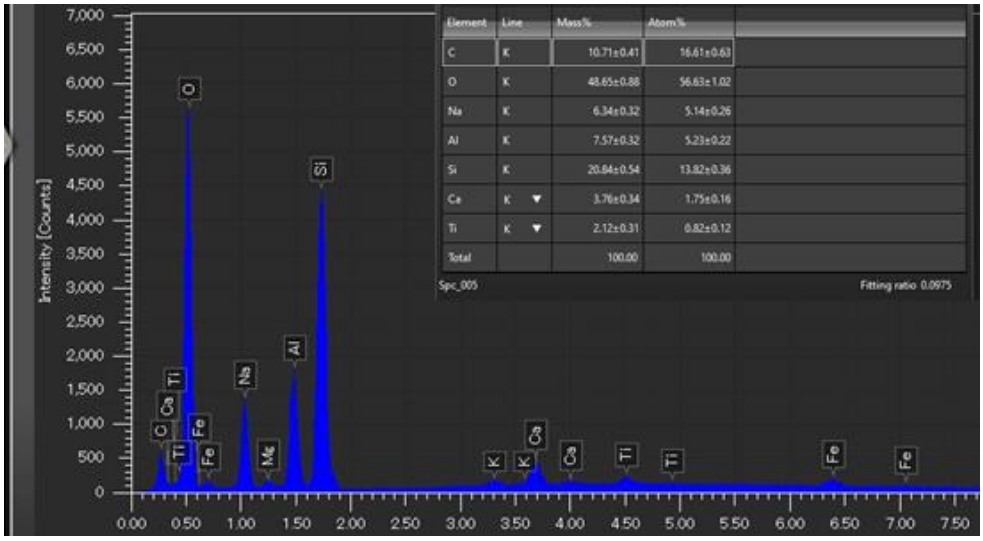

Figure 4.23. 2NS+75% BOFS (CO_2 curing)

The presence of fly ash particles is noticed in the fissures (Figure 24). Fly ash particle size is equivalent to the fracture of geopolymer concrete, which improves the characteristics. Partially reacted fly ash particles are common, as are some fully reacted particles in Figure 22, 23. There is a porous, heterogeneous combination of unreacted or partially reacted fly ash grains, residual alkaline precipitates, and geopolymer gel. There are evident cracks emerging at the site of fly ash particle collection. On the surface, it seems to be denser than all other concrete. Fly ash particles create weak linkages in the matrix, allowing cracks to spread. Crack development is noticed at random in standard grade concrete. The separation of particles from the concrete's surface is also visible in Figure 22, 23. In the same magnification scale, the light density of geopolymer concrete is detected in Figure 22, 23.

4.4.3. Drying shrinkage

The Figure 25 and 26 presents the shrinkage behavior and weight change of the GPM mixture. During the polymerization process, binders, AAS, and water react with each other to form geopolymerization products. This reaction causes chemical shrinkage in the GPM matrix. Also, the volume changes due to autogenous shrinkage (self-desiccation) and the volume change through capillary pores (drying shrinkage) dominate the overall shrinkage behavior of GPM. As shown in Figure 25, the GPM mixture containing 100% RS and 50% RS, and 50% BOFS aggregate (1 and 1.5 ratios of AAS) has higher shrinkage than other mixtures, about -1.4%, and more length change. These results match the early-age compressive strength development of both mixtures illustrated in Figure. The higher the shrinkage, the higher the compressive strength. This trend also fits the GPM mixture with the lowest shrinkage and compressive strength development. Interestingly, the 2NS+50% BOFS mixture shows the lowest shrinkage under the same condition and mix proportion. Therefore, the combined effect based on all different types of shrinkage influences the total shrinkage behavior of the GPM mixture.

According to Sun et al., 2021 and Siddique and Cachim 2018, he evaporation of internal free water in the set mortar or concrete mix in the environment causes drying shrinkage, which is a sort of independent stress deformation. This relates to the hydrated cement stone's meso- and macroporous structure. Because of the low capillary tension (pressure), free water evaporates first from the macropores. This behavior is seen in the image, which corresponds to a significant initial drying shrinkage lasting up to 10 days. Due to continual evaporation, there is less free water in

macropores. As a result, the water in the mesoscale pores gradually evaporates, causing considerable capillary tension and continuous contraction. As demonstrated in Figure 25, this effect is connected with drying shrinkage after 10 days.

Shehata et al., 2022 review paper shows that FA-based geopolymers with the content of free lime and sulphite, 11% and 4%, respectively, may reduce the drying shrinkage of geopolymer mortar/concrete by 60.65% compared to OPC concrete. The F-FA used in this study indicates calcium oxide (CaO) and Sulfur trioxide (SO_3), 1.86% and 0.31%. Therefore the shrinkage might show a slighter decrease than in the previous study.

According to Sandybay et al., 2022 study, when mortar mixes with BOFS and GGBFS were dried, the percentage of GGBFS rose, resulting in more significant drying shrinkage. The fact that GGBFS has better cementitious properties than F-FA, which contains inert phases such as dicalcium ferrite (C_2F) and Magnetic oxide (Fe_3O_4), may cause this outcome. Due to the GGBFS's gypsum component, adding more GGBFS to the mortar mixture improves the cement's hydration and increases the amount of ettringite. Hence, drying shrinkage increases with GGBFS content.

Figures 25 shows (a), (b), and (e) shows that with the increasing ratio of sodium silicate to sodium hydroxide, the shrinkage of GPM specimens increases together, similar to Xu et al. 2022 study. The control mixture after six months shows only -1.2% of shrinkage with 1NS+0% BOFS, and it increases to -1.3% and -1.45% with 1.5NS+0% BOFS and 2NS+0% BOFS mixtures, respectively. As same the mixtures with 25% of BOFS (-1.1%, -1.2%, and -1.3% at 1, 1.5, and 2 ratios of AAS respectively) and 100% BOFS (-1.05%, -1.1%, and -1.25% at 1, 1.5 and 2 ratios of AAS respectively) have the same results for drying shrinkage durability test. This negative effect of sodium silicate on GPM might be related to an increase in sodium silicate, which can make a material more porous, increasing the likelihood of internal water flow and, as a result, reducing shrinkage since the specimen has enough moisture. A rise in sodium silicate, on the other hand, may speed the hydration rate of alkali-activated materials and increase shrinkage.

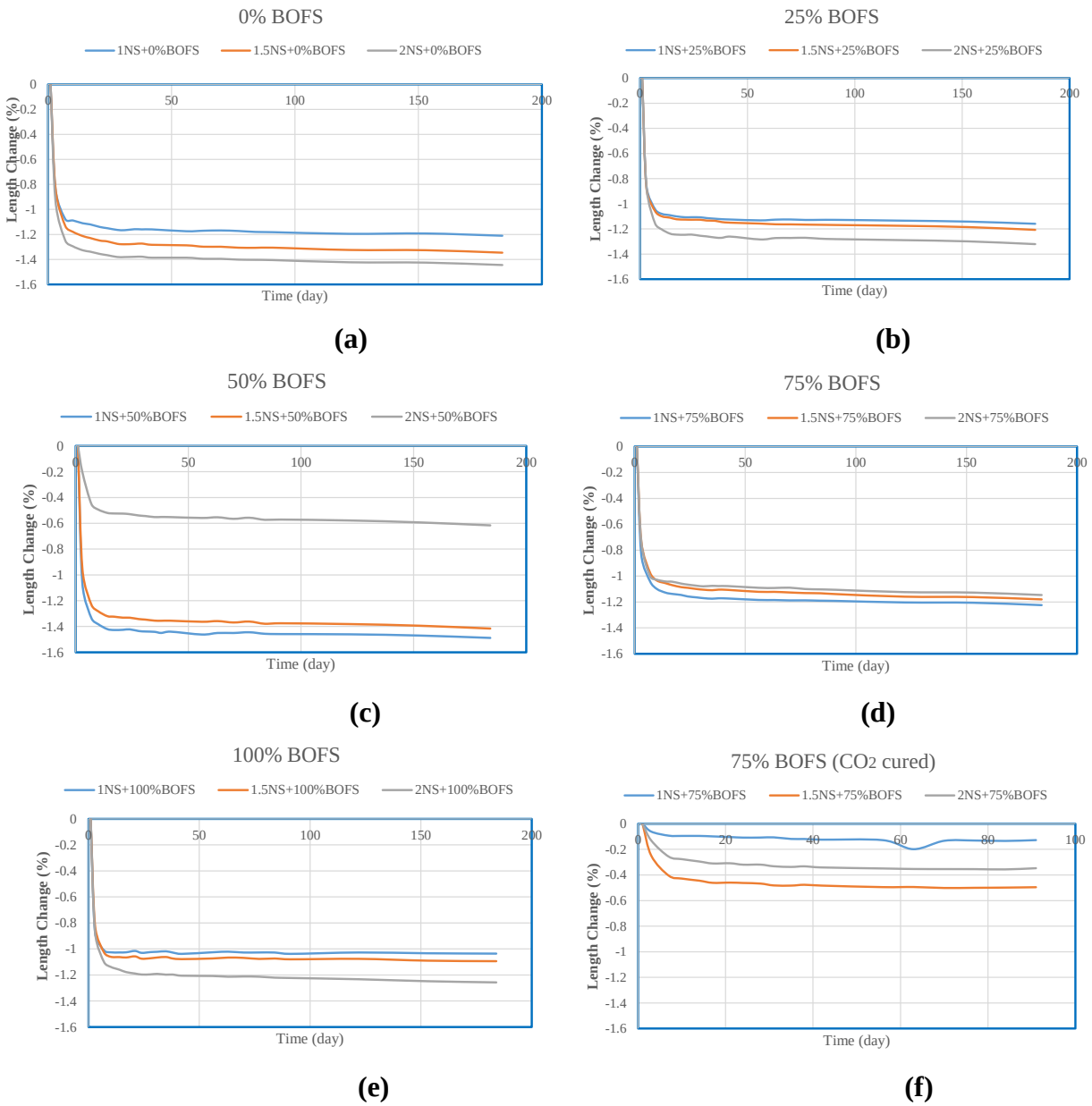

Figure 4.24. Drying shrinkage (length change) of GPM mixture. (a), (b), (c), (d), and (e) ambient cured samples; (f) CO_2 cured sample

Surface energy, capillary tension, and disjoining pressure were identified as the three primary causes of drying shrinkage. Compared to ambient-cured 75% BOFS GPM, the carbonation-cured samples show fewer shrinkage results. If under room temperature condition the shrinkage were about -1.2%, then after CO_2 treatment the shrinkage was less than -0.5%. It means that CO_2 treatment control and positive effect on the form change of GPM. After the carbonation curing polymerization process could control the GPM, the gel, by this process, could maintain the samples form from their initial shape.

The study demonstrates how the calcium carbonate generated by the carbonation process filled up the gaps in the Alkali Activated solution pastes and reduced their overall porosity. Overall porosity and pore-size distribution were altered by CO_2 curing. The overall porosity and the percentage of holes smaller than 25 nm were found to have significantly decreased. The pores were coarsened by decalcification of C-(A)-S-H, which increased the median pore size from 7.2 nm to 14.3 nm. When AASC drying shrinkage was compared to AASC cured in air at the same temperature and RH, capillary pressure decreased as pore size rose [Cai et al ., 2019].

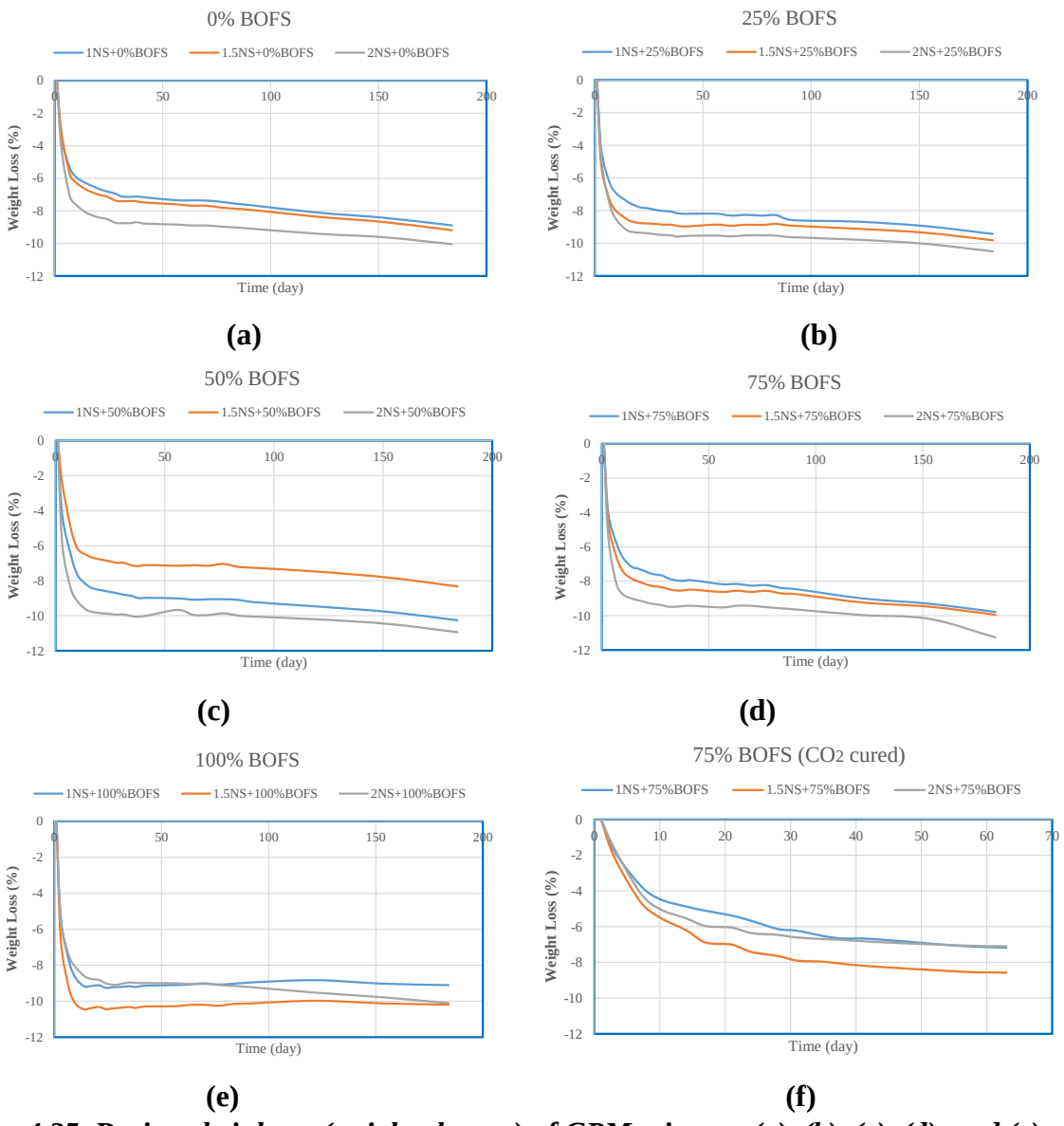

Figure 4.25. Drying shrinkage (weight change) of GPM mixture. (a), (b), (c), (d), and (e) ambient cured samples; (f) CO_2 cured sample

4.5. RSM

Table 4.3. Central Composition Design of RSM

Central Composite Design			
Factors:	2	Replicates:	1
Base runs:	13	Total runs:	13
Base blocks:	1	Total blocks:	1
Two-level factorial:	Full factorial		
Cube points:	4		
Center points in the cube:	5		
Axial points:	4		
Center points in axial:	0		
α: 1			

The RSM was conducted by the ratio of NA_2SiO_3 to NaOH, and by percentage of BOFS content, Compressive strength results at 28 days, and ASR expansion results also at 28 days, to compare the correlation. The R square, the optimum equation for compressive strength and ASR expansion provided. Furthermore, for the last step, the optimum ratio for sodium silicate and percentage of BOFS have been calculated and occurred by the graph. For this research work with the control group (100% river sand+0%BOFS) and increasing percentage of BOFS content, overall, 15 mixtures were designed, and conducted all tests. For the RSM analyzer, 15 mixtures were grouped into 3 groups. Group A includes 0%, 25%, and 50% BOFS aggregate-based GPM, with the same 25% period. Group B has 25%, 50%, and 75% of BOFS; it also has a 25% difference between the mixtures. The last Group is C, which is 0%, 50%, and 100% BOFS-based GPM; the period is 50%.

4.5.1. Group A. 25%, 50%, and 75% BOFS-based GPM

Table 4.4. Values of Na_2SiO_3 and BOFS

Uncoded values		Coded values	
Na_2SiO3	BOFS	Na_2SiO3	BOFS
1	25	-1	-1
1.5	50	0	0
2	75	1	1

Compressive strength = 26.967 - 8.508 Na2SiO3 + 5.377 BOFS - 1.213 (Na2SiO3)2 + 11.882 (BOFS)2 + 0.583 Na2SiO3*BOFS (17)

Eq (17) shows the best compressive strength equation. Accurate data and the model's predictions must be compared in order to evaluate the developed model equations for the dependability of the

RSM findings. For this reason, the set of quadratic equations above is used as the foundation for the prediction model, and corresponding comparison graphs are created. Via the R square, the RSM shows the compatibility of the equation. The equation shows that R^2= 98.49% is applicable.

Figure 26 and 27 depicts the response surface and contour plots for Group A mix design, which show that the combination comprising 1, 1.5 and 2 ratio Na_2SiO_3 (coded as -1, 0 and 1) and 25%, 50% and 75% BOFS aggregate has the greatest hardened compressive strength of 98.49% and feasible durability factor of 91.89%.

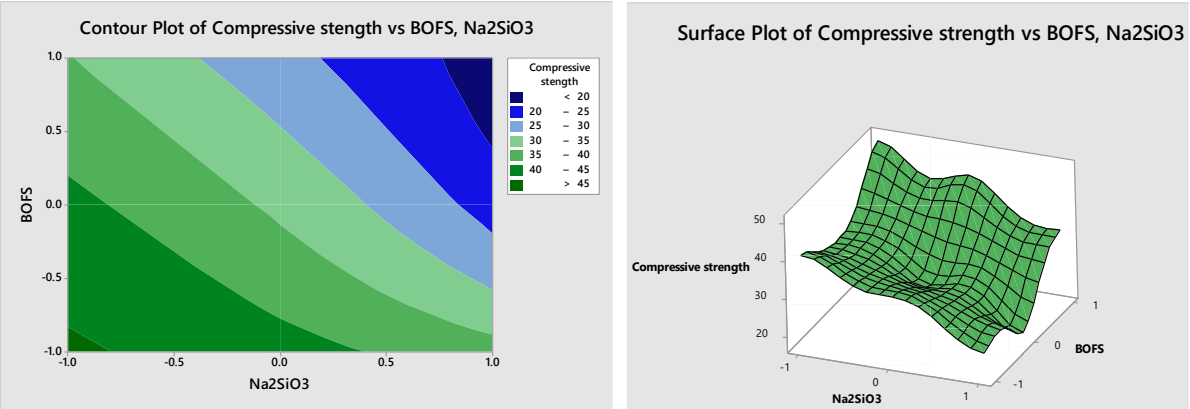

Figure 4.26. Counter plot (a) and Surface plot of Compressive strength vs. BOFS, Na_2SiO_3

ASR expansion = 0.03403 - 0.02300 Na2SiO3 + 0.03433 BOFS - 0.0176 (Na2SiO3)2 + 0.0324 (BOFS)2 - 0.02800 Na2SiO3 *BOFS (18)

The Eq (18) is ASR expansion, which the DOE analyzer gave the R^2=91.89% match able results for using this equation

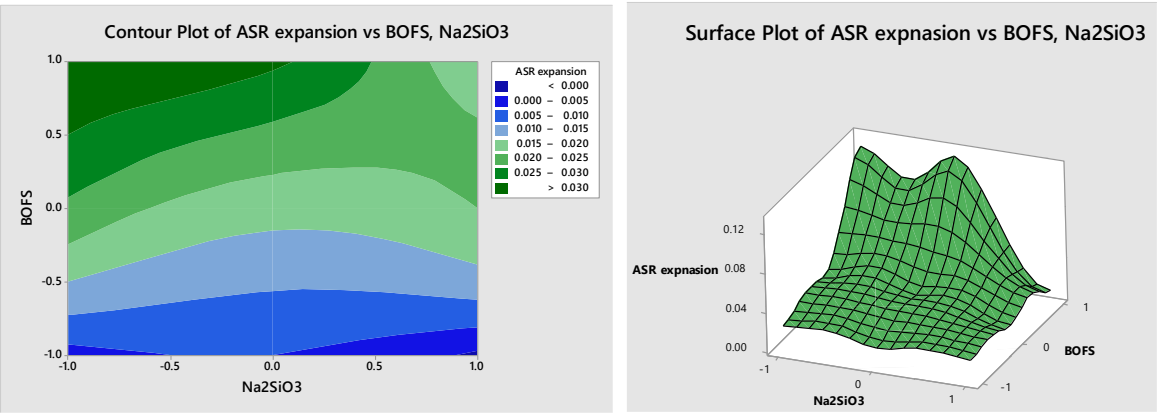

Figure 4.27. Counter plot (a) and Surface plot of ASR expansion vs. BOFS, Na_2SiO_3

Figure 4.28. The optimum mix design for BOFS-based GPM

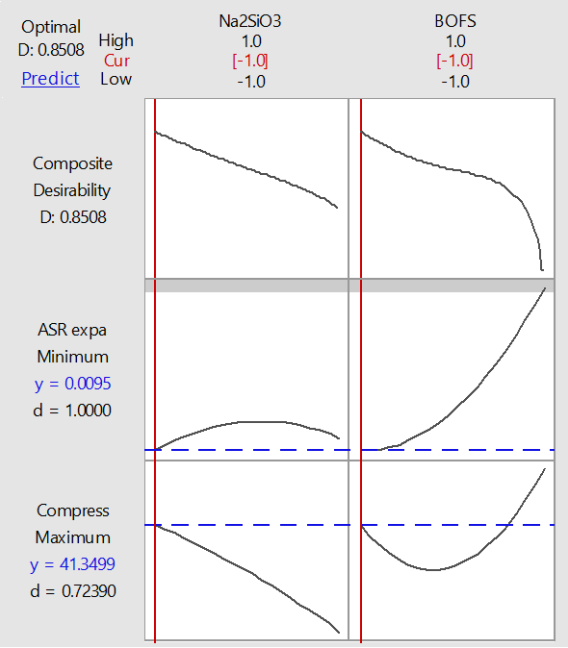

The Figure 28 shows the optimum mix design, where the ratio of sodium silicate is – 1.0 and -1.0 by the coded values. The uncoded values mean the 1 ratio of Na_2SiO_3 to NaOH and 25% of BOFS is the most optimized version for Group A.

4.5.2. Group B. 50%, 75%, and 100% BOFS aggregate-based GPM

Table 4.5. Values of Na_2SiO_3 and BOFS

Uncoded values		Coded values	
Na_2SiO_3	BOFS	Na_2SiO_3	BOFS
1	50	-1	-1
1.5	75	0	0
2	100	1	1

$$\textit{Compressive strength} = 45.046 - 8.937\ Na2SiO3 + 3.585\ BOFS - 1.796\ (Na2SiO3)2 - 13.671\ (BOFS)2 - 0.820\ Na2SiO3*BOFS \quad (19)$$

Figure 29 and 30 depicts the response surface and contour plots for Group B mix design, which show that the mixture including 1, 1.5 and 2 ratio of sodium silicate to sodium hydroxide (coded as -1, 0 and 1) and 50%, 75% and 100% BOFS has the maximum strength of compressive 99.59% and feasible ASR expansion durability factor of R^2= 86.92%.

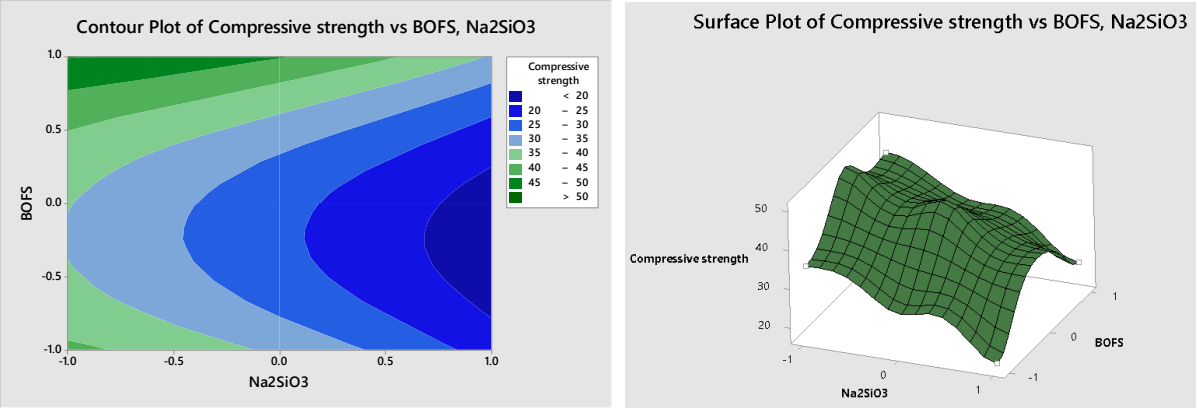

Figure 4.29. Counter plot (a) and Surface plot of Compressive strength vs. BOFS, Na_2SiO_3

ASR expansion = 0.1141 + 0.0052 Na2SiO3 + 0.0495 BOFS - 0.0037 (Na2SiO3)2 - 0.0357 (BOFS)2 + 0.0457 Na2SiO3*BOFS (20)

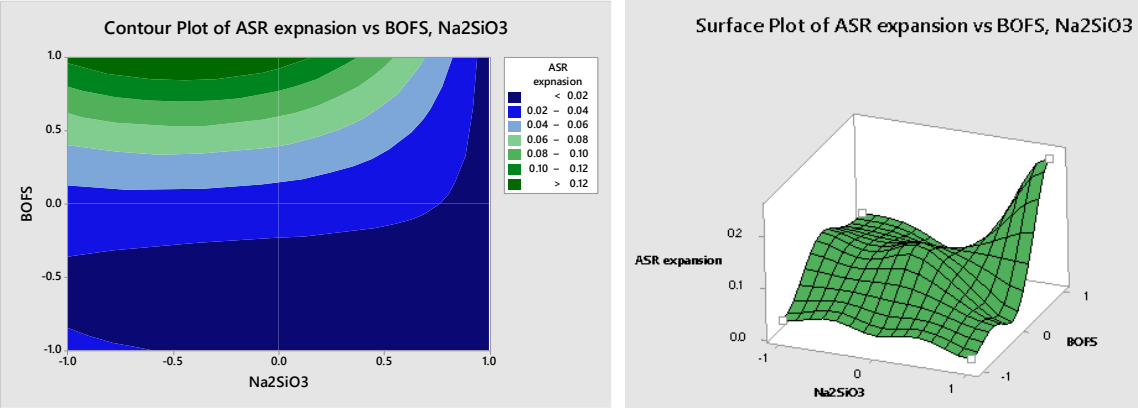

Figure 4.30. Counter plot (a) and Surface plot of ASR expansion vs. BOFS, Na_2SiO_3

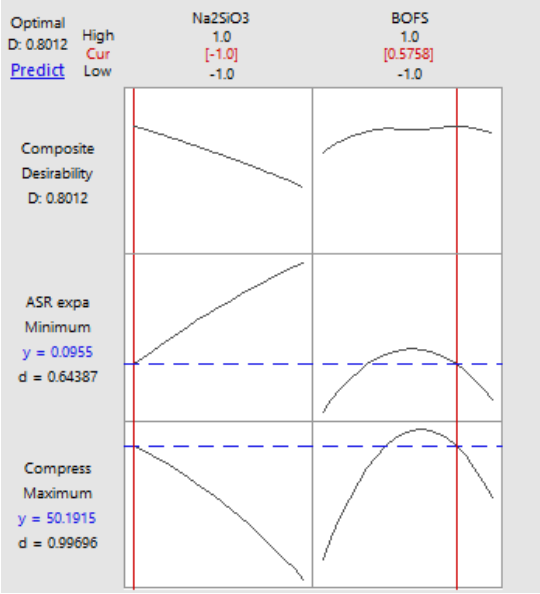

Figure 4.31. The optimum mix design for BOFs-based GPM

The optimum mix design for Group B is shown in Figure 31. It indicates that for both cases, compressive strength and ASR expansion are the most matched variables for sodium silicate and BOFS is 1 ratio and 89%, respectively.

Summary

	Compressive strength	Hardened Density	Flexural strength	Dielectric constant	Drying shrinkage	Water expansion (under limit)	ASR expansion (under limit)
Group 1 (0% BOFS)	↑	↓	↑	↓	↓	OK	OK
Group 2 (25% BOFS)	↑	↓	↑	↓	↓	OK	OK
Group 3 (50% BOFS)	↑	↓	↑	↓	↓	OK	OK
Group 4 (75% BOFS)	↑	↓	↑	↓	↓	OK	1NS+75%BOFS & 1.5NS+75%BOFS
Group 5 (100% BOFS)	↑	↓	**No trend**	↓	↓	1NS+100%BOFS	2NS+100%BOFS

This research work have been used 15 mixtures with 5 various proportion of river sand to BOFS. The 5 group summarized the hardened properties and durability performance of GPM. It shows increasing trend of compressive strength with the increasing of time. At the same time

hardened properties, which is directly related to compressive strength shows the decreasing of results, because of the decreasing hydration of GPM samples. The flexural strength also, similar to compressive strength illustrates increasing of flexural strength with increasing of age of GPM, except 100% based GPM. The permittivity shows overall decreasing of results. The durability shows also good performance. All the mortars, except 100% BOFS GPM, showed good water expansion results. All the results is under 0.1% of expansion, which means non-reactive aggregate. ASR expansion showed similar results. Control group, 25% and 50% BOFS based GPM non-reactive aggregate and 1NS and 1.5 NS + 75% BOFS based and 2NS+100% BOFS based GPM showed that they are potential reactive aggregate.

Chapter 5 . Conclusion and Recommendation

5.1. Conclusion

This study has evaluated whether geopolymer mixture can become a key material to utilize basic oxygen furnace slag (BOFS) as an aggregate without causing high expansion. The following results have been obtained:

- Up to 75% replacement of RS with BOFS aggregate, increasing BOFS aggregate content increases the relative flowability of the GPM mixture.
- The air content and setting time of the GMP mixture decrease with increasing BOFS aggregate content.
- For compressive and flexural strengths, the GPM mixtures containing BOFS aggregate had comparative strength or higher strength than that containing 100% RS.
- The GPM mixture with higher compressive strength showed higher shrinkage than other mixtures.
- The Dielectric constant results shows that BOFS based GPM permittivity decrease with increasing of BOFS content, and the GPM very sensitive to environmental condition as temperature and humidity where mortar is exposed.
- Regardless of water and 1 M NaOH solution submersions, all GPM mixtures have less than 0.1% expansion value except for the mixture having 25% RS and 75% BOFS aggregate submersed in NaOH solution.
- Through the SEM pictures and EDS results it shows that manifestation CSH gel clearly identified, which control the behavior of BOFS, even after reaction with water and1 M NaOH.
- Drying shrinkage is a sort of independent stress deformation, and with the increasing of BOFS percentage in GPM the shrinkage percentage is decrease.
- It has been effectively demonstrated that geopolymer technology can stabilize BOFS because the matrix of the GPM combination contains a considerable amount of free silicon (Si), which combines with free CaO or free MgO to form stable silicate compounds, hence resolving the problem of BOFS expansion.
- Additionally Carbonation curing helped geopolymerization process to control the characterization of durability performance GPM.

References

Rao A. K., Kumar D. R. Comparative study on the behavior of GPC using silica fume and fly ash with GGBS exposed to elevated temperature and ambient curing conditions, Mater. Today: Proc. 27 (2020) 1833-1837. https://doi.org/10.1016/j.matpr.2020.03.789

Azarsa P., Gupta R. Durability and leach-ability evaluation of K-based geopolymer concrete in real environmental conditions, Case Stud. Constr. Mater. 13 (2020) e00366. https://doi.org/10.1016/j.cscm.2020.e00366

Ma M., Mendizadeh H., Guo M. Z., Ling T. C. Effect of direct carbonation routes of basic oxygen furnace slag (BOFS) on strength and hydration of blended cement paste, Constr Build Mater. 304 (2021) 124628. https://doi.org/10.1016/j.conbuildmat.2021.124628

Ding Y.-C., Cheng T.-W., Liu P.-C., Lee W.-H. Study on the treatment of BOF slag to replace fine aggregate in concrete, Constr Build Mater. 146 (2017) 644-651. http://dx.doi.org/10.1016/j.conbuildmat.2017.04.164

Lee W.-H., Cheng T.-W., Lin K.-Y., Lin K.-L., Wu C.-C., Tsai C.-T. Geopolymer technologies for stabilization of basic oxygen furnace slags and sustainable application as construction materials, Sustainability, Sustainability 12 (2020) 5002. https://www.mdpi.com/2071-1050/12/12/5002

Yunxia L., Mingkai Z., Xiao C., Fang X. Methods for Improving Volume Stability of Steel Slag as Fine Aggregate, J. Wuhan Univ. Technol. Mater. Sci. Ed. 23 (2008) 737–742. doi:10.1007/s11595-007-5737-3

Kabay N., Miyan N., Ozkan H. Basic oxygen furnace and ground granulated blast furnace slag based alkali-activated pastes: Characterization and optimization, J. Clean. Prod. 327 (2021) 129483. https://doi.org/10.1016/j.jclepro.2021.129483

Huijgen W.J.J., Carbon dioxide sequestration by mineral carbonation (2007). https://edepot.wur.nl/121870

Pradhan P., Dwibedy S., Pradhan M., Panda S., Panigrahi S. K. Durability characteristics of geopolymer concrete - Progress and perspectives, Journal of Building Engineering 59 (2022) 105100. https://doi.org/10.1016/j.jobe.2022.105100

Ahmed H. U., Mahmood L. J., Muhammad M. A., Faraj R. H., Qaidi S. M A., Sor N. H., Mohammed A. S., Mohammed A. A. Geopolymer concrete as a cleaner construction material: An overview on materials and structural performances, Cleaner Materials 5 (2022) 10011. https://doi.org/10.1016/j.clema.2022.100111

Hamdane H., Tamraiui Y., Mansouri S., Ouman M., Bouih A., Ghaillassi T. E., Boulif R., Manoun B., Hannache H. Statistical modeling of geopolymers from dual-alkali activation of un-calcined phosphate sludge and their potential applications as sustainable coating materials,

Journal of cleaner production 283 (2021) 125421. https://doi.org/10.1016/j.jclepro.2020.125421

Farooq F., Xin J., Jave M. F., Akbar A., Shah M. I., Aslam F., Alyousef R. Geopolymer concrete as sustainable material: A state of the art review, Construction and Building Materials 306 (2021) 124762. https://doi.org/10.1016/j.conbuildmat.2021.124762

Shehata N., Mohamed O.A., Sayed E.T., Abdelkaeem M. A., Olabu A.G. Geopolymer concrete as green building materials: Recent applications, sustainable development and circular economy potentials, Science of the Total Environment 836 (2022) 155577. http://dx.doi.org/10.1016/j.scitotenv.2022.155577

Ghafoor M. T., Khan Q. S., Qazi A. U., Sheikh M. N., Hadi M. N. S. Influence of alkaline activators on the mechanical properties of fly ash based geopolymer concrete cured at ambient temperature, Construction and Building Materials 273 (2021) 121752. https://doi.org/10.1016/j.conbuildmat.2020.121752

I.G. Lodeiro, A. Palomo, F. Jim´enez, Alkali-aggregate reaction in activated fly ash systems, Cement Concr. Res. 37 (2007) 175–183. https://doi.org/10.1016/j.cemconres.2006.11.002

Chen X., Zhang J., Lu M., Chen B., Gao S., Bai J., Zhang H., Yang Y. Study on the effect of calcium and sulfur content on the properties of fly ash based geopolymer, Construction and Building Materials 314 (2022) 125650. https://doi.org/10.1016/j.conbuildmat.2021.125650

Lee S. H., Kim H. J., Sakaib E., Daimon M. Effect of the particle size distribution of fly ash–cement system on the fluidity of cement pastes DOI:10.1016/S0008-8846(02)01054-2

Amran M., Debbarma S., Ozbakkaloglu T. Fly ash-based eco-friendly geopolymer concrete: A critical review of the long-term durability properties, Construction and Building Materials 270 (2021) 121857. https://doi.org/10.1016/j.conbuildmat.2020.121857

Law D. W., Adam A. A., Molyneaux T K., Patnaikuni I.,Wardhono A. Long term durability properties of class F fly ash geopolymer concrete, Materials and Structures (2015) 48:721–73. DOI 10.1617/s11527-014-0268-9

Bellum R. R., Khazaleh M. A., Pilla R. K., Choudhary S., Venkatesh C., Effect of slag on strength, durability and microstructural characteristics of fly ash-based geopolymer concrete, Journal of Building Pathology and Rehabilitation 7(1). DOI:10.1007/s41024-022-00163-4

Karthik A., Sudalaimani K., Kumar C.T. Investigation on mechanical properties of fly ash-ground granulated blast furnace slag based self curing bio-geopolymer concrete, Materials Science, Engineering Construction and Building Materials. DOI:10.1016/J.CONBUILDMAT.2017.05.139

Yaping Y., Xiaoqiang Z., Weilan Q., Mingwen W. Synthesis of pure zeolites from supersaturated silicon and aluminum alkali extracts from fused coal fly ash, https://doi.org/10.1016/j.fuel.2007.12.002

Multon, S., Barin, F., Godart, B., and Toutlemonde, F. (2008). "Estimation of residual expansion of concrete affected by alkali silica reaction." J. Mater. Civ. Eng., 20(1), 54–62.

Kupwade-Patil K, Allouche E. N, Eng P. Impact of Alkali-Silica Reaction on Fly Ash-BasedGeopolymer Concrete, International Journal of Science and Research (IJSR) 6(9)

Ahmad J, Kontoleon K. J., Majdi A. , Naqash M. T., Deifalla A. F., Kahla N. B., Isleem H. F., and Qaidi A. A Comprehensive Review on the Ground Granulated Blast Furnace Slag (GGBS) in Concrete Production, Sustainability 2022, 14(14), 8783. https://doi.org/10.3390/su14148783

Ganesh, P.; Murthy, A.R. Tensile Behaviour and Durability Aspects of Sustainable Ultra-High Performance Concrete Incorporated with GGBS as Cementitious Material. Constr. Build. Mater. 2019, 197, 667–680. https://doi.org/10.1016/j.conbuildmat.2018.11.240

Duos, C., Eggers, J., 1999. Evaluation of ground granulated blast furnace slag in concrete (Grade 120). Rpt. No. FHWA/LA-99/336, Louisiana Trans. Res. Center, Baton Rouge, Louisiana.

Hadi N.S., Farhan N. A., Sheikh M.N. Design of geopolymer concrete with GGBFS at ambient curing condition using Taguchi method, Construction and Building Materials 140 (2017) 414-431. http://dx.doi.org/10.1016/j.conbuildmat.2017.02.131

Malhotra, V.M., 2008. Mineral admixtures. In: Nawy, E.G. (Ed.), Concrete Construction Engineering Handbook. CRC Press, London

Shahmansouri A. A., Nematzadeh M., Behnood A. Mechanical properties of GGBFS-based geopolymer concrete incorporating natural zeolite and silica fume with an optimum design using response surface method, Journal of Building Engineering 36 (2021) 102138

Hansen, W.C., 1944. Studies relating to the mechanism by which alkali-aggregate reaction produces expansion in concrete. J. Am. Concr. Inst. 15, 213 217.

Maeda, Y., 2015. Slag cement-related products which utilized a property of the ground granulated blast furnace slag, Technical Report, Nippon Steel & Sumitomo Metal Technıcal Report No. 109

Wei, Y., Hansen, W., Biernacki, J.J., Schlangen, E., 2011. Unified shrinkage model for concrete from autogenous shrinkage test on paste with and without ground-granulated blast-furnace slag. ACI Mater. J. 108 (1), 13 20.

Brand A.S. and Fanijo E.O., (2020), A Review of the Influence of Steel Furnace Slag Type on the Properties of Cementitious Composites, applied sciences, doi:10.3390/app10228210

Martins A.C.P., Carvalho J. M. F., Costa L. C. B. et al., (2021), Steel slags in cement-based composites: An ultimate review on characterization, applications, and performance, Construction and Building Materials, doi.org/10.1016/j.conbuildmat.2021.123265

Piemonti A., Conforti A., Cominoli L., Sorlini S., Luciano A., Plizzari G., (2021), Use of Iron and Steel Slags in Concrete: State of the Art and Future Perspectives, sustainability, doi.org/10.3390/su13020556

Naidu T. S., Sheridan C. M., Dyk L. D., (2020), Basic oxygen furnace slag: Review of current and potential uses, Minerals Engineering, doi.org/10.1016/j.mineng.2020.106234

Carvalho S.Z., Vernilli F., Almeida B., Demarco M., Silva S. N., (2017), The recycling effect of BOF slag in the portland cement properties, Resources, Conservation & Recycling, doi.org/10.1016/j.resconrec.2017.08.021

Omur T., Muyan N., Kabay N., Ozkan H. Utilization and optimization of unweathered and weathered basic oxygen furnace slag aggregates in cement based mortar, Journal of Building Engineering 64 (2023) 105634. https://doi.org/10.1016/j.jobe.2022.105634

Kuo W., Gao., Juang C., (2019), Influence of BOF and GGBFS Based Alkali Activated Materials on the Properties of Porous Concrete, materials, doi:10.3390/ma12142214

Mastali M., Alzaza A., Shaad K. M., Kinnunen P., Abdollahnejad Z., Woof B., and Illikainen M. (2019), Using Carbonated BOF Slag Aggregates in Alkali-Activated Concretes, materials, doi:10.3390/ma12081288

Lee W. H., Cheng T. W., , Lin K Y., Lin K.L., Wu C. C., and Tsai C. T. Geopolymer Technologies for Stabilization of Basic Oxygen Furnace Slags and Sustainable Application as Construction Materials, Sustainability 2020, 12(12), 5002. https://doi.org/10.3390/su12125002

Ding Y. C., Cheng T. W., Liu P. C., Lee W. H. Study on the treatment of BOF slag to replace fine aggregate in concrete, Construction and Building Materials 146(2017) 644-651. http://dx.doi.org/10.1016/j.conbuildmat.2017.04.164

Ozkan, O., Saribiyink, M., 2011. Alkali silica reaction of BOF and BFS wastes combination in cement. J. Civ. Eng. Manage. 19, 110–113.

Sarabia L. A. and Ortiz M. C., University of Burgos, Burgos, Spain Response Surface Methodology. DOI:10.1016/B978-044452701-1.00083-1

Awolusia T.F., Okea O.L., Akinkurolerea O.O., Sojobi A.O. Application of response surface methodology: Predicting and optimizing the properties of concrete containing steel fibre extracted from waste tires with limestone powder as filler

Prakash C. G, Dhurvey P.,and Shaik N. Optimization and Prediction of Concrete with Recycled Coarse Aggregate and Bone China Fine Aggregate Using Response Surface Methodology. https://doi.org/10.1155/2022/2264457

Dinh H. Q., Nguyen T. B. Composition of ground granulated blast-furnace slag and fly ash-based geopolymer activated by sodium silicate and sodium hydroxide solution: multi-response optimizationusing Response Surface Methodology

Law D. W., Adam A. A., Molyneaux T. K., Patnaikuni I., Wardhono A. Long term durability properties of class F fly ash geopolymer concrete, Materials and Structures (2015) 48:721–731

Tsai C.J., Huang R., Lin W.T., Wang H.N., Mechanical and cementitious characteristics of ground granulated blast furnace slag and basic oxygen furnace slag blended mortar, Mater. Des. 60 (2014) 267–273, https://doi.org/10.1016/j.matdes.2014.04.002.

Apostolidou Ch., Georgakopoulos A. Morphology, Mineralogy, and Chemistry of Fly Ash from the Ptolemais Power Stations, Northern Greece, and its potential as partial Portland cement substitute

Styszko-Grochowiak K., Golas J., Jankowsli H., Kozinski S. Characterization of the coal fly ash for the purpose of improvement of industrial on-line measurement of unburned carbon content. doi:10.1016/j.fuel.2004.03.005

Verma M., Dev N., Rahman I., Nigam M., Ahmed M., Mallick J. Geopolymer Concrete: A Material for Sustainable Development in Indian Construction Industries, Crystals 2022, 12, 514. https://doi.org/10.3390/cryst12040514

M. Harini, G. Shaalini, G. Dhinakaran, KSCE J. Civ. Eng. 16 (1) (2012) 163-168. DOI 10.1007/s12205-012-1283-4

Tian X., Xu W., Song S., Rao F., Xia L. Effects of curing temperature on the compressive strength and microstructure of copper tailing-based geopolymers, Chemosphere 253 (2020) 126754. https://doi.org/10.1016/j.chemosphere.2020.126754

S. Solomon, DVN T. Flach, In: M. Mercedes Maroto-Valer, editor, Developments and Innovation in Carbon Dioxide (CO2) Capture and Storage Technology: Carbon Dioxide (CO2) Capture, Transport and Industrial Applications, 1st ed. Woodhead Publishing, 2010

Cai Y., Yu L., Yang Y., Gao Y., Yang C. Effect of Early Age-Curing Methods on Drying Shrinkage of Alkali-Activated Slag Concrete. Materials (Basel). 2019 May 18;12(10):1633. doi: 10.3390/ma12101633.

Shi, C.; Liu, M.; He, P.; Ou, Z. Factors affecting kinetics of CO2 curing of concrete. J. Sustainable Cem.Based Mater. 2012, 1, 24–33. [CrossRef]

Shi, C.; Wang, D.; He, F.; Liu, M. Weathering properties of CO2 cured concrete blocks. Resour. Conserv. Recy.2012, 65, 11–17. [CrossRef]

Han S. H., Jun Y., Shin T. Y., Kim J. H. CO2 Curing Efficiency for Cement Paste and Mortars Produced by a Low Water-to-Cement Ratio, Materials 2020, 13, 3883; doi:10.3390/ma13173883

Skvara, F., Kopecky, L., Nemecek, J., and Bittnar, Z., 2006, “Microstructure of geopolymer materials based on fly ash”, Cermaics – Silikaty, Vol. 50, 208 – 215 pp

E. Álvarez-Ayuso, X. Querol, F. Plana et al., "Environmental, physical and structural characterisation of geopolymer matrixes synthesised from coal (co-)combustion fly ashes," Journal of Hazardous Materials, vol. 154, no. 1–3, pp. 175–183, 2008.

Schmitt, R. Electromagnetics Explained: A Handbook for Wireless/RF, EMC, and High-Speed Electronics; Newnes: London, UK, 2002. [Google Scholar]

Hanjitsuwan, S.; Hunpratub, S.; Thongbai, P.; Maensiri, S.; Sata, V.; Chindaprasirt, P. Effects of NaOH concentrations on physical and electrical properties of high calcium fly ash geopolymer paste. Cem. Concr. Compos. 2014, 45, 9–14. [Google Scholar] [CrossRef]

Topark-Ngarm, P.; Chindaprasirt, P.; Sata, V. Setting time, strength, and bond of high-calcium fly ash geopolymer concrete. J. Mater. Civ. Eng. 2015, 27, 04014198. [Google Scholar] [CrossRef]

Nuruddin, M.F.; Malkawi, A.B.; Fauzi, A.; Mohammed, B.S.; Almattarneh, H.M. Geopolymer concrete for structural use: Recent findings and limitations. In Proceedings of the IOP Conference Series: Materials Science and Engineering, Guangdong, China, 1 June 2016; IOP Publishing: Bristol, UK, 2016; p. 012021. [Google Scholar]

Kantakam, S.; Pimraksa, K.; Ngamjarurojana, A.; Chindaprasirt, P.; Chaipanich, A. Investigation on the dielectric properties of 0–3 lead zirconate titanate-geopolymer composites. Ferroelectrics 2013, 451, 84–89. [Google Scholar] [CrossRef]

Aradoaei, M.; Pepenar, I. Considerations on the dielectric properties and thermal profile of geopolymeric composites with ferro/ferrimagnetic inserts. In Proceedings of the 2014 International Conference and Exposition on Electrical and Power Engineering (EPE), Iasi, Romania, 16 October 2016; IEEE: Piscataway, NJ, USA, 2016; pp. 891–896. [Google Scholar]

Vlasceanu, I.N.; Gharzouni, A.; Tantot, O.; Lalande, M.; Elissalde, C.; Rossignol, S. Geopolymer as dielectric materials for ultra-wideband antenna applications: Impact of magnetite addition and humidity. Open Ceram. 2020, 2, 100013. [Google Scholar] [CrossRef]

Jumrat, S.; Chatveera, B.; Rattanadecho, P. Dielectric properties and temperature profile of fly ash-based geopolymer mortar. Int. Commun. 2011, 38, 242–248. [Google Scholar] [CrossRef]

Hanjitsuwan, S.; Chindaprasirt, P.; Pimraksa, K. Electrical conductivity and dielectric property of fly ash geopolymer pastes. Int. J. Miner. Metall. 2011, 18, 94–99. [Google Scholar] [CrossRef]

Tukaziban A., Shon C.-S., Orynbassarov I., Sandybay S., Syzdykov D., Zhang D., Kim J.R. Mechanical, swelling, and thermal properties of geopolymer mixture containing basic oxygen furnace slag aggregates, In: IOP Conf. Ser.: Earth Environ. Sci. 1050 (2022) 012021. DOI 10.1088/1755-1315/1050/1/012021

Qiu X., Chen J., Ye G., Schutter G.D. Insights in the chemical fundamentals of ASR and the role of calcium in the early stage based on a 3D reactive transport model, Cem. Concr. Res .157 (2022) 106778. https://doi.org/10.1016/j.cemconres.2022.106778

Sun, K., Peng, X., Chu, S.H., Wang, S., Zeng, L., Ji, G. (2021). Utilization of BOF steel slagaggregate in metakaolin-based geopolymer. Construction and Building Materials, 300, 124024.

Xu S., Gao P.,Huang L. , Tang L., Gu X. and Wang L. Experimental Research on Mechanical and ShrinkageProperties of Alkali Activated Low-Carbon Green Concrete, Materials (Basel). 2022 Aug 30;15(17):5984. doi: 10.3390/ma15175984.